THE EFFECT OF METAL ION EXCHANGE AND ALKALI METAL DOPING ON THE ELECTRICAL CONDUCTIVITY OF THE FAUJASITE-TYPE ZEOLITE 13X.

A thesis submitted to the
UNIVERSITY OF CAPE TOWN

in fulfilment of the requirements for the degree of

MASTER OF SCIENCE

by

STEPHEN SWART
B.Sc (Hons)

National Institute for Materials Research
Council for Scientific & Industrial Research
Pretoria 0001, South Africa.

December 1983.

ACKNOWLEDGEMENTS

I sincerely thank Dr J. Coetzer for his encouragement and guidance throughout the course of this work.

Thanks are also due to Professor L.R. Nassimbeni for his advice and interest in this work.

Dr P.J. Johnson is thanked for his assistance in setting up the automated data collection system and for the computer software associated with it.

I also wish to thank Mr C.D.N. Hertzog for the invaluable technical support he gave, as well as Mrs J. Harris and Mr J. Albain for their help with the Chemical Analyses and X-ray work.

My colleagues of the Electrometallurgy Division, NIMR, particularly Dr M.J. Nolte and Mr B.U. Köhler, are thanked for their general interest and encouragement during the course of this work.

Dr J.B. Clark, Chief Director of the National Institute for Materials Research, CSIR, is thanked for the use of the laboratory facilities of the Electrometallurgy Division.

The Anglo American Corporation of S.A. is acknowledged for its financial support.

Finally I wish to thank Mrs M. Dorling for her competent typing of this thesis and my mother for her support and encouragement enabling me to complete this work.

ABSTRACT

Zeolite 13X was synthesized in the sodium form. Some Group I, Group II and transition metal cations were introduced into the zeolite framework by ion exchange reactions.

These different cationic zeolite forms were doped or impregnated with sodium metal, utilizing the adsorptive properties of the zeolite.

An A.C. technique was used to determine the electrical conductivity of the dehydrated ion exchanged zeolites and the sodium impregnated zeolite samples as a function of temperature. The conductivity value obtained was used to determine some thermodynamic parameters relating to the conduction process.

For the dehydrated ion exchanged zeolites the electrical conductivity showed a general decrease with a decreasing ion exchange capacity.

The sodium impregnated zeolites showed an increase in conductivity with respect to the dehydrated unimpregnated samples. This was attributed to the presence of Na_6^{5+} centres in the impregnated zeolites. The reduction of some of the metal cations by the sodium on impregnation did not appear to have any significant effect on the overall ionic conductivity of the samples.

The conductivity as a function of temperature and pressure for the dehydrated sodium form of zeolite 13X and its impregnated counterpart was determined. The conductivity was found to increase with increasing pressure and temperature.

I N D E X

C H A P T E R 1

INTRODUCTION: ZEOLITES; THEIR STRUCTURE AND PROPERTIES.

1.1 Definition and General History

Zeolites have been known for many years, the first mineral zeolites being discovered in 1756. An appropriate definition of a zeolite is that given by Smith (1) which states that a zeolite is an aluminosilicate with a framework structure enclosing cavities occupied by large ions and water molecules, both of which have considerable freedom of movement permitting ion exchange and reversible dehydration.

The framework structure consists of a three-dimensional network of oxygen-sharing $A\ell O_4$ and SiO_4 tetrahedra, arranged in such a way that each zeolite species has its own structure with specific cavity dimensions.

Zeolites were first recognised as cation exchangers, but their real potential in the chemical industry was only realised in the 1920's and 1930's when the first crystal structure of a zeolite was determined (2,3).

The ion exchange and reversible dehydration properties made the zeolites useful ingredients in different catalytic processes, particularly since it was realised that dehydrated zeolites, instead of adsorbing watermolecules only, were able to selectively and reversibly adsorb various inorganic vapours. This principle laid the foundation for the now

well known concept of molecular sieving. The great potential of the zeolites in the chemical industry soon led to many species, both natural and synthetic, being produced in the laboratory.

Nowadays the importance of zeolites, with many fields of application, is reflected by the fact that in annual production value they rank about fortieth in a list of industrial chemicals, including sulphuric acid, ammonia and plastics.

Zeolite uses include the separation and recovery of normal paraffin hydrocarbons, catalysis of hydrocarbon reactions, drying of refrigerants, separation of air components, cracking catalysts in the petrochemical industry (4,5) and the recovery of radioactive ions from radioactive waste solutions (6). More recently, the possibility of using zeolites in solid state battery systems has been investigated (7,8). It was for this purpose that the work reported here was carried out, with specific reference to the ionic conductivities of the zeolite and how this might be affected by adsorption and ion exchange.

1.2 Zeolite Structure

Zeolites are hydrated crystalline aluminosilicates of general composition (9):

$$M\ (\text{Group I or Group II})_x\left[(A\ell_x Si_y)O_{2x+2y}\right]Z.H_2O\ \text{w.G.}$$

metal cations	aluminosilicate framework	water and included guest species

The zeolite structure consists of an anionic three-dimensional framework of SiO_4 and $A\ell O_4$ tetrahedra, formed by the mutual sharing of oxygens alone. This essentially means that there are no unshared oxygens in the framework, resulting in the ratio (Si + Aℓ) : oxygen being 1:2 (10). The linkage of the

tetrahedra by the oxygens is such that there exists a series of interconnecting channels and cavities of definite and uniform dimensions within the framework structure (11,12,13). A variety of channel systems are found in zeolites, viz. one, two or three dimensional, linear, zig-zag, etc (14).

Each tetrahedrally co-ordinated aluminium is associated with a net negative charge, hence creating the anionic framework. This net negative charge is neutralised by the so-called zeolite cations, most commonly of Group I and II metals. The metal cations are situated in specific sites located within the channels and cavities of the zeolite structure (15).

In silicate framework structures of which zeolites are a sub-class it is quite common for $A\ell^{3+}$ ions to substitute for Si^{4+} ions in the framework, thus creating the anionic aluminosilicate framework found in the zeolites (16). The maximum substitution of $A\ell^{3+}$ for Si^{4+} is found to be in the ratio 1:1 (17,18), since no two $A\ell$ ions can occupy the centres of tetrahedra linked by a single oxygen (19). The minimum substitution in zeolites occurs in zeolite Mordenite where the ratio of $Si:A\ell = 5:1$.

Zeolite frameworks have been described in terms of stacking sequences of certain building blocks, formed from the Si and $A\ell$ tetrahedra, such as six-membered double or single rings. These building blocks have been termed secondary building units (SBU) (20).

These SBU can combine in certain ways to form polyhedra such as cubes, hexagonal prisms and truncated octahedra in forming the zeolite framework. Figure 1(a) gives an illustration of some typical SBU and Figure 1(b) some of the polyhedra formed by linking the SBU together.

FIGURE 1(a): Some S B U involved in the zeolite structure.

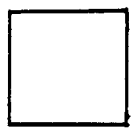

Single 4 ring

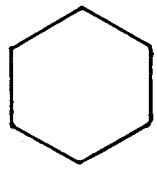

Single 6 ring

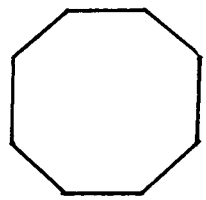

Single 8 ring

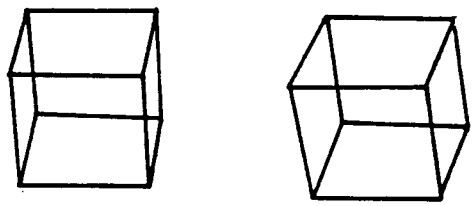

Double 4 ring

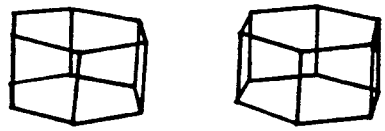

Double 6 ring

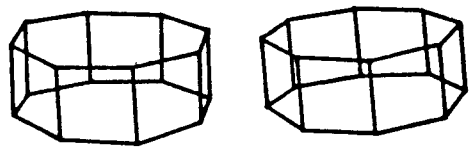

Double 8 ring

FIGURE 1(b): Some polyhedra formed by the linking together of the S B U.

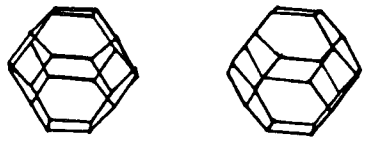

14 hedron of type I.

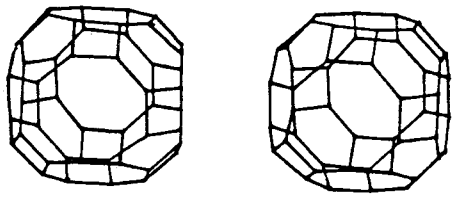

26 hedron of type I

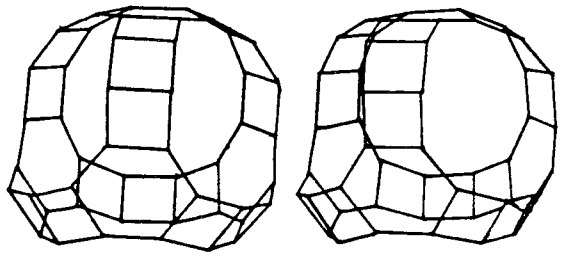

26 hedron of type II

A typical polyhedral building block found in zeolites is what is termed the sodalite unit, since it closely resembles the main structural unit found in the mineral sodalite. It contains 24 (Si,Aℓ) ions, interconnected with 36 oxygen anions. The oxygens form 6 octahedrally positioned rings containing 4 oxygen ions, and one set of cubically positioned or 2 sets of tetrahedrally positioned 6 element rings of oxygen ions (Figure 1(c)).

These sodalite units are arranged in different ways, so producing different zeolite structures. This can be readily illustrated by considering the synthetic A type zeolite and the synthetic faujasite type X zeolite. In the former, the sodalite units are symmetrically located at the corners of a cubic unit cell. The latter case has the sodalite units placed in tetrahedral co-ordination as in a diamond structure (12). Figure 1(d)(i and ii) illustrates this concept.

The zeolitic water is located within the cavities and channels in the framework structure. Nuclear Magnetic Resonance (NMR) (21), neutron diffraction (22), and X-ray studies have revealed three types of water molecules within the zeolite 13X dependent on its location and environment. Zeolite waters are commonly found clustered around the metal cations forming a hydration sphere (23), which is hydrogen bonded to the aluminosilicate framework. These hydrated spheres are located in the small channels and cavities (termed cages) as well as in the large cavities (termed supercages).

1.3 Classification and Nomenclature

The classification of zeolites is based on the aluminosilicate framework topology of the zeolites for which structures are known. The classification consists of seven groups. Within each group, the zeolites have a common subunit of

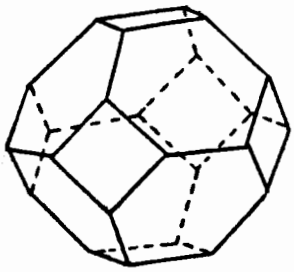

FIGURE 1(c) Sodalite Unit

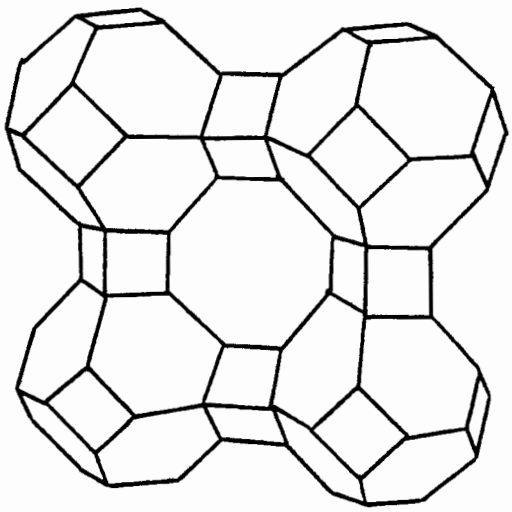

FIGURE 1(d) (i)
Linkage of sodalite units in forming Zeolite 4A

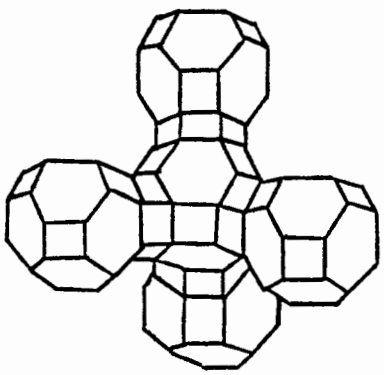

FIGURE 1(d) (ii)
Linkage of sodalite units in forming Zeolite X

structure which is a specific array of $(Si,Al)O_4$ tetrahedra. Each group is named after a representative member such as the "mordenite group", "natrolite group", etc (24).

Zeolite nomenclature has basically followed the rules of mineralogy, with the natural zeolites being designated this way.

The synthetic zeolites are referred to by single letters (where possible), assigned to them by the original investigators. These zeolites are then grouped under the group of natural zeolites which have a very similar structure. The synthetic zeolites type X and Y are members of the faujasite type of zeolites, having a structure very similar to the mineral faujasite.

The letters assigned to the zeolites designate them as synthesized, e.g. the zeolite A designates the synthetic zeolite $Na_{12}[(AlO_2)_{12}(SiO_2)_{12}].27H_2O$. Hence, the letters refer to the variation in compositions of the different zeolites (25).

When dealing with treated zeolites (e.g. ion exchanged,zeolites) the most suitable nomenclature is one which specifies the treatment applied to the starting material, e.g. dehydrated Ca-exchanged type Y zeolite, for brevity referred to as Ca-Y.

The IUPAC Committee on Zeolite Nomenclature (26) has recommended a format which gives analytical and structural information about the zeolite. An example of this is given below:

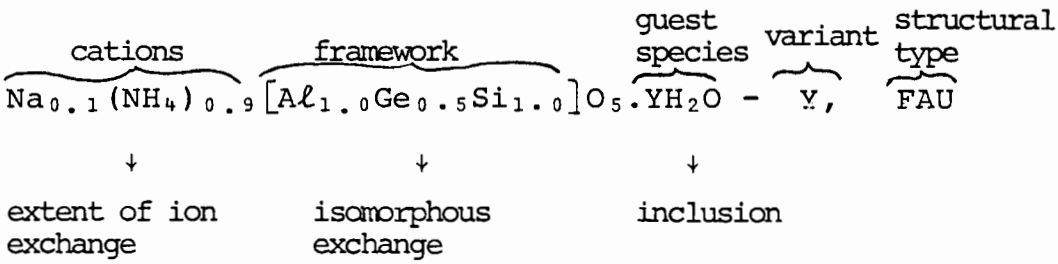

OR

$Na_{56}[Al_{56}Si_{136}]O_{384}.250H_2O$ - Y, FAU

which designates the synthetic zeolite Y.

1.4 Ion Exchange

Zeolites have long been known for their ion exchange properties. Their ability to readily exchange their framework cations for other cations in solutions or molten salts is a direct result of the open three-dimensional framework structure. The cations balancing the anionic framework charge are loosely attached to the aluminosilicate tetrahedra forming the framework, hence they are fairly mobile and can be readily exchanged.

The framework structures of the zeolites are quite rigid, and therefore most zeolites do not undergo any appreciable dimensional changes when subject to an ion exchange reaction. This means that the different zeolites, each with their own specific geometric parameters, which essentially remain unaltered, tend to be selective as to which ions are readily exchanged and which are not, setting up a type of "ion-sieve" effect. There are various factors governing the exchange behaviour of the zeolites, contributing to the "sieve" effect. They are the nature of the exchanging cation with respect to its charge and size, the temperature at which the exchange is carried out, the anion species associated with the cation in solution, the concentration of the cation species in solution (27) and the structure of the zeolite. Perhaps the most important factor affecting the exchange is the steric factor, dependent upon the size of the exchanging ion and the size of the zeolite cavity or channel. This is illustrated in Table 1(a) (28).

TABLE 1(a)

Zeolite	Minimum Channel Width	Exchange Cation	Non Exchangeable Cation
Analcime	2.6Å	Rb^+	Cs^+
Chabazite	3.7Å	Cs^+	$N(CH_3)_4^+$
Zeolite A	4.3Å	$NH(CH_3)_3^+$	$N(CH_3)_4^+$
Faujasite	∿ 9Å	$N(CH_3)_4^+$	$N(C_2H_5)_4^+$

A great deal of research has gone into ion exchange reactions involving zeolites (29,30,31,32) producing some remarkable results. Ion selectivity series for many zeolites have been set up. An example of this is the monovalent cation series for zeolite A, in the order of decreasing selectivity:

$$Ag > T\ell > Na > K > NH_4 > Rb > Li > Cs \quad (30)$$

For small ions such as Li^+ and Mg^{2+} the exchange does not occur very readily, due possibly to the high energy of hydration associated with these ions in solution.

Ion exchange in zeolites causes a dramatic alteration of the zeolite properties such as stability, adsorption behaviour and selectivity and catalytic activity. The effect of different ion exchanged forms on the electrical conductivity of the zeolites will be considered specifically in this work.

1.5 Adsorption

A normal hydrated zeolite contains between 5 and 30% water by weight, the water molecules being located mainly in the cavities and channels of the structure. On dehydration these water molecules are lost thus forming a crystalline solid permeated by a series of micropores and channels. When exposed to gases and vapours, these cavities within the

anhydrous zeolite fill rapidly with the molecular species concerned, making the dehydrated zeolite a highly selective adsorbent for gases, vapours and liquids.

The rigid framework structure of the zeolites remaining after dehydration maintains the dimensional characteristics of the specific zeolite. This means that on adsorption, the zeolites can imbibe those molecules which are small enough or of the right shapes to pass through their surfaces and enter the intracrystalline pores, but are unable to sorb those molecules having the wrong sizes or shapes. This has been illustrated by Babo (33) who showed that chabazite was able to sorb molecules such as methyl alcohol, CO_2 and methyl amine , but was unable to sorb the vapours of such compounds as pentane, benzene and ether. From these results, and those of other workers (34,35,36), the concept of molecular sieving developed whereby zeolites are used to separate mixtures of various chemicals due to their selective sorption. This has a particularly wide application in the petrochemical industry (37,38).

Sorption in zeolites is not confined to organic vapours and inert gases, but also includes sorption of inorganic materials such as mercury, sulphur and phosphorous (39). An interesting feature of zeolite sorption is their ability to sorb alkali metals from the vapour phase, particularly sodium metal (40). The adsorption of the sodium causes a colour change in the zeolites, attributed to the formation of Na_4^{3+} and Na_6^{5+} paramagnetic centres, particularly in the zeolites Y and X respectively (35). This adsorption characteristic is extensively used in this work to investigate the effect it has on the electrical conductivity of the zeolites.

The chemical composition of a zeolite has been found to greatly affect its adsorption capability. Ion exchanged forms of the zeolite can slightly alter the cavity and channel

dimensions within a zeolite and hence its selectivity for different materials can either be reduced or enhanced. Examples of this are revealed in chabazite where it was found that chabazite from different localities with different compositions showed a marked difference in adsorption character (41). Zeolite A has been shown to adsorb and hence separate n-paraffins from other hydrocarbons when in the Ca exchanged form.

Polar molecules are more selectively adsorbed by zeolites than are non polar molecules, since zeolites themselves are very polar.

It is obvious that the adsorption property of zeolites has great potential within the realm of the chemical industry, and has already, to a large extent, been usefully exploited.

1.6 Thermal Stability

Generally zeolites are thermally fairly stable compounds. There is, however, a limit to their stability, dependent on the pressure and environment under which they are heated.

When heated at elevated temperatures in air, the crystal structure of the zeolite ultimately breaks down, forming an amorphous solid and recrystallising to a non zeolite species.

Examples of this are illustrated below:

Zeolite A $\xrightarrow{800°C}$ β-Cristoballite

Zeolite X $\xrightarrow{1000°C}$ Carnegeite

Zeolite Y $\xrightarrow{1000°C}$ Glass

Table 1(b) (42) lists the stability of some zeolites in air.

TABLE 1(b)

Thermal stability of some zeolite forms in air.

Zeolite	Si/Aℓ	t(a)	t(b)
NaA	2	660	755
KA	2	800	825
CaA	2	540	830
NaX	2.5	660	770
KX	2.5	600	720
CaX		710	880
NaY	3.4	710	795
KY	3.4	780	810
CaY	3.5	780	890

t(a) = Temperature in °C at which structural degradation in first observed.

t(b) = Temperature in °C at which structure is 50% decomposed.

It is obvious from these few examples that the thermal stability of the zeolites generally increases with an increasing Si/Aℓ ratio. Hence, zeolite A is thermally less stable than zeolite X, which in turn is less stable than zeolite Y.

When heated in an atmosphere of water at 350°C, zeolite X was found to lose its structure. Zeolite A is sensitive to even small amounts of water vapour at 600°C. Zeolite Y retains its structure and crystallinity when subjected to water vapour at 410°C.

At very high pressures and temperatures the zeolites generally transform to denser aluminosilicates. This is illustrated in Table 1(c) which shows the transformation of zeolite Y to different products at various temperatures and pressures (42).

TABLE 1(c)

Some products of the transformation of Zeolite Y at high pressure

Temperature (°C)	Pressure (kilobars)	Product
300	15	zeolite P
400	10	analcime
400	25	jadeite
500	5	analcime
500	20	jadeite
600	25	jadeite
700	15	albite

1.7 Acid-base stability

The acid-base stability of zeolites is rather varied, although in general most zeolites are affected by strong acids and strong bases.

When aluminosilicates are treated with mineral acids, there may be exchange of their cations by hydronium ions or there may be hydrolysis of the Aℓ-O-Si bonds. Hydrolysis occurs very readily for most aluminous materials, resulting in a complete disintegration to colloidal silica and aluminium salts. As the silica content of the zeolites is increased, the formation of a silica gel and not colloidal silica becomes more favoured (43).

Most zeolites are also unstable to strong bases. This is revealed by the fact that although most zeolites are formed under basic conditions, prolonged exposure to the base results in conversion to another species. This is typified by zeolite A, which when exposed to dilute NaOH for prolonged periods of time, converts to zeolite P. In more concentrated solutions, it converts to the hydroxysodalite hydrate.

The general trend of zeolite stability towards acids and bases can be summarised as follows:

Zeolites with a high Si/Aℓ ratio tend to be more stable to acids and unstable to bases, while those with a low Si/Aℓ ratio (i.e. higher aluminium content) tend to be unstable to acids and more stable to bases.

C H A P T E R 2

THE STRUCTURE OF FAUJASITE-TYPE ZEOLITES.

The faujasite-type zeolites, specifically the synthetic type X and Y have the most open framework structure known so far in zeolites, with the void space accounting for about 50% by volume of the dehydrated crystal. It is this structural feature, among others, which contributes to the great importance enjoyed by the zeolites in the chemical industry.

The framework structures of the mineral faujasite and the synthetic zeolites X and Y are basically the same, hence their classification into the same group. The differences occurring in these zeolites are due to composition, and other physical properties brought about by the compositional differences. The compositional difference found in these zeolites is illustrated in Table 2.1 (44).

TABLE 2.1

The unit cell composition of some faujasite-type zeolites.

Zeolite	Composition of Unit Cell
Faujasite (natural)	$(Na_2,Ca,Mg)_{60}[(A\ell O_2)_{60}(SiO_2)_{132}].260H_2O$
Synthetic Zeolite X	$Na_{86}[(A\ell O_2)_{86}(SiO_2)_{106}].264H_2O$
Synthetic Zeolite Y	$Na_{56}[(A\ell O_2)_{56}(SiO_2)_{136}].264H_2O$

The polyhedral structural unit of these zeolites is a cub-octahedral aluminosilicate cage, also known as a truncated

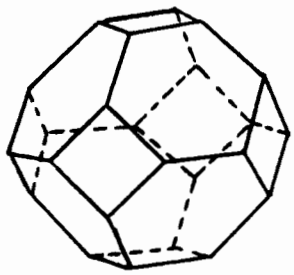

FIGURE 2.1 (a): Sodalite 14-Hedron or truncated octahedron forming a β-cage

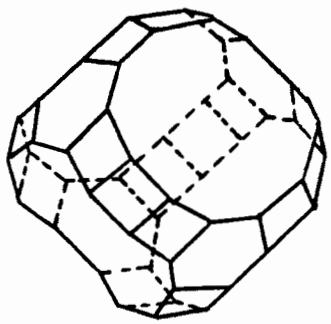

FIGURE 2.1 (b): Faujasite 26-Hedron of Type II forming a α-cage.

octahedron (Figure 2.1(a)), consisting of 24 (Si,Aℓ) atoms and 36 oxygen atoms. The space surrounded by such a truncated octahedron is referred to as the sodalite cage or the β-cage. These truncated octahedra are tetrahedrally arranged in the same way as the carbon atoms in the diamond structure. They are joined to each other by bridging oxygen atoms from the $(Si,A\ell)_6O_6$ faces of the octahedra, outlining a hexagonal prism or double six ring (D6R), one of the basic secondary building units of the structure. Only four of the eight six-rings in any one truncated octahedron are engaged in the bonding of these units to each other.

The large cages formed by this arrangement of cuboctahedra have a diameter of approximately 16.3Å, measured from the centres of two opposing oxygen ions. These cages, termed α- or supercages are interconnected tetrahedrally by holes outlined by near circular 12-membered $(Si,A\ell)_{12}O_{12}$ rings, which measure approximately 10Å from the centre to centre of two opposing oxygen ions (Figure 2.1(b)). Figure 2.2 clearly illustrates the framework structure obtained from the above described linkage. There are in total eight α-cages, eight β-cages and sixteen hexagonal prisms per unit cell.

This open framework structure can contain up to 260 water molecules per unit cell and, depending on the Si/Aℓ ratio, different amounts of exchangeable cations (Table 2.1) (45,46,47,48,49). The water molecules in the framework are distributed mainly in the large α-cages and the smaller β-cages.

There are essentially six possible cation sites within the faujasite zeolites that have been defined. The location of these sites is illustrated in Figure 2.3 (49,50).

The site S_I is a 16-fold site located at the centre of each D6R or hexagonal prism. Site S_I, is on the inside of the

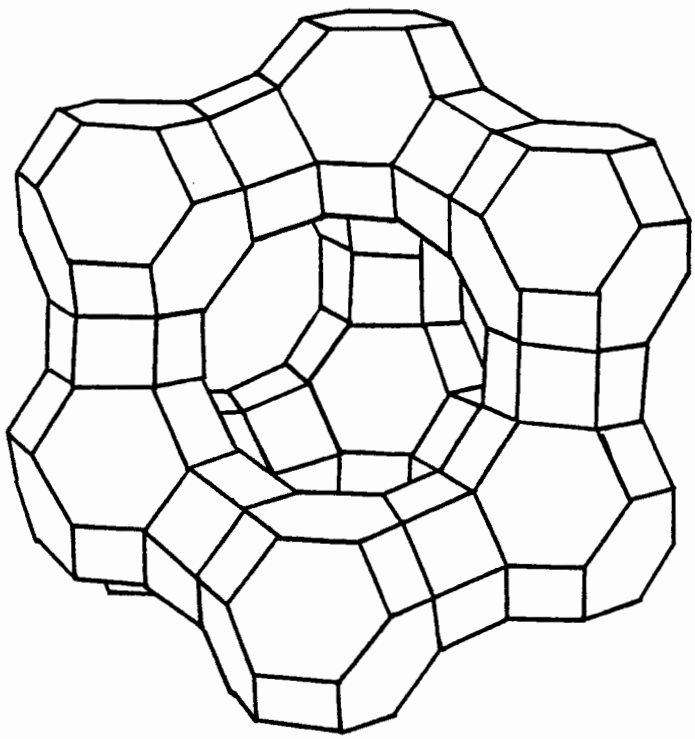

FIGURE 2.2: Framework structure of Zeolite X

FIGURE 2.3: Representations of the cation site positions in Zeolite X

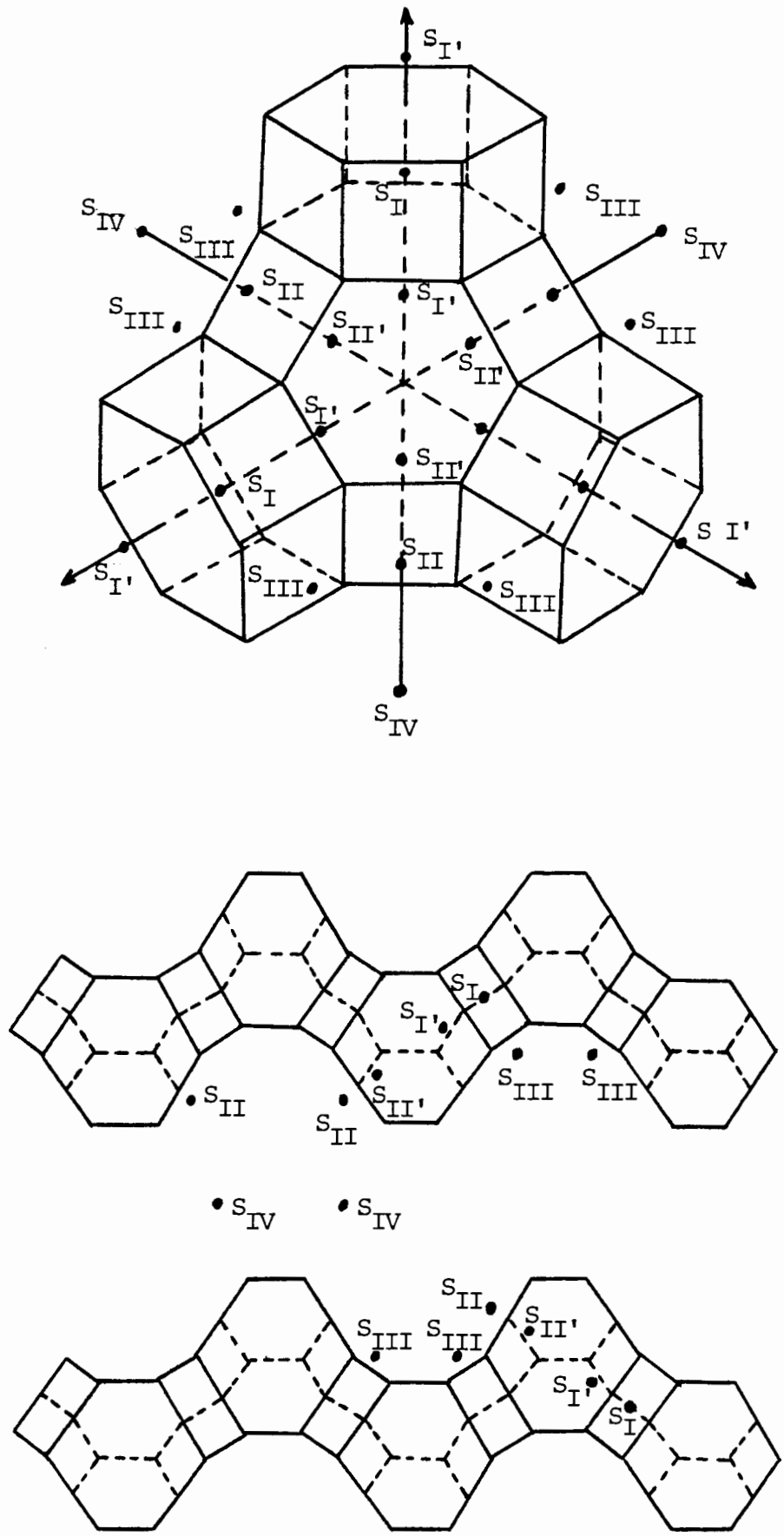

sodalite or β-cage next to the D6R. Site S_{II} is located outside the sodalite cage (i.e. inside the supercage) adjacent to the single six ring. Site $S_{II'}$ is inside the β-cage next to the S6R, opposite S_{II}. Site S_{III} refers to the positions in the wall of the large cavity in the large 12-ring aperture. Site S_{IV} is near the centre of the 12-membered ring between the supercages.

Site S_I is the only one permitting a cation to be enclosed by framework oxygens, since the cation is surrounded by six oxygens in an octahedral arrangement. This then is the only site in the dehydrated framework which provides full coordination of the cations by the framework oxygens. Sites $S_{I'}$, $S_{II'}$, and S_{II} permit only one-sided coordination to oxygens of the adjacent six rings. Hence site S_I is the generally preferred site, unless other considerations such as electrostatic repulsion or cation-molecule attraction become important.

A structural investigation by Baur (45) on the hydrated mineral faujasite of undetermined cationic composition, based upon the assumption of a total of 43 sodium and calcium ions per unit cell, has shown that 17 cations are located within the β-cages at the site now designated $S_{I'}$. These cations are in a tetrahedral arrangement with four water molecules. The remaining 26 cations were not definitely located, but could occupy sites next to the single six-rings inside the β-cages ($S_{II'}$).

Initial structural studies on hydrated zeolite NaX have assigned 48 of the 80 odd sodium ions to sites S_I and S_{II} (46). There is considerable evidence that the remaining cations are coordinated to water molecule oxygens in the crystal, and hence tend to behave as a strong electrolytic solution. This concept is supported by techniques such as infrared spectroscopy and electrical conductivity studies. The Infrared spectrum shows the stretch and deformation frequencies of normal water,

while the electrical conductivity studies have revealed that the cations in the hydrated zeolite behave in the same way as they do in normal salt solutions.

Later studies on hydrated zeolite X assigned cations to sites S_I, $S_{I'}$, and S_{II}. In the small pore system (β-cages and D6R) the sodium ions are distributed between sites S_I and $S_{I'}$. The total number of ions which can occupy sites in the small pore is sixteen. The unlocated cations in the zeolite unit cell are assumed to be coordinated to the water molecules and are statistically distributed on sites S_{III} and $S_{II'}$(51).

The occupation of different cation sites, together with the compositional variations in the zeolites having the same basic framework structure are among the features which distinguish the different zeolites within a particular group.

This can be illustrated by considering sodium-rich faujasite and NaX. In the faujasite, site S_I is not occupied by cations, while in NaX, site S_I is occupied by nine sodium ions. This is a direct result of the higher number of cations required in the X zeolite to maintain electrical neutrality (see Table 2.1).

Table 2.2 gives the probable locations of some cations in the different hydrated zeolites (49).

In hydrated zeolites, the water molecules form hydration complexes with the cations and interact electrostatically with the framework oxygens. For monovalent cations, these hydration complexes are weakly bonded, while with polyvalent cations, these complexes are more strongly bonded.

On dehydration, the cations in the zeolite must move from the positions where they are coordinated with the water molecules into the positions near the framework oxygens. This is illustrated by the fact that on dehydration of a potassium-

TABLE 2.2

The cation distribution of some zeolites (49)

	Faujasite			Zeolite X		Zeolite Y
	Site	Na^+	Ca^{2+}	Na^+	Ca^{2+}	Na^+
Deh.	$16S_I$	10	14.2	4	13.3	7.5
Hyd.		-	-	9	-	-
Deh.	$32S_{I'}$	9	2.6	32	5.0	19.5
Hyd.		14	9.7	8	13(0)	-
Deh.	$32S_{II'}$	-	-	-	6	-
Hyd.		15	11.5		26	-
Deh.	$32S_{II}$	32	11.4	32	25	30
Hyd.		11	23.4	24	27	-
Deh.	$48S_{III}$	-	-	4	-	
Hyd.		-	-	-	-	
Deh.	$16S_{IV}$	-	-	-	-	
Hyd.		-	-	32	-	

exchanged zeolite X (KX), there is an increase in the populations of sites S_I, $S_{I'}$, and S_{II} and a corresponding decrease in the number of cations on sites S_{III} (52,53).

For divalent ions, site S_I is generally the preferred site, especially for calcium and nickel ions. In zeolite X, Ca^{2+} and Sr^{2+} ions prefer sites S_I, $S_{I'}$, and S_{II}.

The change in positions of cations upon dehydration is also illustrated by the case in NiY. On dehydration, it was found that the Ni^{2+} ions moved into S_I (54). In dehydrated

zeolites, the unlocated cations probably lie close to the walls in the large cavities in many crystallographic equivalent sites and hence cannot be located by X-ray techniques.

The maximum occupancy of sites S_I and $S_{I'}$ is such that the sum of the number of cations on site S_I and half the number on site $S_{I'}$ should never exceed sixteen. Hence site S_I although providing the optimum coordination possibilities, is never filled due to the fact that neighbouring sites S_I and $S_{I'}$ (that is, sites on opposite sides of the same six ring) are never occupied simultaneously (52).

In hydrated zeolites the relative occupancy of the different ion exchange sites might be explained on the basis of a statistical distribution of the cations. In the dehydrated case, the absence of the water molecules with a high dielectric constant will most likely result in a less homogeneous charge distribution. Therefore, the exchangeable cations will be fixed preferentially on the sites with the highest charge density, or on the sites S_I where the most favourable co-ordination conditions are realised.

In most zeolites there are generally many more available cation sites than are exchangeable cations in the framework structure. This creates the possibility of ionic migration by the cations and hence leads to electrical conductivity of an ionic nature which is a characteristic of the zeolites.

C H A P T E R 3

IONIC CONDUCTIVITY.

3.1 General Theory

Electrical conductivity, generally speaking, occurs by the movement of charged particles such as cations, anions and electrons within a substance. In practically all cases the electrical conductivity σ can be written as the sum of the partial conductivities σ_i of the different types of charged particles i which contribute to the conductivity (55);

$$\sigma = \sum_i \sigma_i \qquad (3.1)$$

assuming that the motion of each particle is independent of that of the others.

The phenomenon of ionic conduction, generally constituted by the movement of ions in the sample, either liquid or solid, is well known. Interest in the ionic conduction of solids has greatly increased, particularly since the use of solid electrolytes in solid state battery systems has become important.

Perhaps the most typical example of ionic conduction in solids is illustrated by the ionic conduction occurring in the alkali halides, such as NaCℓ where the ionic conduction can be satisfactorily explained in terms of lattice defects and the laws of thermodynamics.

The most common types of defects in solid lattices are illustrated in Figure 3.1. These are:

(a) the location of an interstitial ion in the lattice with a corresponding vacancy site. This situation

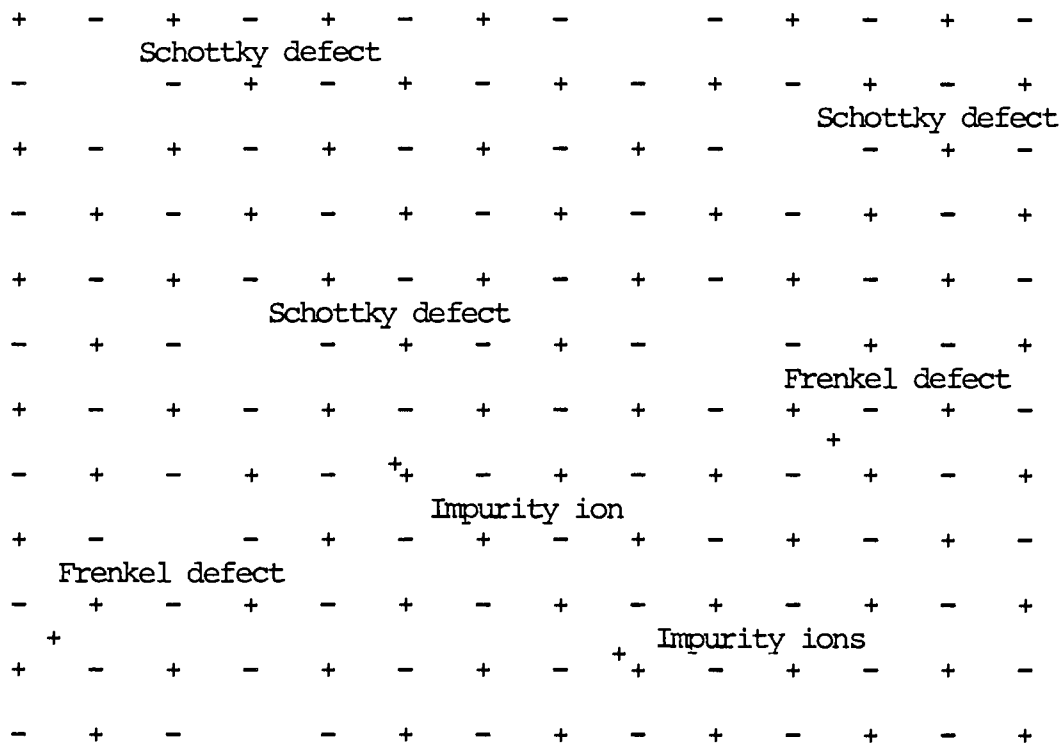

FIGURE 3.1: Illustration of the common types of defects found in a solid crystal lattice.

arises when a cation in the lattice moves from its normal lattice site into an interstitial site, leaving a vacant site. Both the interstitial and the vacancy are then able to migrate through the lattice. Defects of this type are known as Frenkel defects.

(b) the occurrence of charged vacancies in the lattice. The vacancies are due to an absence of ions in a normal lattice, i.e. the vacancies are essentially missing ions compared to the ideal lattice. Such defects are termed Schottky defects.

(c) the presence of foreign ions (in the form of impurities) which may be on interstitial sites or substituted for those which are normally on the lattice.

These defects behave as mobile "charged particles" and generally cause the partial ionic conductivity found in solids such as the alkali halides.

Another lattice disorder very favourable to a high ionic conduction is one in which at high temperatures there is a larger number of lattice sites present than are ions in the lattice. In this situation a small disorder energy is sufficient to change the ordered state of the ions to a statistical distribution over many lattice sites. There are four possible types of ionic movement within such a system. These are the movement of ions:

(i) from normal occupied sites to adjacent empty normal sites,

(ii) from normal occupied sites to adjacent empty interstitial sites,

(iii) from occupied interstitial sites to adjacent empty interstitial sites,

(iv) from occupied interstitial sites to adjacent empty normal sites.

An example of a material in which such movement of ions can take place is β-alumina. Such a disorder seems to be very important in many good solid electrolyte systems.

For a solid of the form MX to possess a high ionic conductivity the species M must have available sites of identical or slightly higher energy largely in excess of the number of M particles present. Only a small energy difference between the ordered and disordered distribution of the mobile M ions over the sites must exist, with the migration energy between these sites being of the order of thermal energy.

One of the characteristic features of the ionic conductivity of a solid salt is its variation with temperature. An extensive series of measurements on ionic conductors by Lehfeldt (56) showed that the logarithm of the conductivity σ is roughly a linear function of the inverse temperature. This variation of σ with T^{-1} can be given as $Ae^{-E/kT}$, thus suggesting that the fundamental process is thermally activated (57).

For simple ionic conductors in which current is carried by only one ionic species, the conductivity σ is related to the concentration of charge carriers by the equation: (58)

$$\sigma = Nze\mu \quad . \quad . \quad . \quad . \quad . \quad . \quad . \quad . \quad . \quad . \quad . \quad (3.2)$$

where N is the number of mobile ions per unit volume and μ is the mobility of these ions. Ze is the charge of the ions.

The mobility μ of the mobile ions can be expressed as (59):

$$\mu T = e^{-\Delta G_m/RT} \quad . \quad . \quad . \quad . \quad . \quad . \quad . \quad . \quad . \quad (3.3)$$

ΔG_m is the free energy for the movement of the mobile ions through the lattice.

$A = Ca^2 e\nu/k$ where

ν = frequency of the vibration of the species in the potential well,

a = the distance between adjacent potential wells in a conduction path,

c = a factor which accounts for the change in ΔHm with T.

Using the laws of thermodynamics and the Boltzmann distribution, the ionic conductivity can be expressed as: (58)

$$\sigma = (\sigma_o/T)\, e^{-Ea/kT} \quad . \quad . \quad . \quad . \quad . \quad . \quad . \quad . \quad (3.4)$$

where Ea is the activation energy for conduction or ionic motion and σ_o is defined by equation 3.5

$$\sigma_o = e^2 f a^2 \alpha \nu N/6k \quad . \quad . \quad . \quad . \quad . \quad . \quad . \quad . \quad (3.5)$$

where

e = charge of the carrier

k = Boltzmann's constant

f = correlation factor which differs from unity only if consecutive jumps are not independent of the motions of other carriers,

a = distance between jumps,

α = fraction of mobile charge carriers. For totally random motion of charge carriers $\alpha = 1$,

ν = average jump frequency,

N = concentration of charge carriers.

A graphical representation of log σT vs T^{-1} (using Eq. 3.4) will yield the activation energy for the conduction process from the slope.

There exists a close relation between the electrical mobility of a particle and its self-diffusion coefficient, given by the Nernst-Einstein relation (57).

$$\sigma = DNq^2/kT \quad . \quad . \quad . \quad . \quad . \quad . \quad . \quad . \quad . \quad . \quad . \quad (3.6)$$

where q is the charge of the ions and D the diffusion coefficient. The other symbols having their normal interpretation.

The self-diffusion coefficient D for ions in a lattice, assuming the diffusion is unidirectional can be expressed by:

$$D = \lambda^2 kT/h \; e^{\Delta S/R} \; e^{-\Delta H/T} \quad . \quad . \quad . \quad . \quad . \quad . \quad (3.7)$$

where λ is the distance between cation sites, the other symbols having their normal interpretation (60).

Combining equations 3.6 and 3.7 yields for the ionic conductivity:

$$\sigma = (N\lambda^2 q^2/h) e^{-\Delta G/RT} \quad . \quad . \quad . \quad . \quad . \quad . \quad (3.8)$$

Equation 3.8 may be used to determine the free energy ΔG for the conduction process, provided N and λ are known for the conducting species. The entropy ΔS and enthalpy ΔH may also be determined from equation 3.8 since

$$\Delta G = \Delta H - T\Delta S \quad . \quad . \quad . \quad . \quad . \quad . \quad . \quad . \quad . \quad . \quad (3.9)$$

3.2 Ionic Conduction in Zeolites

Zeolites, with their loosely bound cations in the anionic framework structure, have available many more lattice sites than are occupied by the cations in the structure. This type of lattice disorder would lead one to expect a good ionic conductivity in the zeolites, especially in cases where the site energies are of comparable magnitude.

It has been shown that the electrical conductivity in zeolites is ionic (61), and occurs by the migration of cations accompanied by an actual mass transfer (11). This

immediately rules out ionic conduction by means of lattice defects such as cation vacancies or negative holes as found in the alkali halides.

The activation energy obtained from the Arrhenius plot, $\log \sigma T$ vs T^{-1} (Equation 3.4), represents the potential energy barrier the cation in the zeolite has to overcome in self diffusion. The presence of an adsorbed species in the zeolite structure has been shown to affect the ionic conductivity in the synthetic zeolite types A and X (62). In most cases, the adsorbed species is associated with the cations, thus decreasing the potential barrier and hence increasing the ionic conductivity.

Water and ammonia adsorption increases the ionic conductivity in both zeolites A and X (62). This is ascribed to the association of the cations with the water or ammonia molecules, thus increasing their mobility in an applied electric field. Adsorption of organic molecules has been found to either increase or decrease the ionic conductivity, dependent on the type and size of the molecule. The cations are associated to these molecules by cation-dipole interactions. The mobility of the cation is then linked to the mobility of the adsorbed organic species. A number of organic molecules are sterically hindered by their size from easy movement and hence the ionic conductivity is retarded with respect to the dehydrated zeolite. Acetonitrile has been found to increase the conductivity, while 2,2 dimethyl= butane and triethylbutane reduce the conductivity (62).

Oxygen and nitrogen adsorption by zeolite X has been found to increase the ionic conductivities of this zeolite. This is once again ascribed to the association of these molecules with the ions in the zeolite lattice. The effect of the adsorption of oxygen and nitrogen on the conductivity of zeolite X at -78°C is illustrated in Table 3.1 (62).

TABLE 3.1

Effect of adsorption of oxygen and nitrogen on zeolite X at -78°C.

Adsorbate	Molecules adsorbed per unit cell	Conductivity ($\Omega^{-1}cm^{-1}$)
None	-	5.0×10^{-10}
O_2	25	8.9×10^{-10}
N_2	25	1.39×10^{-9}

The relative increase in the conductivity of a zeolite on adsorption of a species will be determined by the strength of the cation-adsorbate interaction.

The electrical conductivity of the zeolites, particularly the zeolites X and Y, is likely to be increased by the adsorption of sodium metal. On adsorption of the sodium metal, Na_6^{5+} and Na_4^{3+} paramagnetic centres are formed in the respective zeolites (35,40). The Na_6^{5+} centres formed in the zeolite X consist of six equivalent sodium ions sharing an electron trapped in the large cavities. Each large cavity is surrounded by six sites, S_{III}, arranged octahedrally in the directions of the four-fold cubic axes, as well as four sites, S_{II}, arranged tetrahedrally in the direction of the three-fold cubic axis. The Na_6^{5+} centre is a result of an electron being trapped or shared among the six Na^+ on the sites S_{III}. The sites S_{II} of the cavity are then necessarily empty. The association of the cations forming the Na_6^{5+} centres, coupled with the available empty sites S_{II} could then facilitate the migration of the charged centres in the zeolite and hence improve the conductivity of the sodium metal adsorbed zeolite provided the various site energies are of comparable magnitude.

C H A P T E R 4

ZEOLITE SYNTHESES BY CRYSTALLIZATION; ION EXCHANGE AND ADSORPTION AND THE CHARACTERIZATION OF THESE ZEOLITES.

4.1 Introduction

Zeolites are formed under hydrothermal conditions and crystallize from aqueous systems containing the necessary chemical components.

A wide variety of zeolites have been synthesized, including new synthetic types with no natural counterpart, and synthetic zeolites related to naturally occurring mineral zeolites. The type of zeolite synthesized depends on a range of factors, such as the temperature at which crystallization is carried out, the nature and type of starting materials and the crystallization time period (63). Most synthetic zeolites are produced under non-equilibrium conditions and are considered in a thermodynamic sense as metastable phases.

Perhaps the most common method of synthesizing zeolites involves the crystallization of the zeolite species from aluminosilicate gels of the alkali metals. It involves the reaction of a freshly prepared aqueous aluminosilicate gel with an alkali metal hydroxide at an elevated temperature (generally in the range 250 - 400°C), in an autoclave for a period of time. Depending on the zeolite species being produced, the time could range from a period of a few hours to a few days. Examples of the zeolites produced in this way include a synthetic analogue of the mineral bikitaite using lithium hydroxide (64) and mordenite using sodium hydroxide (65).

A number of synthetic zeolites have been synthesized at lower temperatures utilising the same technique discussed above. Among these types of zeolites are the synthetic faujasite zeolites X and Y, which crystallize in the temperature range of 20 - 120°C and 20 - 175°C respectively, both forming from the sodium hydroxide basic system.

Alkaline earth zeolites can also be synthesized in a very similar manner. The basic principle involved is the use of an alkali earth metal hydroxide instead of the alkali metal hydroxide. Typical examples of this are the synthesis of a calcium zeolite, formed at 250°C, related to the mineral epistlebite, and another related to mordenite which is formed at 390°C (66).

A novel method for producing zeolites, particularly the types A and X from the alkali metal-aluminosilicate gel systems, is that reported by Charnell (67). Instead of an alkali metal hydroxide an organic base is used, and the crystallization is carried out in the temperature range 75 - 90°C, without the use of an autoclave.

Other methods of zeolite crystallization include the use of quaternary ammonium ions instead of alkali metals. Zeolites formed in this manner include the zeolite termed N-X (described as the nitrogenous form of zeolite X) and zeolite N-Y (66).

Synthetic zeolites can crystallize from reactive amorphous substrates other than aluminosilicate gels. The most common process involves the use of minerals of the kaolin group. The kaolin is converted to the metakaolin phase by thermal treatment at 600°C. The amorphous metakaolin is then reacted with aqueous sodium hydroxide at about 100°C.

The zeolite so formed depends on the composition of the reaction mixture e.g. if only NaOH is used, zeolite type A is formed (68).

Once crystallized, different forms of a zeolite can be synthesized by means of ion exchange reactions.

The ion exchange process in a zeolite in solution can be represented by the following equation (69):

$$Z_A B^{Z_B^+}_{(Z)} + Z_B A^{Z_A^+}_{(S)} \rightleftharpoons Z_A B^{Z_B^+}_{(S)} + Z_B A^{Z_A^+}_{(Z)} \qquad (4.1)$$

where Z_A and Z_B are the charges of the cations A and B respectively, and the subscripts (S) and (Z) refer to the solution and the zeolite respectively. The separation factor α_B^A is defined by equation 4.2 and indicates the preference of the zeolite for one of two ions (69).

$$\alpha_B^A = (A_Z B_S / B_Z A_S) \quad . \quad . \quad . \quad . \quad . \quad . \quad . \quad . \quad . \quad (4.2)$$

$\alpha_A^B > 1$ indicates a preference of the zeolite for ion B.

The equivalent fractions of the exchanging cation in the solution and the zeolite are defined by the quantities A_S and A_Z, respectively. These fractions are given in equations 4.3 and 4.4

$$A_S = Z_A M_S^A \; / \; Z_A M_S^A + Z_B M_S^B \quad . \quad . \quad . \quad . \quad . \quad . \quad (4.3)$$

$$A_Z = Z_A M_Z^A \; / \; Z_A M_Z^A + Z_B M_Z^B \quad . \quad . \quad . \quad . \quad . \quad . \quad (4.4)$$

M_S^A and M_S^B are the molalities of the cations A and B in the solution. M_Z^A and M_Z^B are similarly defined for the zeolite phase.

There are various factors affecting the ion exchange capacity of a zeolite, such as the structural characteristics of the zeolite, the cation species, etc (see Chapter 1),

leading to the ion selectivity series for the different zeolites. The ion selectivity series essentially indicates the preference exercised by the zeolite in exchanging a particular ion. This is neatly illustrated in Figure 4.1 which shows the possible selectivity curves of a zeolite for a cation (69). Ultimately, the exchange capacity depends on the chemical composition of the zeolite; a lower Si/Aℓ ratio favouring a higher exchange capacity.

A very thorough investigation of ion exchange reactions in the synthetic faujasites X and Y has been carried out by Barrer and Rees (70,71) and Sherry (72,73). Essentially what they have shown is that alkali metals with large cation radii such as Cs^+ and Rb^+ cannot completely exchange with all the Na^+ ions in NaX and NaY. This is probably due to the fact that the sodium ions which could not be replaced by these cations are located in the small cavities of the zeolite, and the exchangeable cations are located in the large cavities or supercages.

An important feature for ion exchange is that in order for an entering ion to replace the Na^+ ions in the sodalite cages or hexagonal prisms, it must diffuse through the ring of 6 tetrahedra which is the window between the supercage and the sodalite cage. In this respect it has been found that Ag^+ and K^+ ions are the largest univalent metal ions that can completely exchange or replace all the Na^+ ions in zeolite X (72).

A great number of ion exchange syntheses of zeolite X have been reported, including exchange of univalent cations such as K^+, Li^+, Cs^+, Rb^+, Ag^+ and $T\ell^+$ (72). Information regarding the cation site selectivity, the type of ingoing ion and the degrees to which complete exchange is achieved has been obtained.

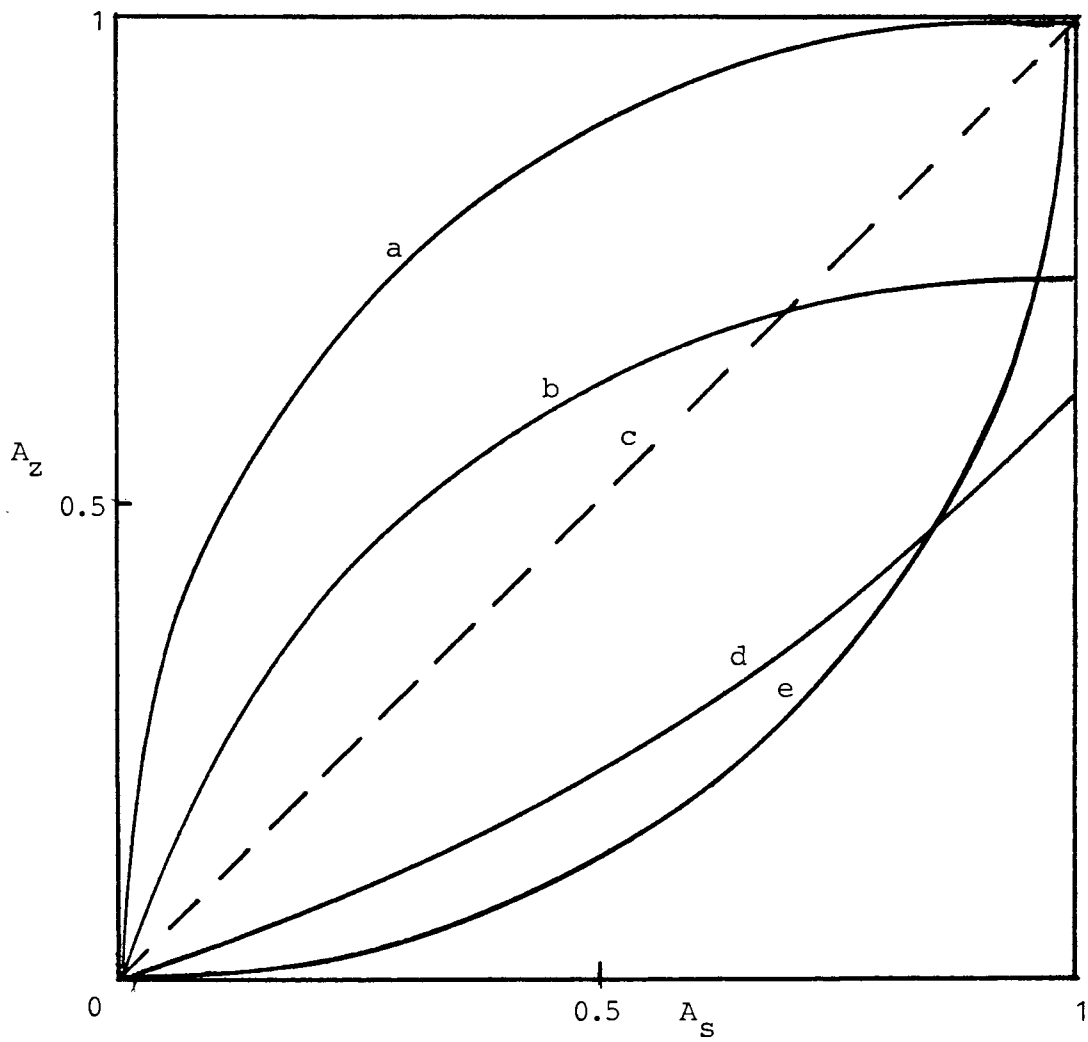

FIGURE 4.1: Probable Selectivity Curves of a Zeolite for a Cation.

(a) $\alpha_B^A > 1$ ion A is selectively sorbed into the zeolite

(b) $\alpha_B^A > 1$ ion A is selectively sorbed until $\alpha_B^A < 1$ then ion B is selectively sorbed. Ion A never fully exchanges with ion B in the zeolite.

(c) $\alpha_B^A = 1$ There is no selectivity for either ion.

(d) $\alpha_B^A < 1$ Ion B is selectively sorbed.

(e) $\alpha_B^A < 1$ Ion B is selectively sorbed. Ion A never fully replaces ion B in the zeolite.

Alkaline earth ion exchange reactions involving mainly the Ca^{2+}, Ba^{2+} and Sr^{2+} ions have been reported (73). For most zeolites it has been found that there is an increasing selectivity for the alkaline earth cations with an increase in reaction temperature.

Rare earth ion-exchange, particularly with La and Ce on zeolite X has been reported (74,75). Ion exchange reactions involving transition metals, particularly the Cu^{2+}, Co^{2+}, Zn^{2+} and Ni^{2+} ions, and also Mg^{2+} ions, have been successfully carried out (76,77).

Exchanges involving organic cations such as the ammonium ion, or some alkyl ammonium ion derivatives have been performed. The success of these reactions was varied, due mainly to the steric factor of the zeolites - the ingoing cations are generally too large for complete exchange to be achieved (78).

Ion exchange in zeolites involving a great variety of the more common ions can be readily achieved with the effects of ion sieving and ion selectivity being important considerations in those reactions. Ion sieving effects are observed with the zeolites having the smallest pore openings and the largest exchanging cations.

Ions successfully entering the pores may differ in their rates of exchange owing to differences in the activation energy required to exchange solvent molecules.

Every zeolite species possesses a different and characteristic pattern of ion exchange selectivity in that certain cationic species, if present, will be preferred or exchanged more readily than certain other species.

The quality of ion exchange separation which may be achieved can be affected by a number of variables such as pH, tempera-

ture, competing cations, choice of solvent, presence of complexing agents, solution strength and types of anions present.

Zeolites can further be synthesized in a different form by adsorption of, or impregnation by different chemical species thus producing a zeolite of high catalytic activity. Often adsorption is used as a technique to obtain a metal dispersed within a zeolite.

An example of this is the adsorption from the vapour phase of an alkali metal, mostly sodium. Rabo *et al* (35) exposed both zeolites NaX and NaY to sodium vapour, observing a dramatic colour change in both species on the adsorption of the sodium. The zeolite X turned dark blue, while the zeolite Y went bright red. This colour was attributed to the formation of Na_6^{5+} and Na_4^{3+} paramagnetic centres in the respective zeolites. Barrer *et al* (40) studied the interaction of sodium vapour on synthetic sodalite and found very similar results, the sodalite changing in colour from bright blue through to black as more sodium was adsorbed. The colours were again attributed to the formation of paramagnetic centres of the Na_4^{3+} type. It was obvious that the sodium being adsorbed was interacting with some of the ions already present in the structure creating these paramagnetic centres.

This initial work lead investigators to consider the effect of an adsorbed phase on the metal ions already in a zeolite structure. Hydrogen was used in many instances as the adsorbent and was found to reduce the metal ions in the zeolite, thus creating a situation in which the metal atoms are finely dispersed within the zeolite matrix. Examples of this are the reduction of Ag^+ ions in zeolite X (79) and the reduction of Pd^{2+} ions in zeolite Y (80). The adsorption of hydrogen and the subsequent reduction of Cu^{2+} and Ni^{2+} has also been reported (35).

The means of synthesizing a metal "loaded" zeolite by means of adsorption reactions creates a situation in which the electrical conductivity of the standard zeolite can be either increased or retarded.

4.2 Characterization Techniques

The characterization of the zeolites synthesized in this study involved using techniques such as XRD, EDAX, and TGA, the basic principles of which are outlined below.

4.2.1. X-Ray Powder Diffraction (XRD)

4.2.1.(a) Bragg's Law: Consider a set of parallel equidistant lattice planes, a distance d apart. When a beam of X-Rays of wavelength λ is incident on these planes at an angle θ, constructive interference of the radiation reflected from successive planes occurs whenever equation 4.5 is satisfied.

$$2d\sin\theta = n\lambda \quad . \; . \; . \; . \; . \; . \; . \; . \quad (4.5)$$

where n is an integer indicating the order of the diffracted beam. Equation 4.5 is known as the Bragg Law, and the angle θ as the Bragg angle.

For any cubic crystal, the spacing of the planes with Miller indices (h,k,ℓ) is given by:

$$d^2 = a^2 / (h^2+k^2+\ell^2) \quad . \; . \; . \; . \; . \quad (4.6)$$

where a is the lattice dimension.

Combining equations 4.5 and 4.6 yields equation 4.7 which gives the condition for coherent diffraction from a cubic material.

$$\sin^2 \theta = (\lambda^2 / 4a^2)(h^2+k^2+\ell^2) \quad . \quad . \quad . \quad (4.7)$$

Equation 4.7 relates the angle of diffraction to the Miller indices of the reflecting planes of the crystal.

4.2.1.(b) Bragg's Law and X-Ray Powder Diffraction

The application of Bragg's Law to X-ray powder diffraction involves the use of monochromatic X-rays, such as the CuKα rays. These rays are allowed to fall on the powdered sample which is rotated through the various diffraction angles. A detector, which picks up the diffracted rays is also rotated through the various diffraction angles. The diffraction intensity is determined as a function of the Bragg angle θ.

The powdered sample contains crystallites orientated randomly at all possible angles. Hence, there will always be some of the crystal faces at the appropriate angles for diffraction at each value θ which satisfies the Bragg equation. For each angle satisfying Bragg's equation, a diffraction line is picked up by the detector and recorded electronically by the deflection of a pen on a recorder. The recorder is calibrated to run in conjunction with the rate of rotation of the sample through the Bragg angles, so that the peaks are translated directly on to the recorder at the angles at which diffraction occurs. A typical diffraction pattern of zeolite NaX is given in Figure 4.2. A full theoretical treatment is given in many texts, for example, the Brown and Forsyth book on crystal structure (81). X-ray diffraction analyses were carried out on a Philips Powder Diffractometer at 40 kV and 20 mA, using a Cu Kα tube. The scan rate was 1°/minute.

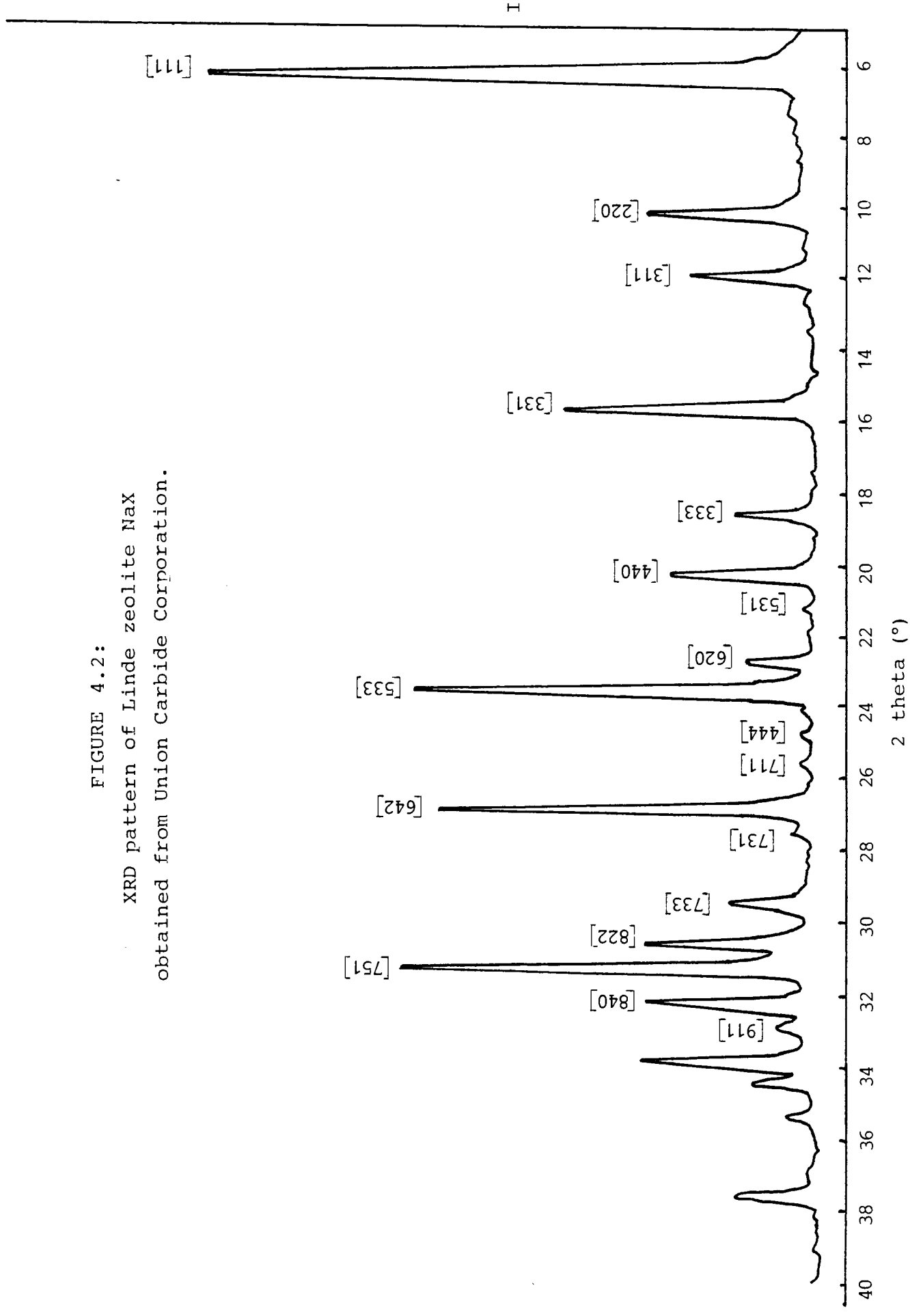

FIGURE 4.2:
XRD pattern of Linde zeolite NaX
obtained from Union Carbide Corporation.

4.2.2. Chemical Analysis by EDAX (82).

The Energy Dispersive Analysis of X-rays (EDAX) is a useful technique whereby both qualitative and quantitative chemical analyses of the elements in a sample can be done. This is, however, only effective for elements with an atomic mass greater than 20.

When an electron beam, commonly generated by a scanning electron microscope strikes a sample, it produces a series of discrete X-ray spectral lines which are then detected by a semi-conductor X-ray detector composed of Si or Ge. These lines are electronically amplified and further analyzed by computer techniques. Each element has its own characteristic X-ray emission lines, hence the elements present in the sample can be qualitatively identified. The intensity of the X-rays emitted gives an indication of the quantity of the particular element present, in the form of weight percent of that element.

Characteristic X-rays of an element are emitted when an electron beam striking a sample has sufficient energy to exceed the excitation potential E_c of the electrons in that element. An electron is then ejected from its parent atom leaving an orbital vacancy behind. The atom is now in an excited state, and any orbital vacancies can be filled quickly by electronic relaxation accompanied by the simultaneous emission of an X-ray photon with a discrete energy corresponding to the difference between the two orbital energy levels.

4.2.3. Thermogravimetric Analysis (TGA) (83,84)

Thermogravimetry may be defined as a technique whereby the weight loss or weight gain of a substance in an environment heated or cooled at a controlled rate, is recorded as a function of temperature. The two basic requirements are therefore a method of heating (or cooling) and a means of accurate weighing.

The basic instrumentation required for a thermogravimetric analysis are a precision balance, a furnace capable of being programmed for a linear rise of temperature with time and a recorder. The recorder should be capable of recording both temperature and weight continuously.

The results are presented as a plot of weight loss or gain of a sample vs. the temperature, producing a thermogravimetric curve as illustrated in Figure 4.3.

Thermogravimetric analysis is a useful technique in characterising the different zeolites synthesized by means of recording the amount of water present in each species of ion-exchanged zeolite. Since the cations are all of differing sizes, the volume of water present in each will vary from the standard zeolite NaX used as the starting material for each synthesis, and hence the extent of the success of the synthesis can be monitored. A Stanton Redcroft TG-750 was used to characterise the zeolites synthesized for this report.

FIGURE 4.3: Thermogravimetric Analysis of Zeolite NaX.

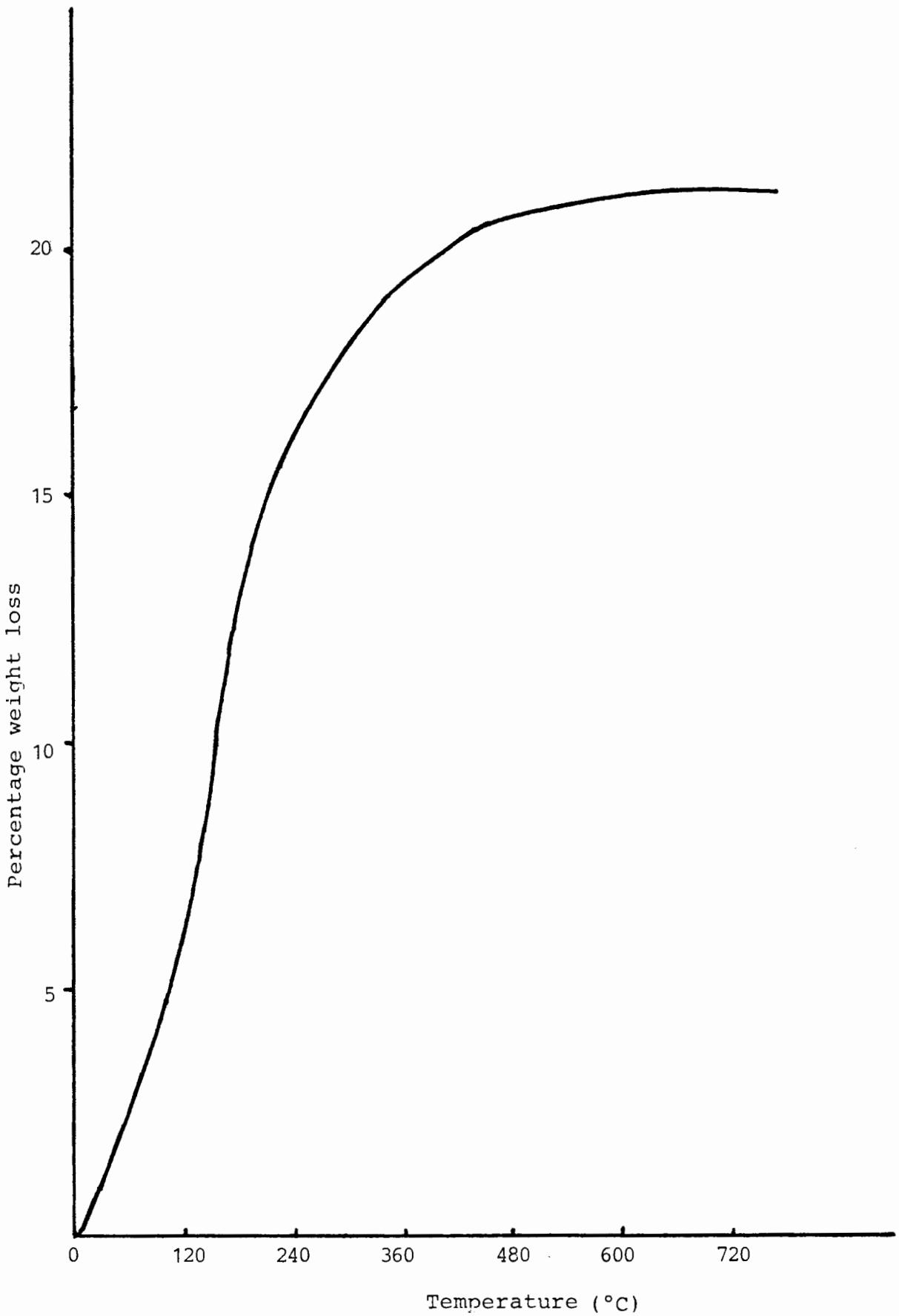

4.3 Experimental - Zeolite Syntheses.

All chemicals used were reagent grade and were obtained from Merck, unless otherwise stated. Distilled water was used as a solvent and all glassware was thoroughly cleaned before use. Dehydration, where necessary, was performed under vacuum, using a glass vacuum line and a Balzers turbo-molecular high vacuum pump. Manipulations involving air-sensitive compounds such as sodium, were performed in a dry box under an inert atmosphere such as argon or nitrogen.

All the zeolites were characterized by X-ray powder diffraction, energy dispersive analysis of X-rays and by thermogravimetric analysis.

Zeolite type NaX was synthesized as described below. Ion exchange and sodium adsorption reactions were done on the Linde zeolite NaX obtained from the Union Carbide Corporation.

4.3.1. Crystallization of Zeolite Type NaX in Reaction Mixtures containing Sodium Aluminate, Sodium Silicate and an Organic Base (67).

The sodium silicate and sodium aluminate used were obtained from Fischer Chemicals (Pty) Ltd, and the organic base triethanolamine was supplied by PAL Chemicals.

100 g of sodium silicate ($Na_2SiO_3.9H_2O$) and 40 g of sodium aluminate ($NaA\ell O_2$) were weighed into separate clean polypropylene beakers. Both the silicate and aluminate were then each dissolved separately in 700 mℓ of distilled water and 100 mℓ of triethanolamine (2,2'-2"-nitrilotriethanol). These solutions were then filtered through Whatman No 542 filter paper using a Buchner funnel. The filtration process was repeated 3 or 4 times to ensure complete removal of any undissolved impurities in the system.

The aluminate solution was slowly stirred into the silicate solution producing a white gel. The beaker containing the gel was covered with a clean polypropylene sheet and placed in a thermostatically controlled waterbath at a temperature in the range of 75 - 95°C until crystallization was complete, usually in a period of about 15-20 days. As the crystallization process progressed, the gel volume diminished until a layer of approximately 1 cm thickness of crystals covered the container bottom.

The crystals were filtered from the mother liquor using Whatman No 1 filter paper and a Buchner funnel and then thoroughly washed with distilled water followed by a rinse with ethanol. The crystals were dried in air at room temperature after which they were characterized.

The optimum temperature for producing reasonable quality crystals was found to be 90°C, with a corresponding crystallization period of 14 days. The zeolite produced under these conditions measured between 15 and 35 microns in diameter. The yield of crystals was in the range of 38 to 40 g for a particular crystallization. The pH of the reaction mixture was 14.

It was found that at a lower temperature, the crystallization time was prolonged, and more impurities such as the zeolite P and some unreacted amorphous starting materials were present in the final crystallized product. This is a direct consequence of the prolonged exposure to a strong base, since zeolite NaX tends to transform to other aluminosilicate species when in contact with the base for a longer period of time. Table 4.1 illustrates some of the reaction conditions and products obtained. The X-ray powder diffraction pattern of the synthesized zeolite NaX is illustrated in Figure 4.4 and the thermogravimetric data is illustrated in Figure 4.3. A chemical analysis is presented in Table 4.2.

FIGURE 4.4: X-ray diffraction pattern of Zeolite 13X synthesized (a) with reference to Linde Zeolite 13X (b).

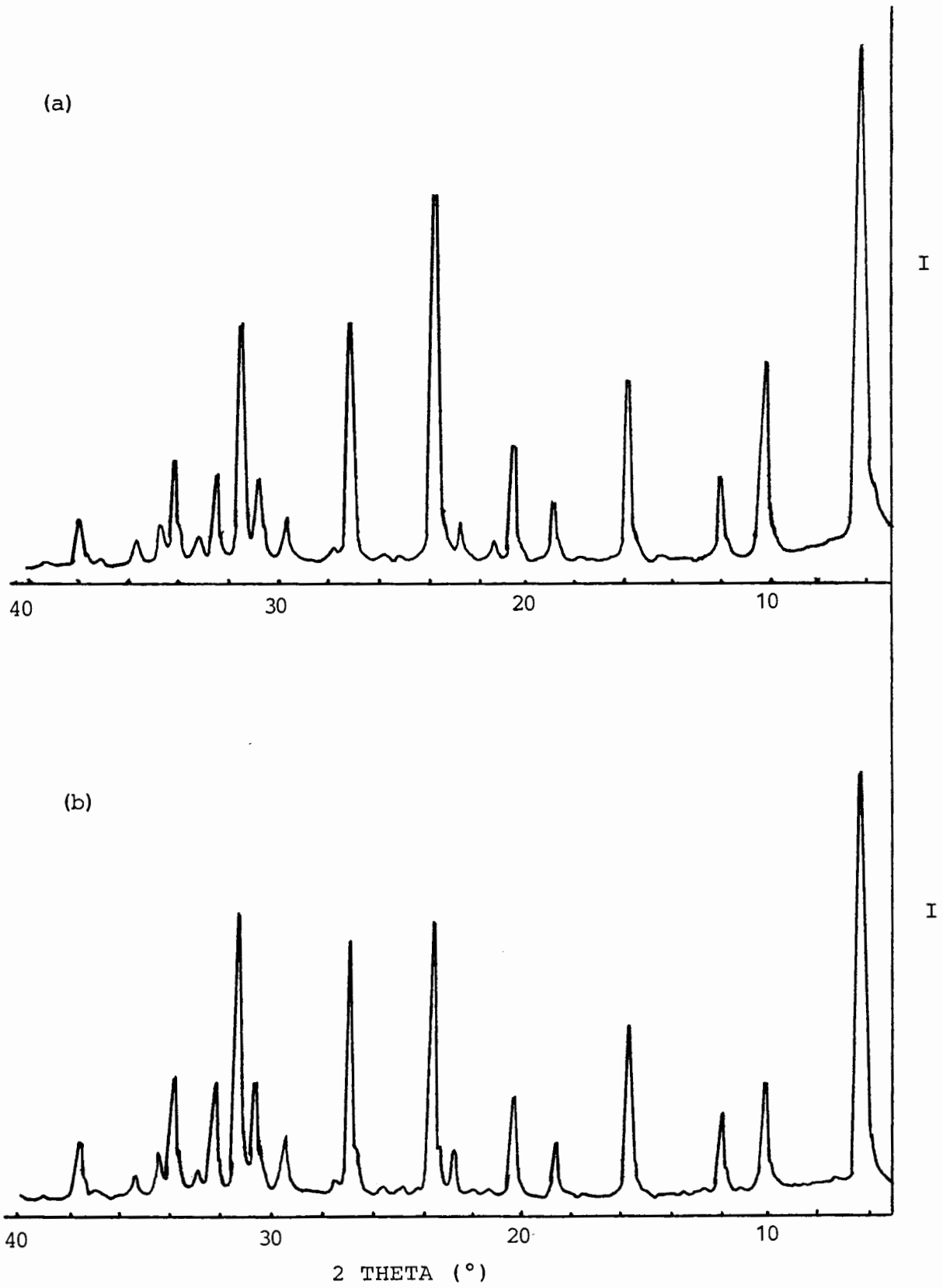

TABLE 4.1

Some reaction conditions and products of zeolite X crystallization at pH 14

Reactants	Temp. (°C)	Time (days)	Product	Size (μ)	Yield (g)
100g $Na_2SiO_3.9H_2O$	90	14	NaX, some P[(a)]	22-28	40.68
700mℓ H_2O	90	15	Good NaX; some P	22-33	36.43
100 mℓ TEA*	90	13	NaX; P; zeolite A	30	48.70
40g $NaAlO_2$	80	24	NaX; P; amorphous reactants	-	15.07
700mℓ H_2O	80	20	NaX; P	13-23	24.00
100mℓ TEA*	78	22	NaX; P; some amorphous material	13-25	22.40
	70	19	P	-	8.78

* TEA = Triethanolamine

(a) = Zeolite species P

TABLE 4.2

Chemical Analysis of Zeolite NaX

Element	Wt %	Ions/unit cell
Na	17	39.3
Aℓ	38	88.0
Si	45	104.0

4.3.2. Synthesis of Zeolites KX, CaX, BaX, CoX, NiX, CuX, ZnX, PbX and AgX by Ion-exchange Reactions

100 g of the zeolite Linde NaX were washed with a 0.1 M solution of $NaNO_3$ to ensure maximum replacement of any H^+ ions present in the zeolite. 10 g quantities of the washed zeolite were used for each exchange reaction.

These quantities were mixed in a 1 M solution of a salt of the desired metal for exchange, and allowed to stand for a period of 10 days. A fresh salt solution was made up and the old one replaced. The solutions were then allowed to stand for a further 11 days. The solution was regularly agitated throughout the exchange period. All the exchanges were carried out at room temperature, except in the case of Ca and Ba, where the solutions were placed in a thermostatically controlled waterbath at 50°C.

The salts used to achieve the different exchanges were: $KC\ell$, $CaC\ell_2$, $BaC\ell_2$, $Pb(NO_3)_2$, $ZnSO_4$, $Ni(NO_3)_2$, $CoC\ell_2$ and $AgNO_3$. The copper exchange was achieved by reacting the zeolites with a $Cu(NH_3)_4SO_4$ complex solution, prepared by dissolving 10.5 g $CuSO_4$ and 15.25 mℓ 25% NH_3 solution in 500 mℓ H_2O.

After completion of the exchange reactions, the solutions were filtered using Whatman No 1 filter paper and a Buchner funnel and then washed with a 0.01 M solution of the respective salt. The copper sample was washed with a 0.01 M $CuSO_4$ solution. The samples were dried and characterised by the methods discussed above.

X-ray powder diffraction data are presented in Figures 4.5 - 4.7 and TGA data are presented in Table 4.3. The chemical analysis data are presented in Table 4.4.

FIGURE 4.5: XRD pattern of ion-exchanged Zeolites with reference to the Linde Zeolite 13X used as starting material.

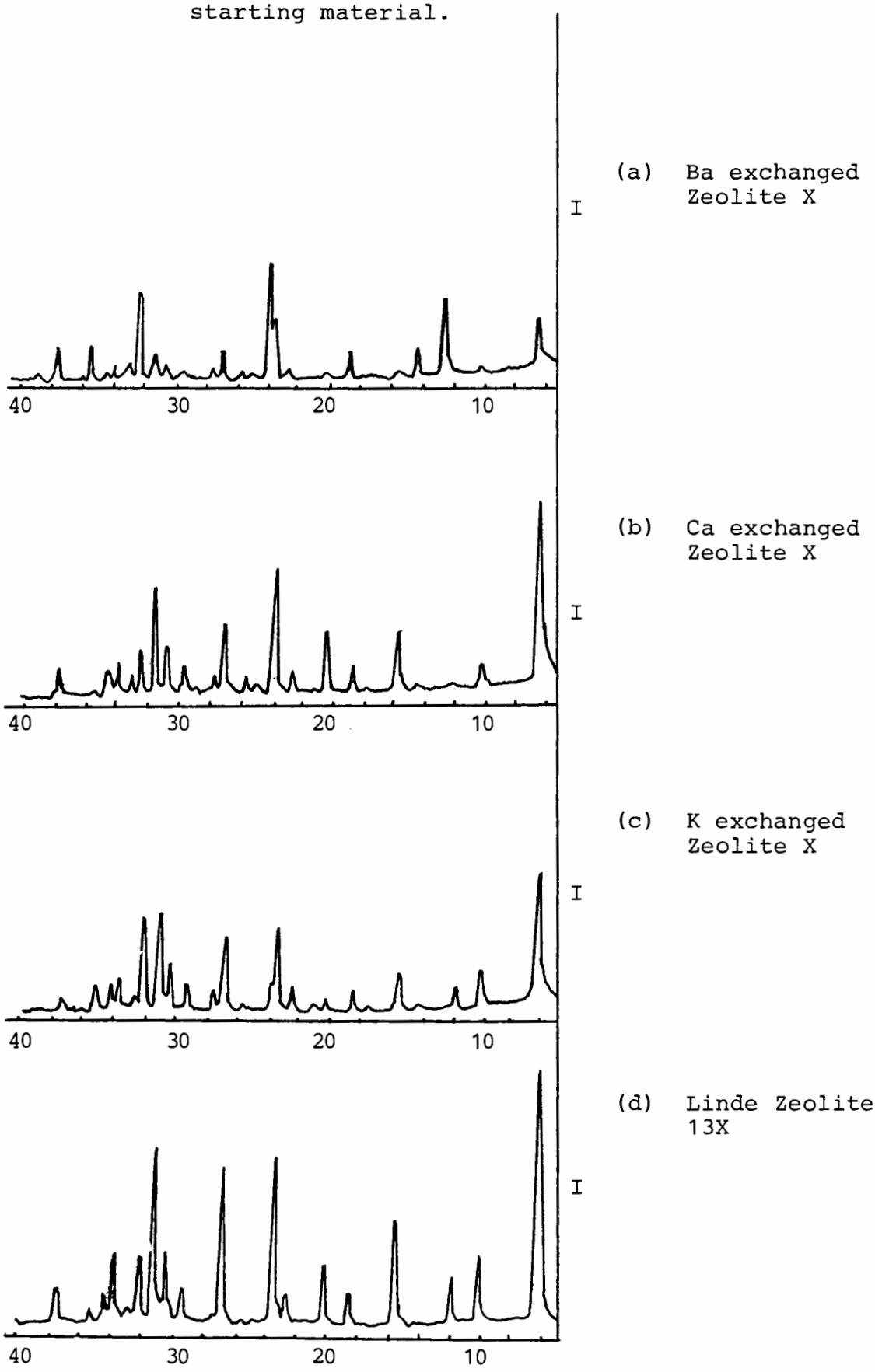

FIGURE 4.6: XRD pattern of ion-exchanged Zeolites with reference to the Linde Zeolite 13X used as starting material.

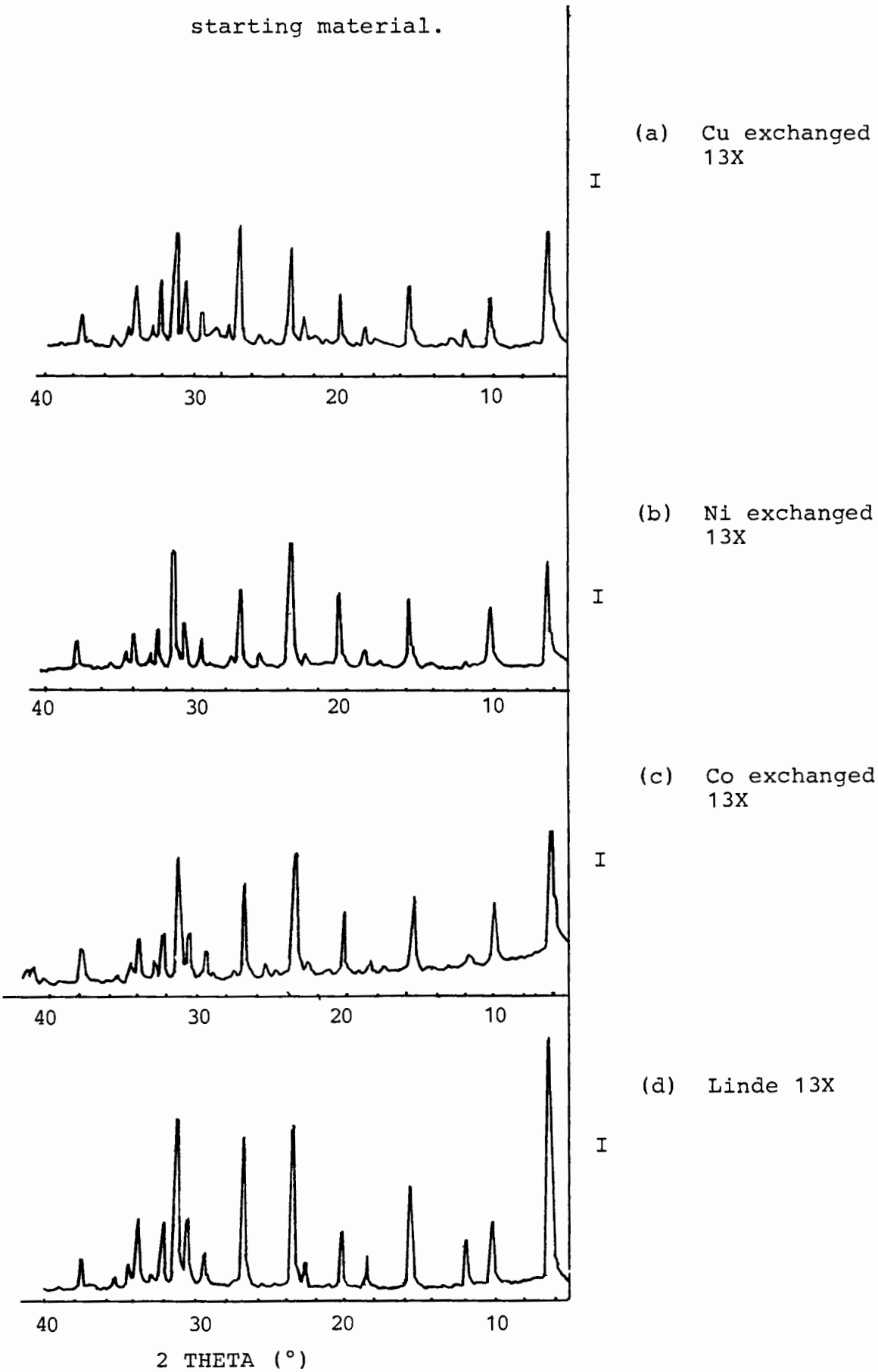

FIGURE 4.7: XRD pattern of ion-exchanged zeolites with reference to the Linde zeolite 13X used as a starting material.

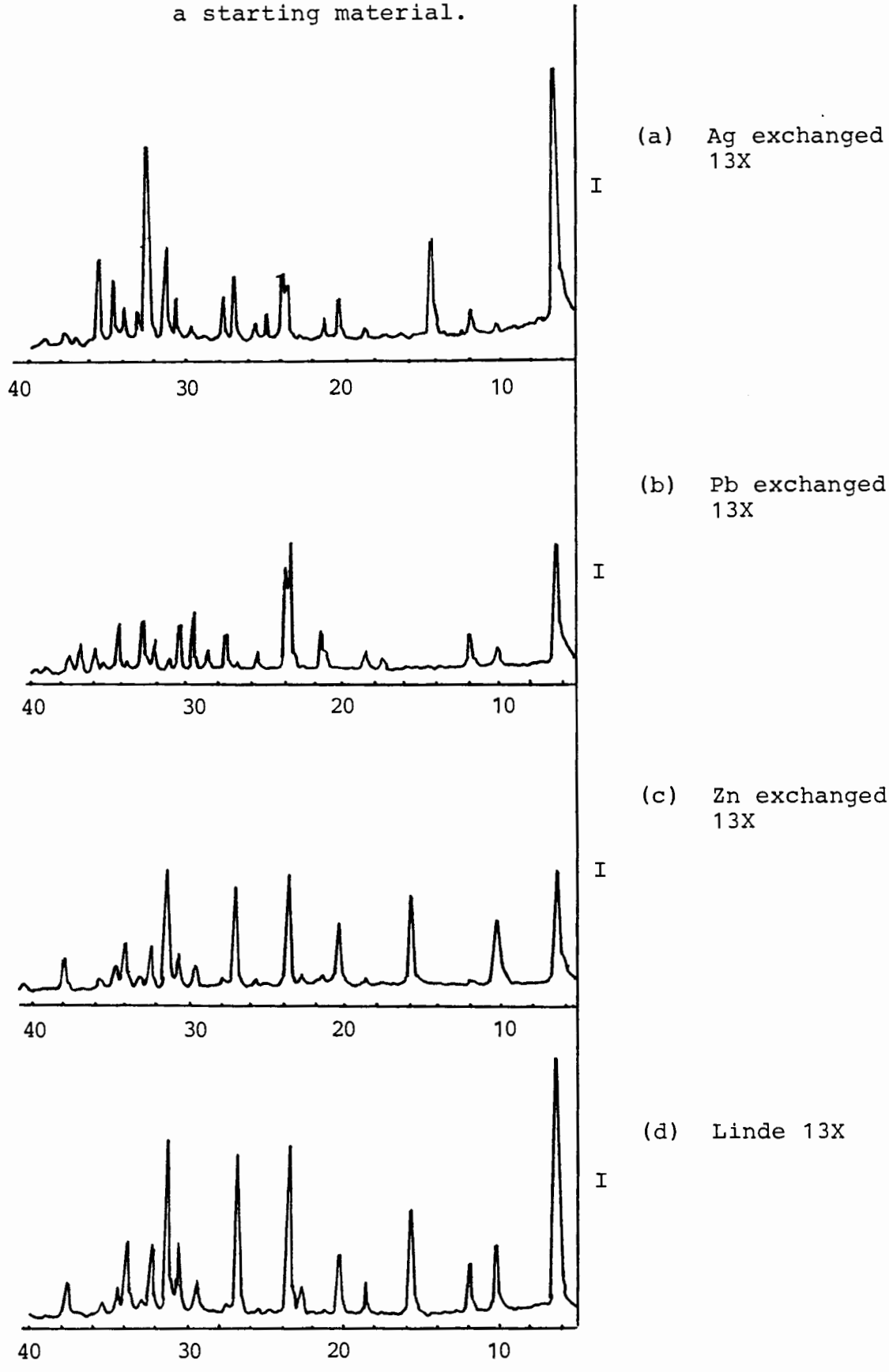

TABLE 4.3

Thermogravimetric Data of Zeolites at 600°C

Zeolite	Water Loss (wt%)
Linde NaX	23.70
KX	21.00
CaX	25.70
BaX	20.00
AgX	19.50
ZnX	26.00
PbX	18.73
CuX	18.64
CoX	23.30
NiX	26.50

Table 4.4 shows that ion exchange did occur in the reactions. The chemical analysis values presented in the table can be considered as good estimates of the true ionic composition of the zeolites. The accuracy of the EDAX technique is somewhat limited, being of the order of 10% for those atoms heavier than phosphorous and as high as 50% relative for sodium determination.

The fact that the zeolite powders were not polished and the non homogeneous packing of the sample analysed are factors which must be taken into consideration when gauging the accuracy of the chemical analyses.

Incomplete ion exchange was observed in the case of Co, Ni, Cu, and Ba. This is evident from the chemical analysis results since there is still some sodium present in the analysis of the end product. The remaining exchanges did not register any sodium content in the final product so we can assume that all of the sodium was exchanged.

The normal sodium ion content in zeolite X is in the region of 77-85 ions per unit cell. Viewing Table 4.4, one can see that none of the exchanges came really near this value.

TABLE 4.4

Chemical Analysis of Ion Exchanged Zeolites

Zeolite	Wt% of element												Number of ions per unit cell*										
Type	Si	Aℓ	Na^+	K^+	Ca^{2+}	Ba^{2+}	Ag^+	Zn^{2+}	Pb^{2+}	Cu^{2+}	Co^{2+}	Ni^{2+}	Si	Aℓ	Na^+	K^+	Ca^{2+}	Ba^{2+}	Ag^+	Zn^{2+}	Pb^{2+}	Cu^{2+}	Co^{2+}	Ni^{2+}
NaX	51	34	15	-	-	-	-	-	-	-	-	-	115	77	41	-	-	-	-	-	-	-	-	-
KX	40	22	-	38	-	-	-	-	-	-	-	-	115	63	-	79	-	-	-	-	-	-	-	-
CaX	50	25	-	-	25	-	-	-	-	-	-	-	115	60.4	-	-	40.6	-	-	-	-	-	-	-
BaX	36	23	3	-	-	39	-	-	-	-	-	-	115	76	13	-	-	25	-	-	-	-	-	-
AgX	29	18	-	-	-	-	53	-	-	-	-	-	115	74	-	-	-	-	63	-	-	-	-	-
ZnX	45	28	-	-	-	-	-	27	-	-	-	-	115	75	-	-	-	-	-	30	-	-	-	-
PbX	24	16	-	-	-	-	-	-	60	-	-	-	115	78	-	-	-	-	-	-	38	-	-	-
CuX	37	22	3	-	-	-	-	-	-	29	-	-	115	71	11	-	-	-	-	-	-	40	-	-
CoX	49	28	3	-	-	-	-	-	-	-	20	-	115	68	9	-	-	-	-	-	-	-	22	-
NiX	47	28	4	-	-	-	-	-	-	-	-	21	115	73	12	-	-	-	-	-	-	-	-	25

* Number of ions per unit cell calculated on the basis that the silica content of the zeolite remained unchanged through all exchange reactions.

This could be attributed to the fact that hydrogen ions present in the aqueous solutions also participate in the ion-exchange reaction. The charge deficiency between the exchanged ions and the anionic framework could be made up by the inclusion of these hydrogen ions which cannot be determined by EDAX.

The cation sites in zeolite X are reasonably well defined and the success of an ion-exchange reaction depends on the number of sites that are accessible to the ingoing cations. This is possibly the reason why the Ba^{2+} ions only partially exchanged. The ionic radius of the Ba^{2+} ion is 1.36 Å, while the diameter of the 6-ring aperture leading into the sodalite cages is 2.6 Å. The Ba^{2+} ion can therefore readily exchange the cations located in the large cavities, but will be sterically restricted from exchanging those ions within the sodalite cages. The size of the hydrated Ba^{2+} ion will further restrict the degree of exchange.

In the case of Co^{2+}, Zn^{2+} and Ni^{2+} exchange, the ionic radii (0.74, 0.74 and 0.72 Å, respectively) are small enough to enter the sodalite cages and hence should have access to all the cation sites. The size of the hydrated ion must be considered in this respect, as well as the ability of these ions to be polarized by the anionic framework charge. Zeolites exchange preferentially with ions that are highly polarizable, such as Ag^{+}.

The Co^{2+} and Ni^{2+} ions with incompletely filled d orbitals tend not to be so easily polarized and one would possibly expect an incomplete ion-exchange reaction. These ions are also octahedrally coordinated to the water molecules in the hydrated state, and hence the hydrated ionic radii could well impose restrictions on the exchange success. Copper, although more readily polarized than Ni and Co, would more than likely also be restrained by the hydrated ion size.

The powder X-ray diffraction patterns (Figures 4.5 - 4.7) show that the aluminosilicate framework structure of the zeolite X was retained after the ion exchange reactions. In particular, the inclusion of the cations into the zeolite matrix by ion exchange does not appear to affect the "a" lattice parameter of the unit cell. This is evident since there is no significant shift in the relative positions of the peaks in the X-ray spectrum. It is evident from the figures that there are differences in peak intensities in the X-ray patterns of the various cationic forms with respect to the reference zeolite NaX used as a starting material for the exchange reactions.

This variation in the peak intensities could be ascribed to the manner in which the zeolite powder was packed before being X-rayed, as well as the particle size distribution within the different zeolite forms.

Each metal exchanged into the zeolite has its own specific atomic scattering power, which directly affects the intensities of the peaks. As the heavier atoms tend to scatter X-rays more strongly, the ion-exchanged zeolites would be expected to show a substantial variation in the intensities of certain reflections. This is observed particularly for the Ba, Ag and Pb exchanges. The appearance of new peaks and the disappearance of some of the peaks already present illustrates the effect on the diffraction of the zeolite by the exchanged cation.

4.3.3. Sorption of Na metal by zeolites NaX; CaX; BaX; KX; CoX; NiX; CuX; ZnX; PbX and AgX.

10 g quantities of each ion-exchanged form of the zeolite X, including the standard Linde type NaX, were dried under vacuum (10^{-3} Pa pressure) at a temperature of 400°C for 12 hours. 5 g lots of sodium metal (50% by weight of the zeolite) were cut into small strips

and added to the different reaction vessels containing the zeolite species. These manipulations were carried out in a dry box under an argon atmosphere.

The reaction vessels were evacuated at 10^{-3} Pa and sealed, the contents of the vessels remaining under vacuum. The sealed vessels were heated in a furnace at 350°C for 24 hours to achieve impregnation of the zeolites by the sodium metal. Characterization of the zeolites was done by X-ray diffraction methods. The powder X-ray diffraction patterns are presented in Figures 4.8 - 4.17.

On adsorption of sodium, the zeolites all turned dark brown to black in colour. They were all stable in air at room temperature, but after a period of 24 hours, there were definite signs of oxidation present.

The X-ray patterns of the sodium-adsorbed zeolites are radically altered as revealed in Figures 4.8 - 4.17. In all the cases, the intensities of the peaks are all drastically reduced, with the majority of the peaks being absent in most of the samples.

This almost amorphous behaviour of the adsorbed zeolites towards X-rays is not fully understood. It does not necessarily indicate a destruction of the zeolite crystal structure, as is evidenced in the case of iodine adsorption by the zeolites (85). The iodine sorbed zeolites appear completely amorphous to X-rays with no crystal structure evident. Once the iodine has been desorbed, the crystal structure reappears, indicating that the crystal structure was not destroyed on adsorption. Sodium, although far removed from iodine in character, could well be interacting with the zeolite framework in a manner similar to iodine, causing a similar effect.

A study on sodium adsorption by sodalite (40), which has an aluminosilicate framework structure similar to that of the X-type zeolites, showed that the framework structure of the sodalite did not break down. On adsorption, the powder X-ray diffraction pattern of the sodalite was essentially retained, with extra diffraction lines not belonging to the supercage appearing. Many changes in the intensity of the sodalite lines were observed. On removing the sodium from the sodalite framework, the X-ray diffraction pattern of the sodalite was essentially retained, with the additional lines present in the adsorbed sample being absent.

In the case of zeolite X, attempts to desorb all the sodium from the framework structure proved unsuccessful, hence it could not be established whether the original X-ray diffraction pattern was regenerated after removal of the sodium.

Adsorption of the sodium metal reduced the metal ions in the Zn, Ag, Pb, Cu, Ni and Co zeolites, while the Ba^{2+}, Ca^{2+}, and K^{+} ions were not reduced. This is plainly evident on examining the X-ray diffraction patterns of these zeolites. Peaks corresponding to the atomic metals are present, while peaks corresponding to the Ca, K and Ba metals are not observed. This is expected because the Ca, Ba and K metals all have higher oxidation potentials than has sodium, hence they will not be reduced by the sodium.

FIGURE 4.8: Na impregnated KX

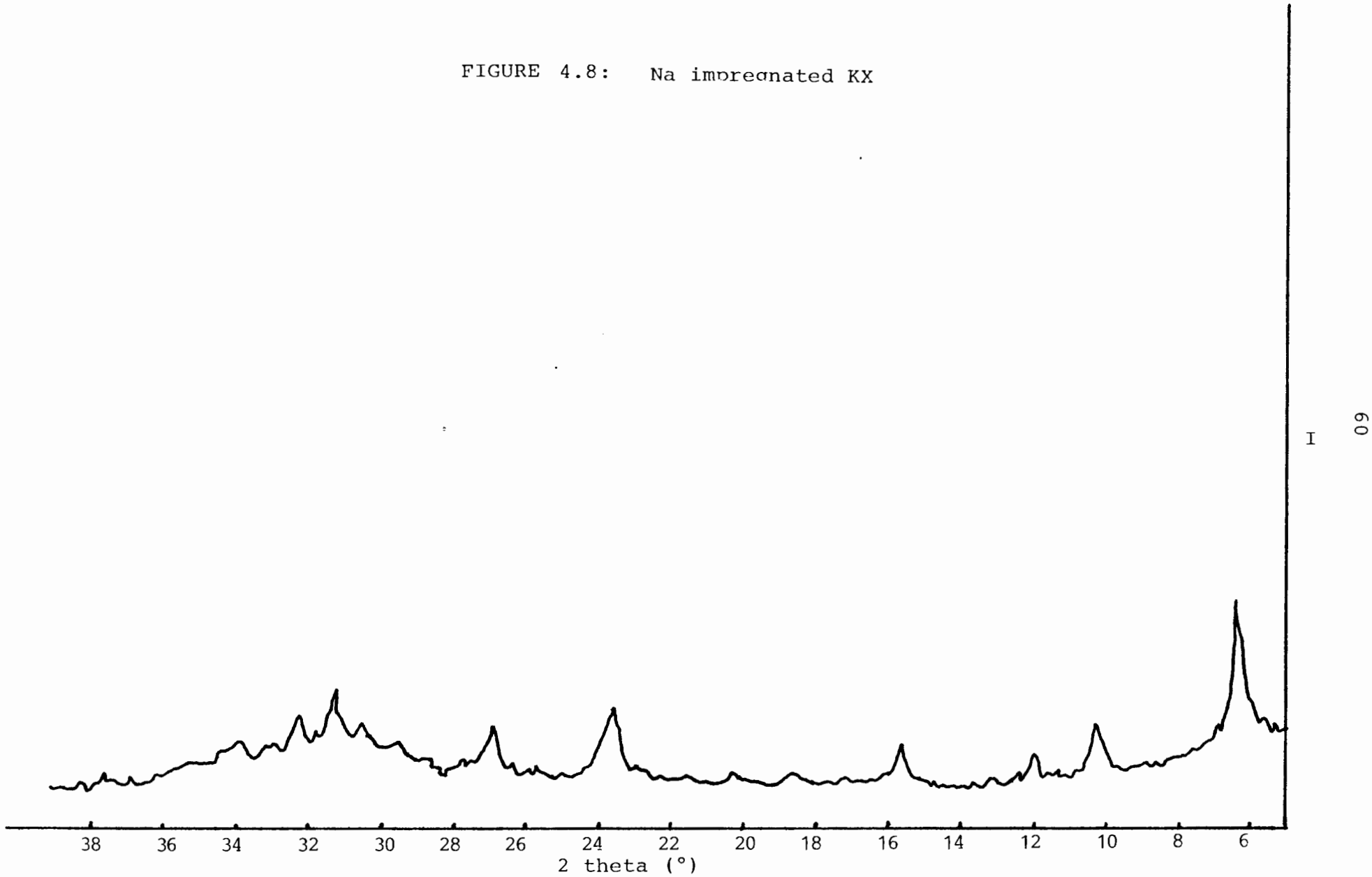

FIGURE 4.9: Na impregnated CaX

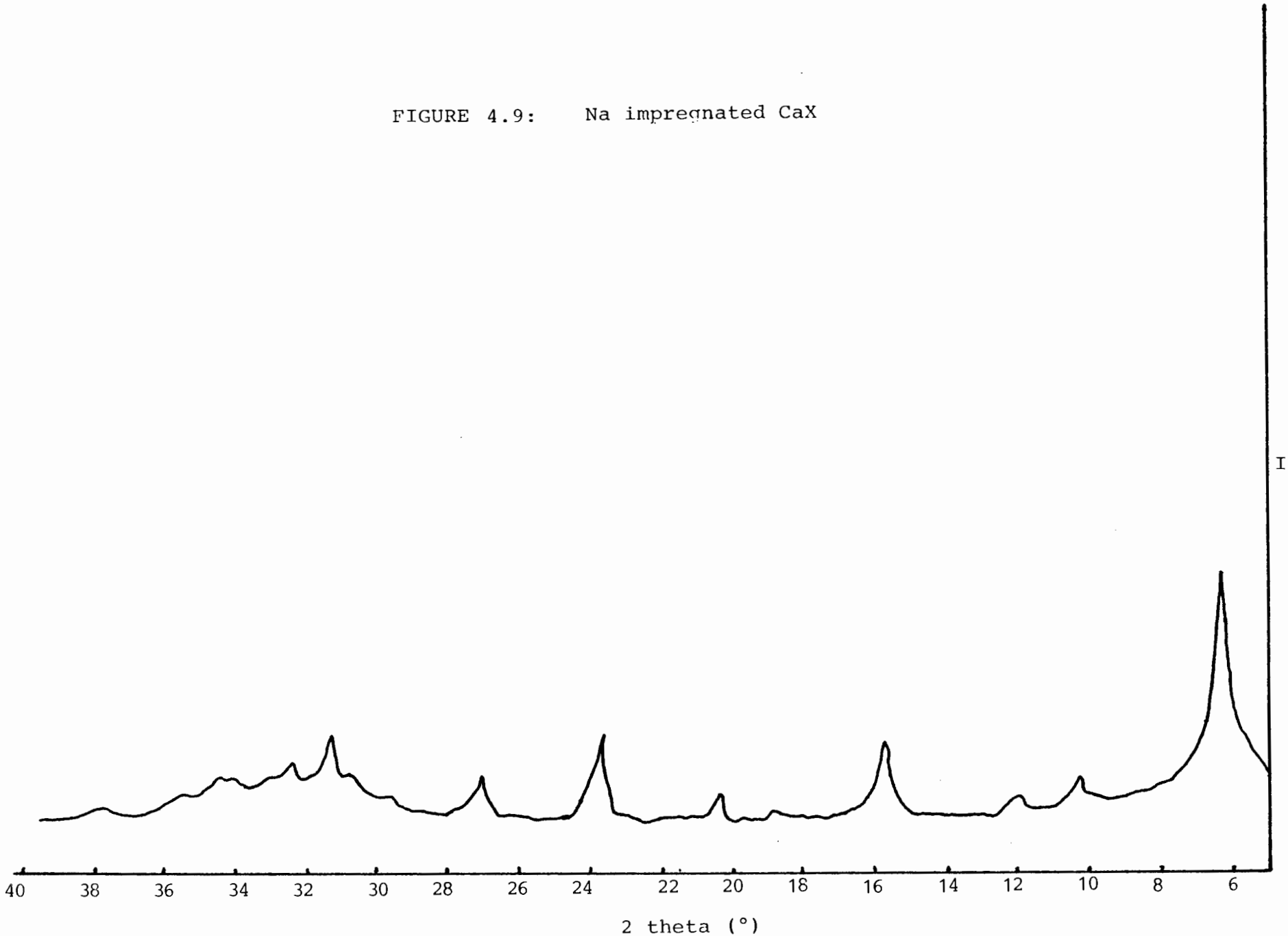

FIGURE 4.10: Na Impregnated BaX

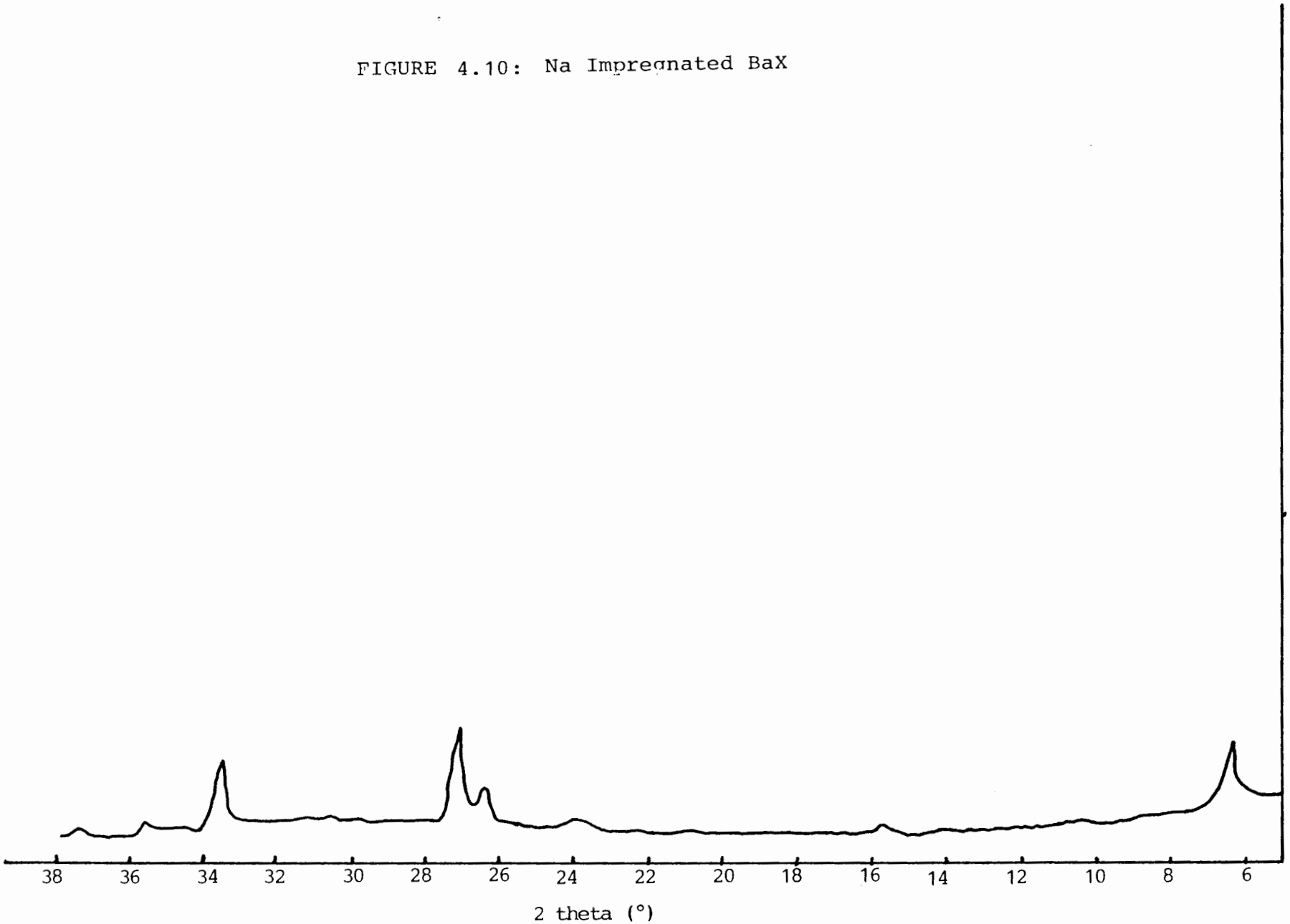

FIGURE 4.11: Na impregnated ZnX

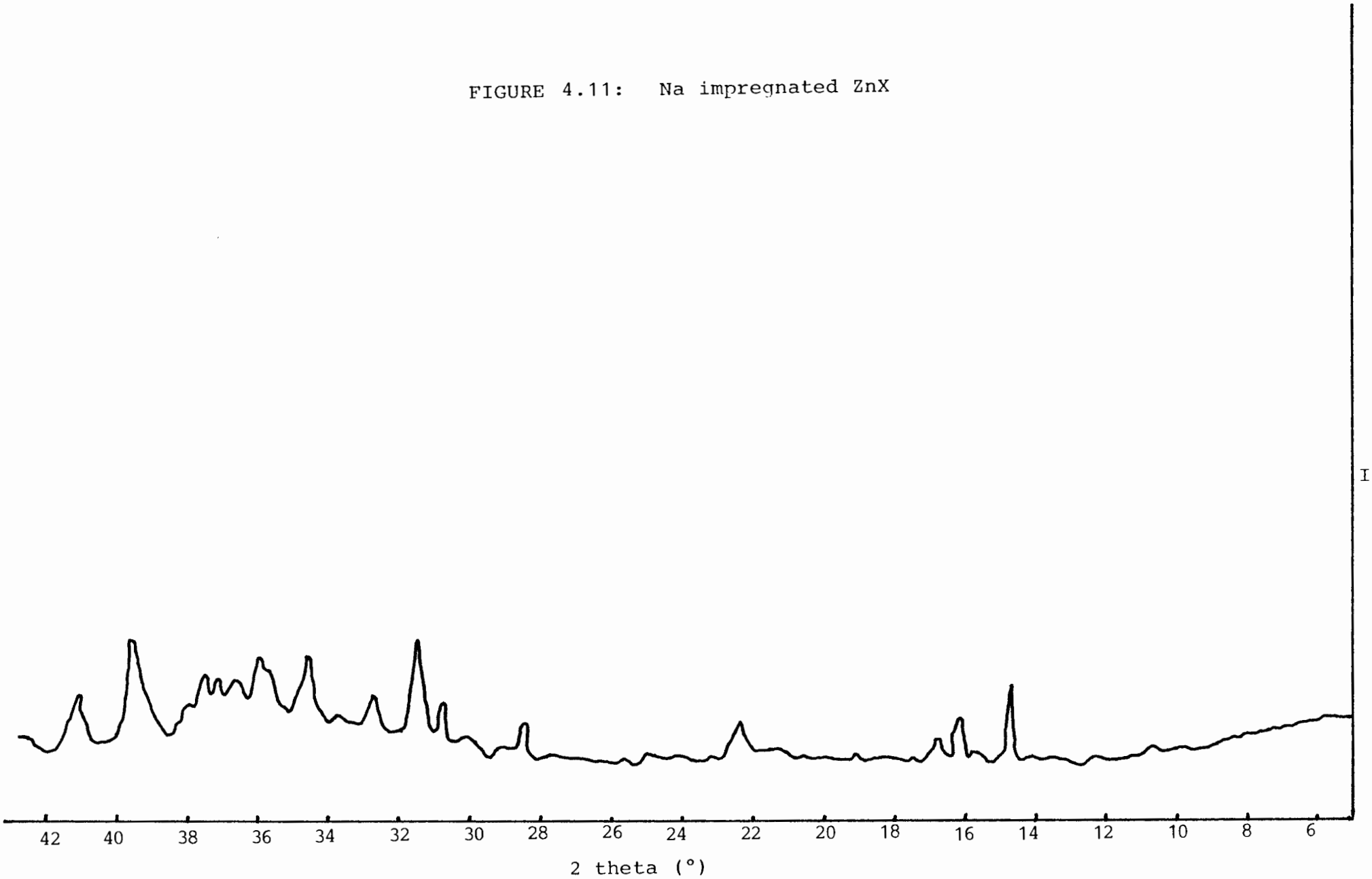

FIGURE 4.12: Na impregnated NiX

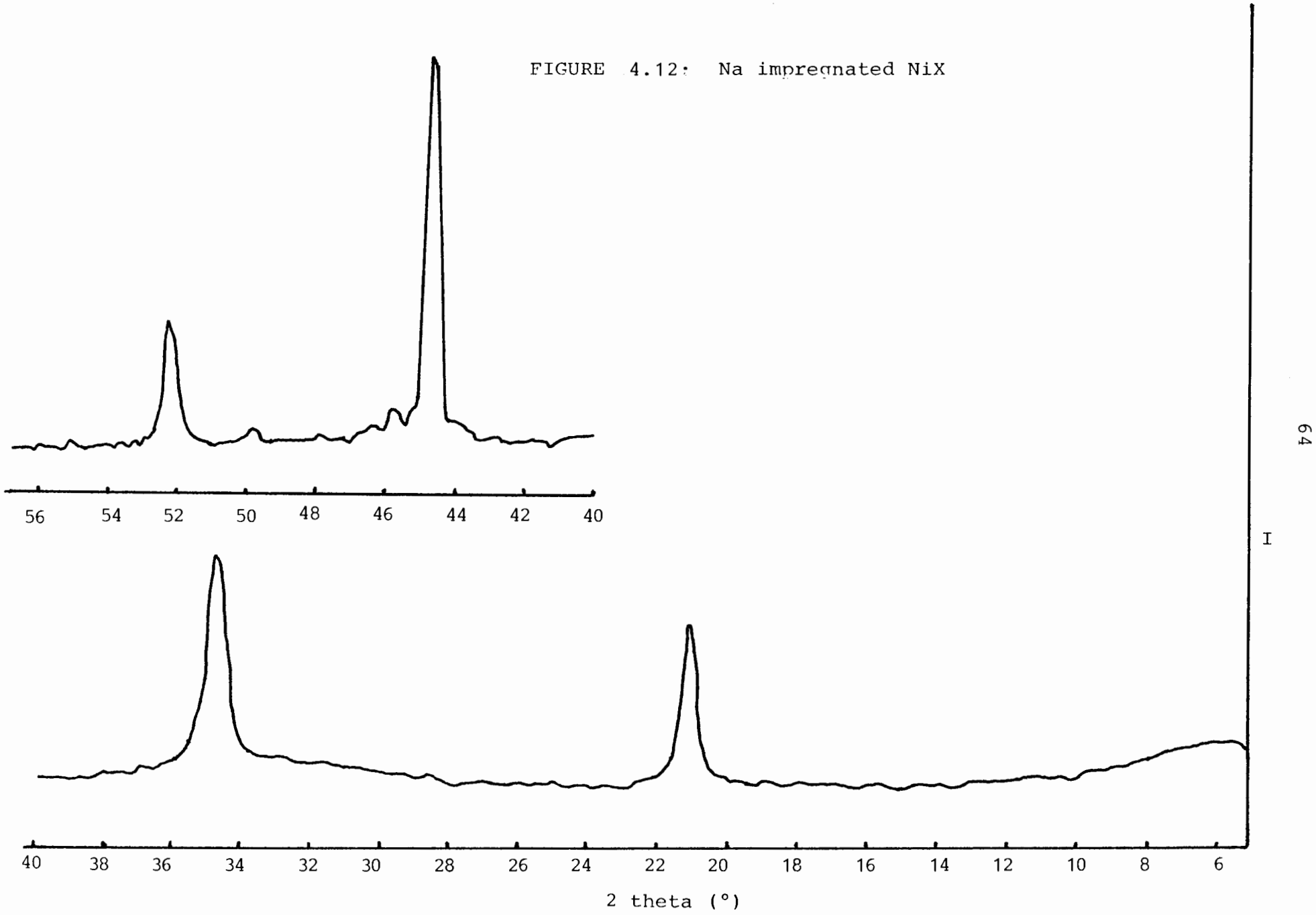

FIGURE 4.13: Na impregnated CoX

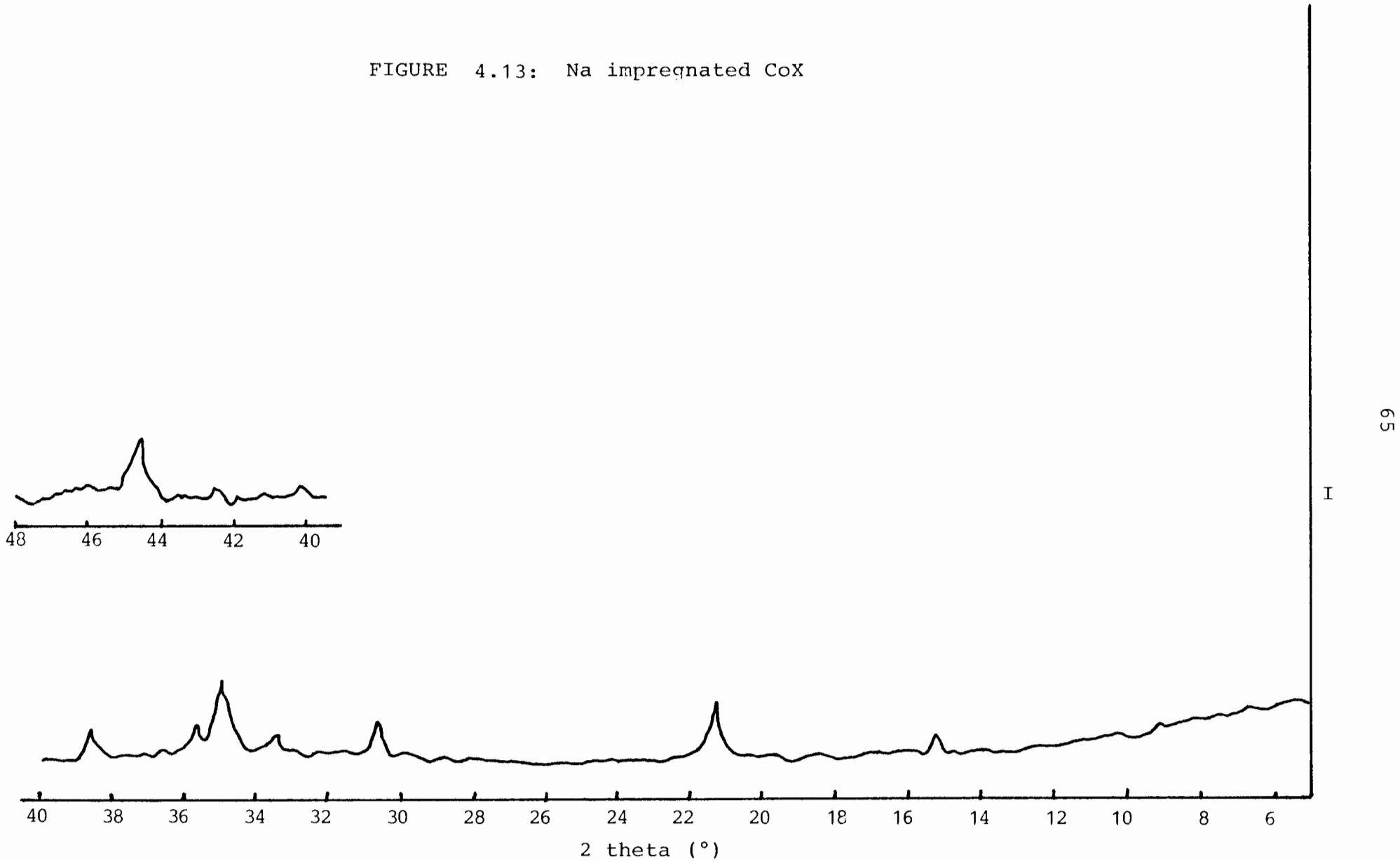

FIGURE 4.14: Na impregnated AgX

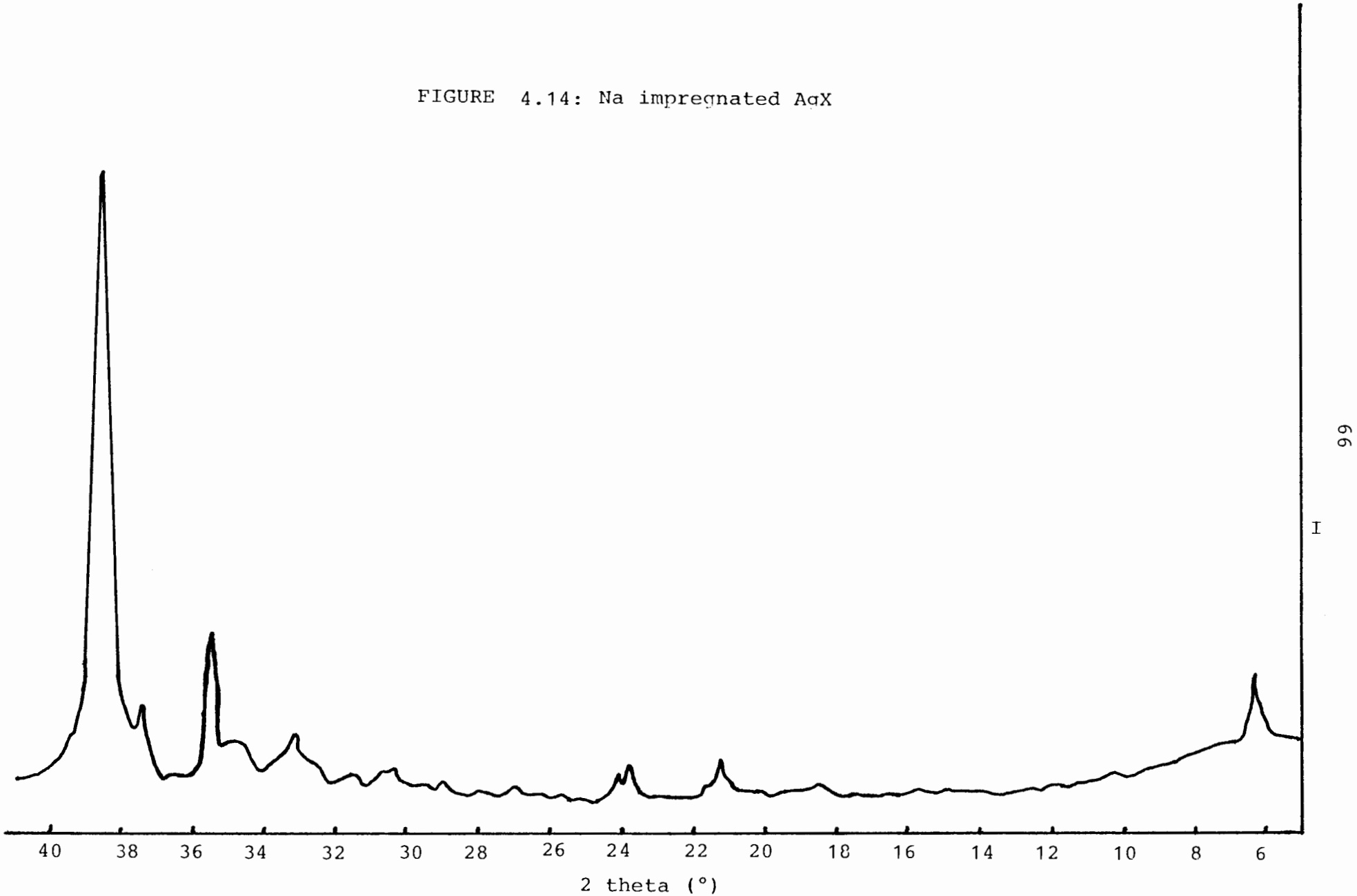

FIGURE 4.15: Na impregnated PbX

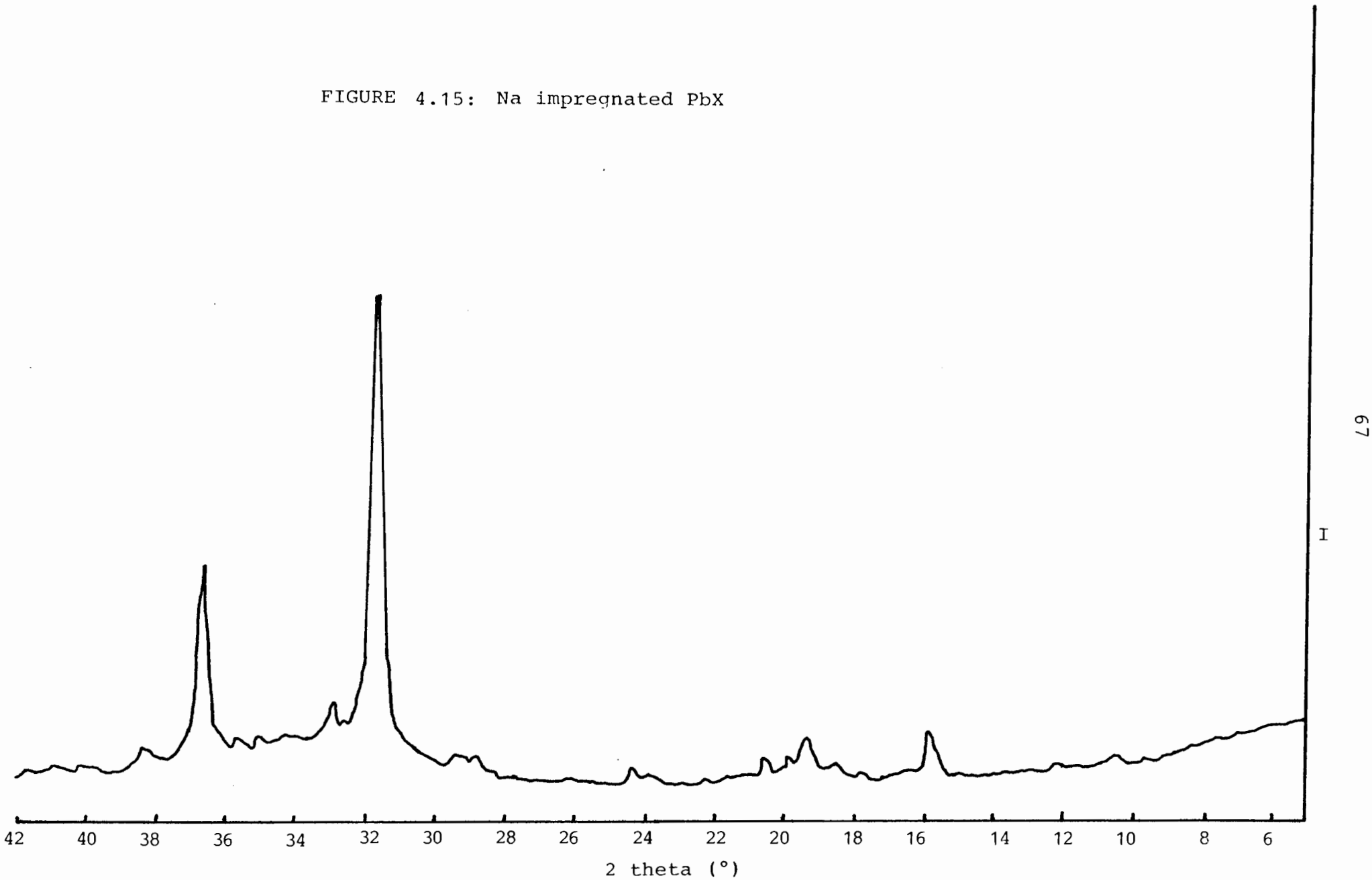

FIGURE 4.16: Na impregnated CuX

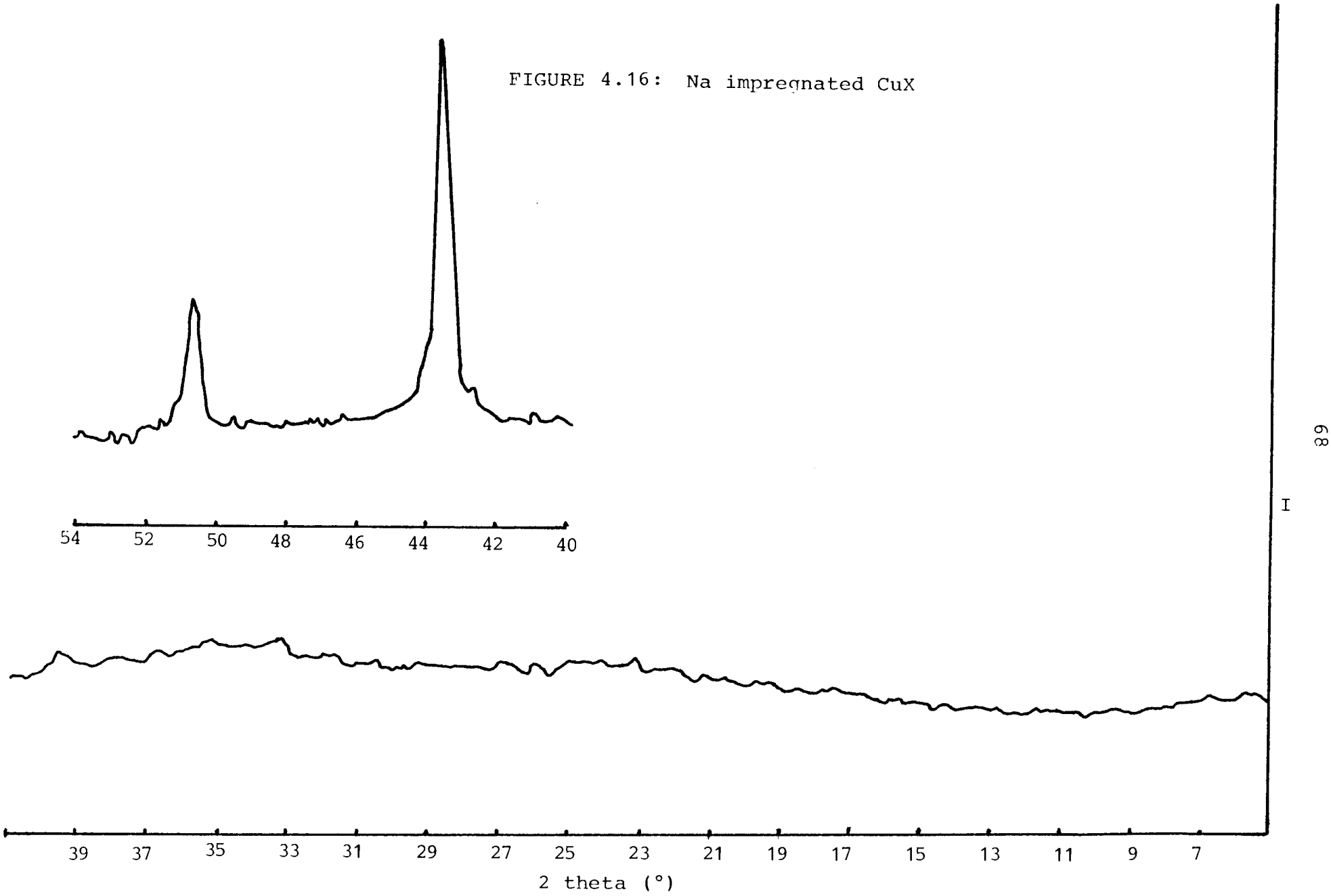

FIGURE 4.17: Na impregnated NaX

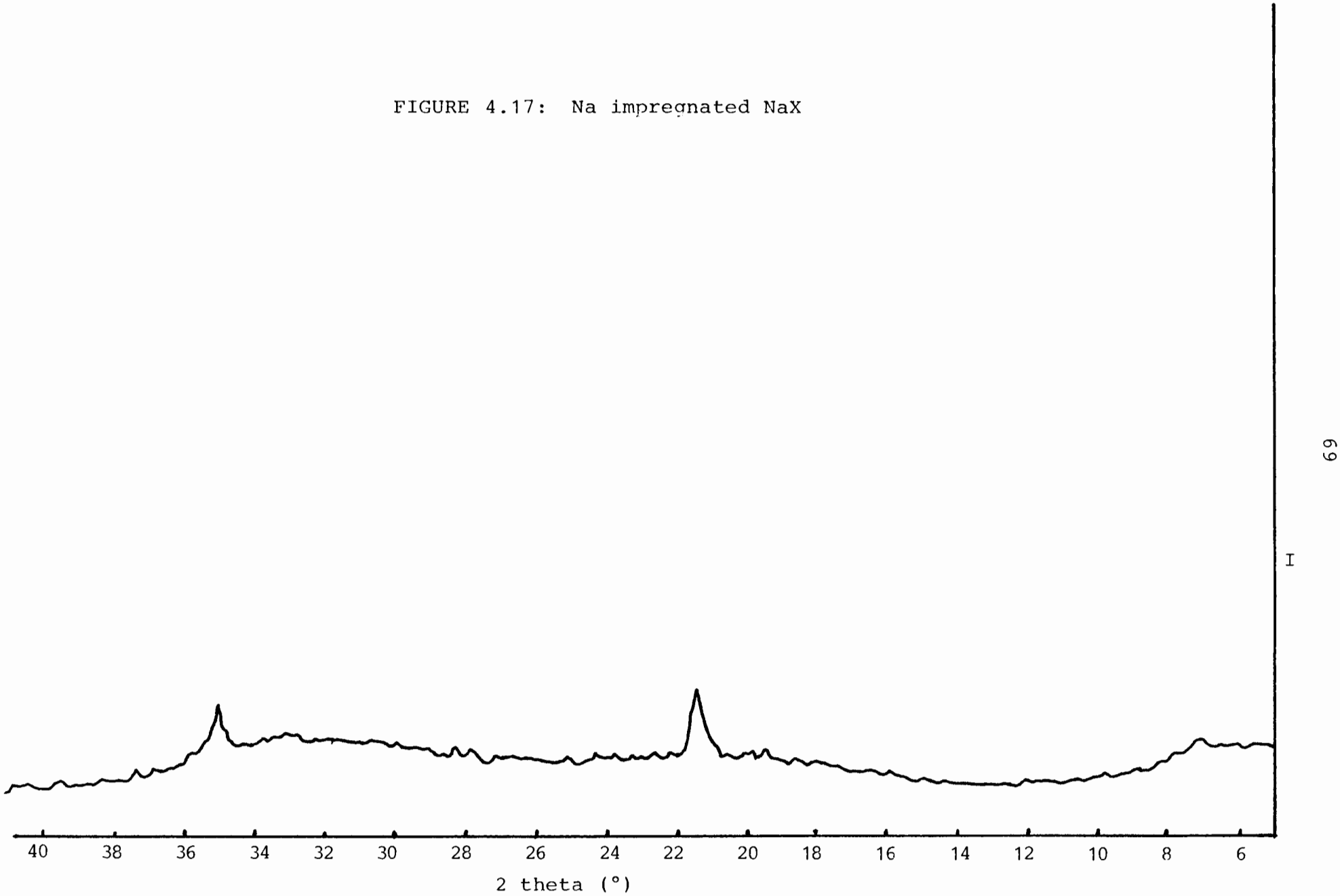

CHAPTER 5

DETERMINATION OF THE ELECTRICAL CONDUCTIVITY AND RELATED THERMODYNAMIC PROPERTIES.

5.1 Introduction

There are several measurement techniques which can be used to evaluate the electrical properties of an ionic conductor. The choice of technique or the combined use of several techniques depends on the type of information sought.

The technique used here involved applying an A.C. signal to a conductivity cell to determine the resistance of the zeolite as a function of temperature.

The conductivity of the zeolite could then be calculated using the standard equation relating the conductivity and the resistance, namely

$$\sigma = \frac{d}{AR} \quad . \quad . \quad . \quad . \quad . \quad . \quad . \quad . \quad . \quad . \quad . \quad . \quad . \quad (5.1)$$

where σ = conductivity, d = thickness or length of conduction path, A = cross-sectional area over which the conduction takes place, and R = resistance of the zeolite sample.

5.2 Sample Preparation and Compaction.

The zeolites were prepared as discussed in sections 3.3.2 and 3.3.3. They were compacted into pellets of the type illustrated in Figure 5.1. The pellets were formed by first compacting 0.1 g of a 1:1 mixture of zeolite and graphite on the base of a 20 mm die. 0.5 g of the desired

zeolite powder was added and gently compressed, followed by a further 0.1 g of the zeolite/graphite mixture. The whole compact was then pressed at 50 mPa in a linear press.

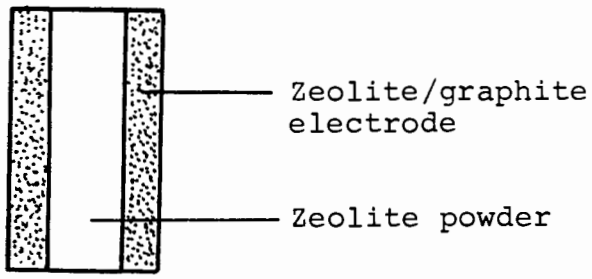

FIGURE 5.1: Illustration of pellet form used in conductivity tests.

5.3 Cell Design and Measurement Technique

The cell was assembled as illustrated in Figure 5.2. It consisted of a pellet, prepared as discussed in Section 5.2, clamped between two aluminium cups which act as current collectors.

These current collectors were connected to a Hewlett Packard model 4262 A LCR meter from which the resistance of the zeolite compact was measured. The cell was mounted in a glass vessel and an inert gas such as argon was passed through the vessel maintaining an inert atmosphere. The temperature in the cell was monitored by means of a chromel-alumel thermocouple, linked via a cold junction to a Keithley 192 programmable digital multimeter, which was inserted into the glass vessel. The glass vessel was inserted into an oven whose heating rate was controlled by a RKC model PS 962 programmable temperature controller.

The Hewlett Packard LCR meter and the Keithley multimeter were linked to a Commodore CBM 8032 computer and disc drive (model CBM 8250). The whole data collection was thus fully automated.

FIGURE 5.2: Conduction cell assembly.

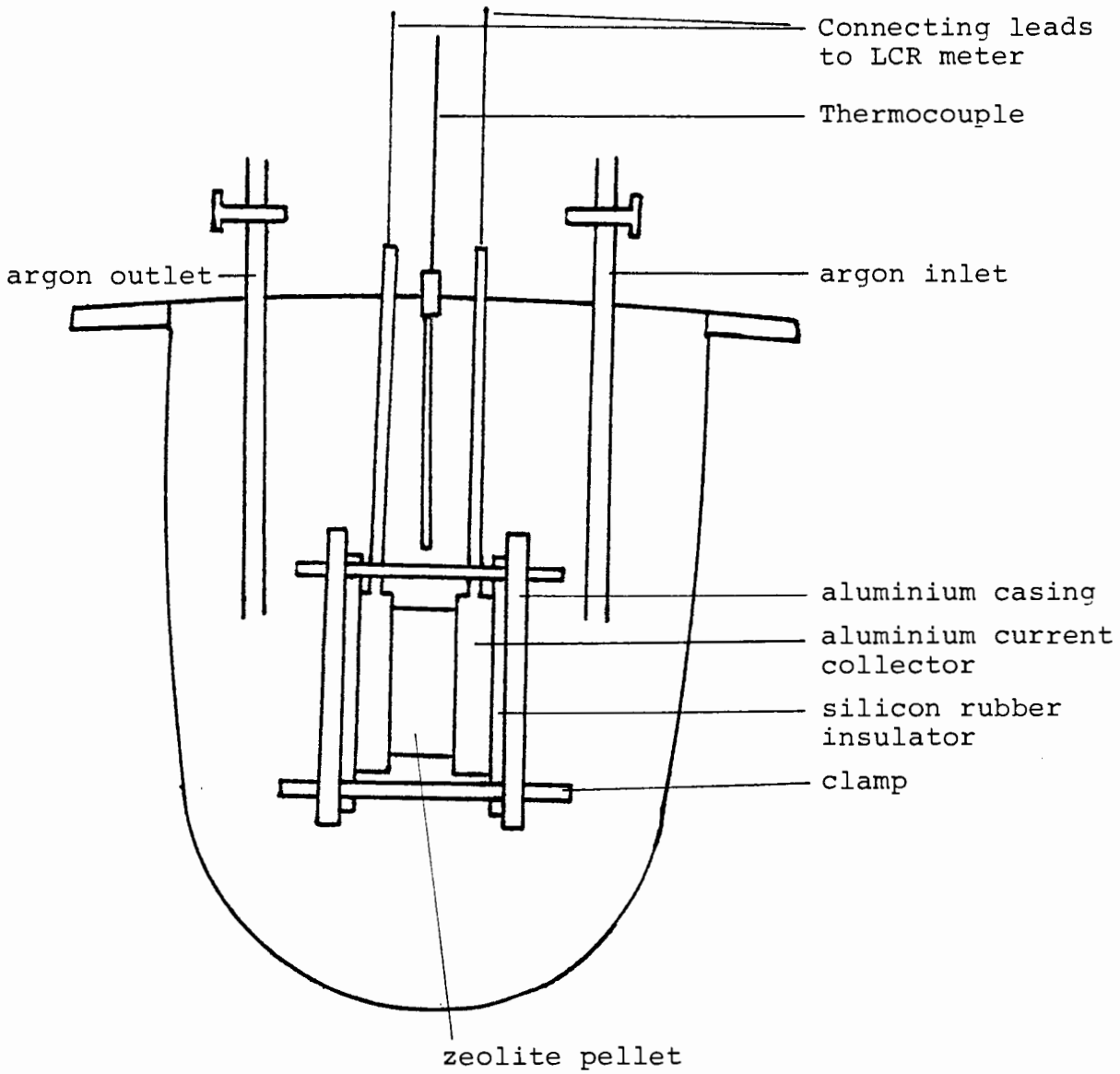

The zeolite/graphite electrodes used in the cell are non-reversible, hence each electrode/electrolyte interface could be modelled as a parallel plate capacitor (86) which accounts for any polarization effects at the interfaces. The rate of charging of these capacitors is determined by the bulk resistance of the electrolyte. An equivalent circuit of the cell is given in Figure 5.3 where R_b is the bulk electrolyte or zeolite impedance and C_i is the combined interfacial capacitance. The interfacial capacitance was minimised by using an A.C. signal to determine the resistance.

Where possible, co-axial leads were used to prevent interference from outside signals affecting the results.

The resistance of the pellet was measured at a signal frequency of 1 kHz, at six minute intervals throughout the heating cycle of the oven up to a temperature of 300°C. The resistance and temperature data were stored on disc in the disc drive.

Pellets of each zeolite sample were tested in this manner, and the electrical conductivity determined from Eq. 5.1.

The activation energies, ΔE, for all the zeolite samples were determined from the slope of a log σT vs T^{-1} plot using Eq. 3.4.

The thermodynamic parameters ΔG, ΔH and ΔS were determined from Eq. 5.2 and 5.3 (refer to Chapter 3).

$$\sigma = (N^2\lambda^2q^2/\eta)\, e^{-\Delta G/RT} \quad . \quad . \quad . \quad . \quad . \quad . \quad . \quad . \quad (5.2)$$

$$\Delta G = \Delta H - T\Delta S \quad . \quad . \quad . \quad . \quad . \quad . \quad . \quad . \quad (5.3)$$

N and λ (see Chapter 3) could be determined assuming that all

FIGURE 5.3: Equivalent Circuit of Conductance Cell.

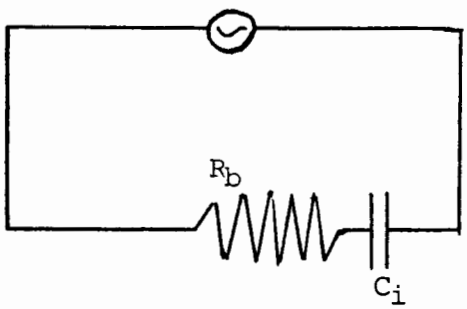

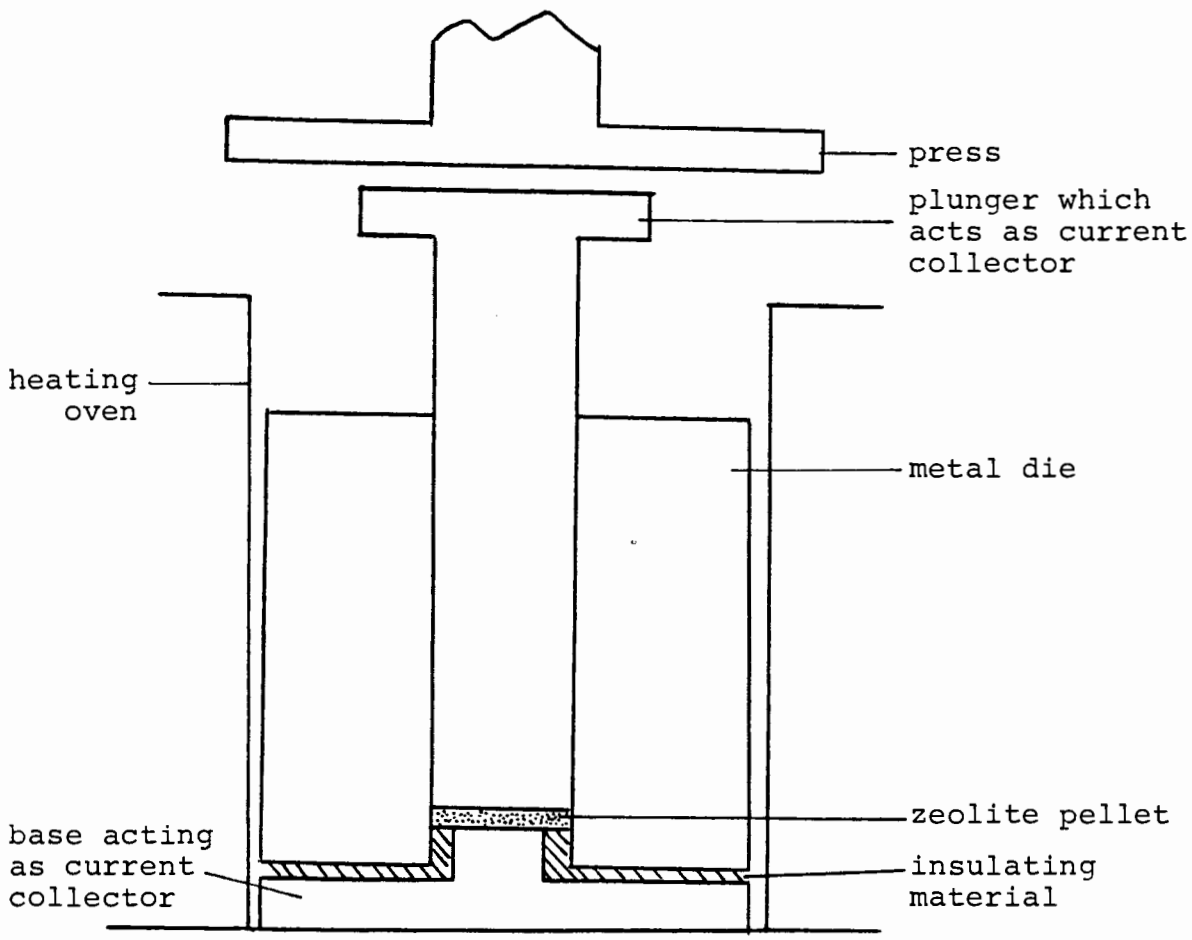

FIGURE 5.4: Conductivity Cell Assembly for Pressure Temperature Measurements.

the ions in the zeolite are charge carriers and that there is a completely random distribution of ions in the unit cell.

Thus N can be given by: $N = (m^+/a^3)$ . . . . . (5.4)

and λ by: $\lambda = (a^3/m)^{1/3}$ . . . . . (5.5)

where m^+ is the number of metal ions in the zeolite and a is the unit cell constant.

For zeolite X $N = 5.55 \times 10^{21}$ ions/cm^3

$\lambda = 5.648 \times 10^{-8}$ cm

The conductivity of the zeolite NaX (unimpregnated and sodium impregnated) as a function of temperature and pressure was determined. A conductivity cell was set up as illustrated in Figure 5.4. The experimental technique employed was similar to that described earlier. It involved heating the sample in the metal die to a desired temperature and measuring the sample resistance at different pressures. The activation volume, ΔV, for the processes was calculated from the slope a $\ell n\ \sigma$ vs P plot using equation 5.6.(87).

$$\Delta V = \left(\frac{\partial \ell n \sigma}{\partial P}\right)_T \quad . \ . \ . \ . \ . \ . \ . \ . \ . \ . \ . \quad (5.6)$$

5.4 Results

5.4.1. Conductivity as a function of temperature.

The conductivity of all the samples was found to increase with an increase in temperature indicating an ionic conduction mechanism. This is clearly illustrated by an Arrhenius type plot, given in Figure 5.5 for the dehydrated metal exchanged forms of zeolite 13X.

At the higher temperatures, the relationship between $\log\sigma T$ and $^1/T$ is characterized by a straight line. At the lower temperatures (< 400 K) positive deviations from the straight line behaviour occur. This is particularly noticeable in the samples where there are two kinds of exchangeable cations present (i.e. those samples in

FIGURE 5.5: Conductivity plot of dehydrated metal exchanged forms of Zeolite 13X.

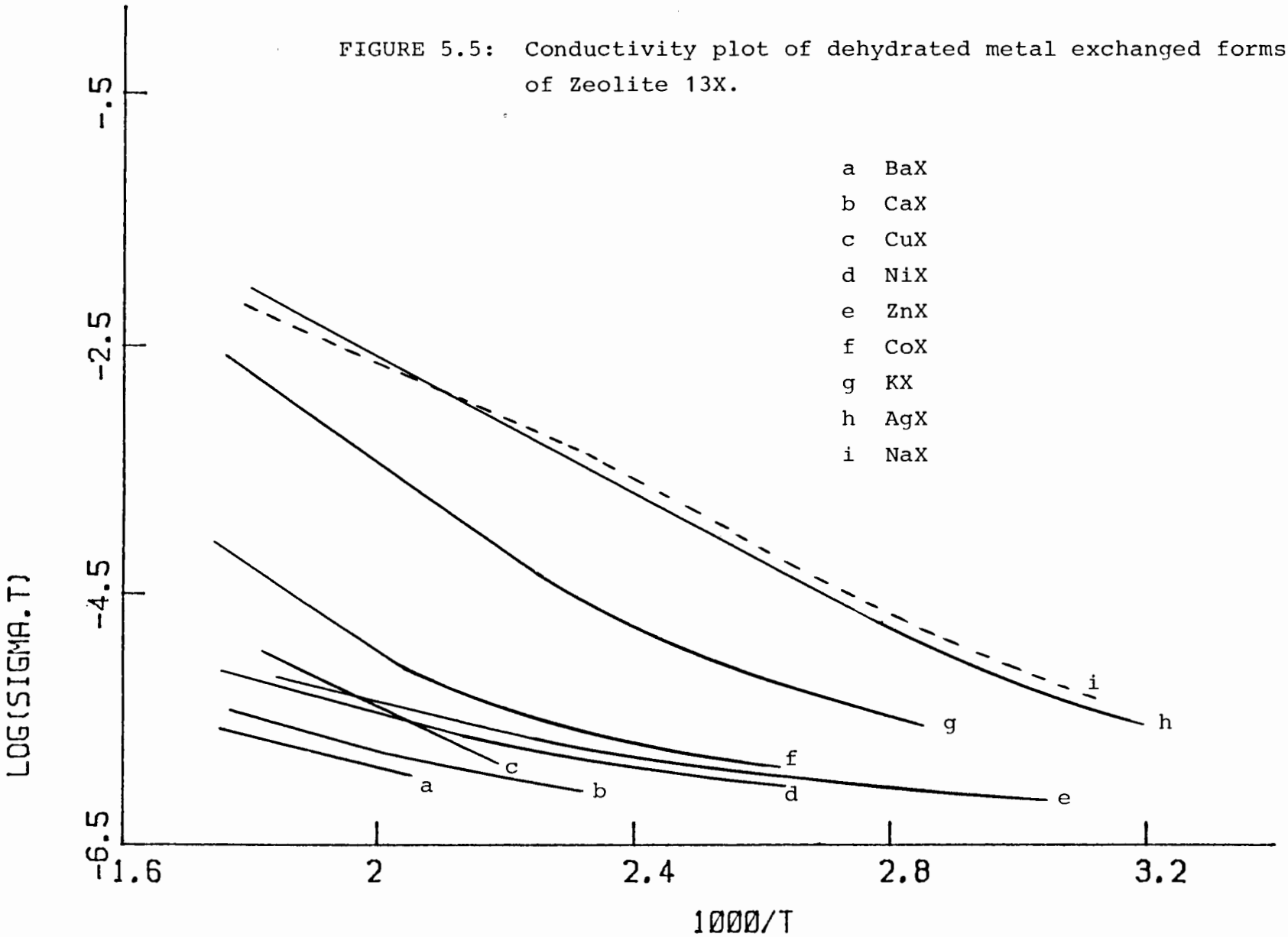

which incomplete ion exchange occurred). This deviation from the straight line behaviour could be attributed to a dielectric absorption which is superposed on the ionic conduction (88). Figure 5.6 presents the conductivity as a function of atomic number of the metal exchanged into the zeolite. For the monovalent cations of Group I the general trend is one of decreasing conductivity with increasing atomic number. This can be attributed to a steric effect due to the increase in the ion size as one descends the group.

The Ag^+ ion, although very similar in behaviour to the Group I metals does not fall into this general trend. Its comparatively high conductivity is not surprising as the good ionic conduction properties of silver in materials such as AgI and $RbAg_4I_5$ is very well known.

The Group II cations of Ca^{2+} and Ba^{2+} also show a decrease in conductivity with increase in atomic number. This too can be attributed to the steric effect of the larger cations as one goes down the group.

The first row transition metals show a remarkable decrease in conductivity with increase in atomic number. Since there is very little difference in ionic size, this trend could be attributed to the degree of exchange achieved in the ion-exchange reactions. The less successful the exchange (see Table 4.4) the higher the conductivity. This is because there are more monovalent ions such as sodium and hydrogen present which are more mobile and could contribute more readily to the conduction mechanism.

The general trend is that the monovalent cations exhibit a higher conductivity than the divalent ions. The number of cations in the divalent metal-exchanged zeolites available for conduction is much lower than in the

FIGURE 5.6: Graph showing Electrical Conductivity at 250°C for unimpregnated metal exchanged forms of Zeolite X.

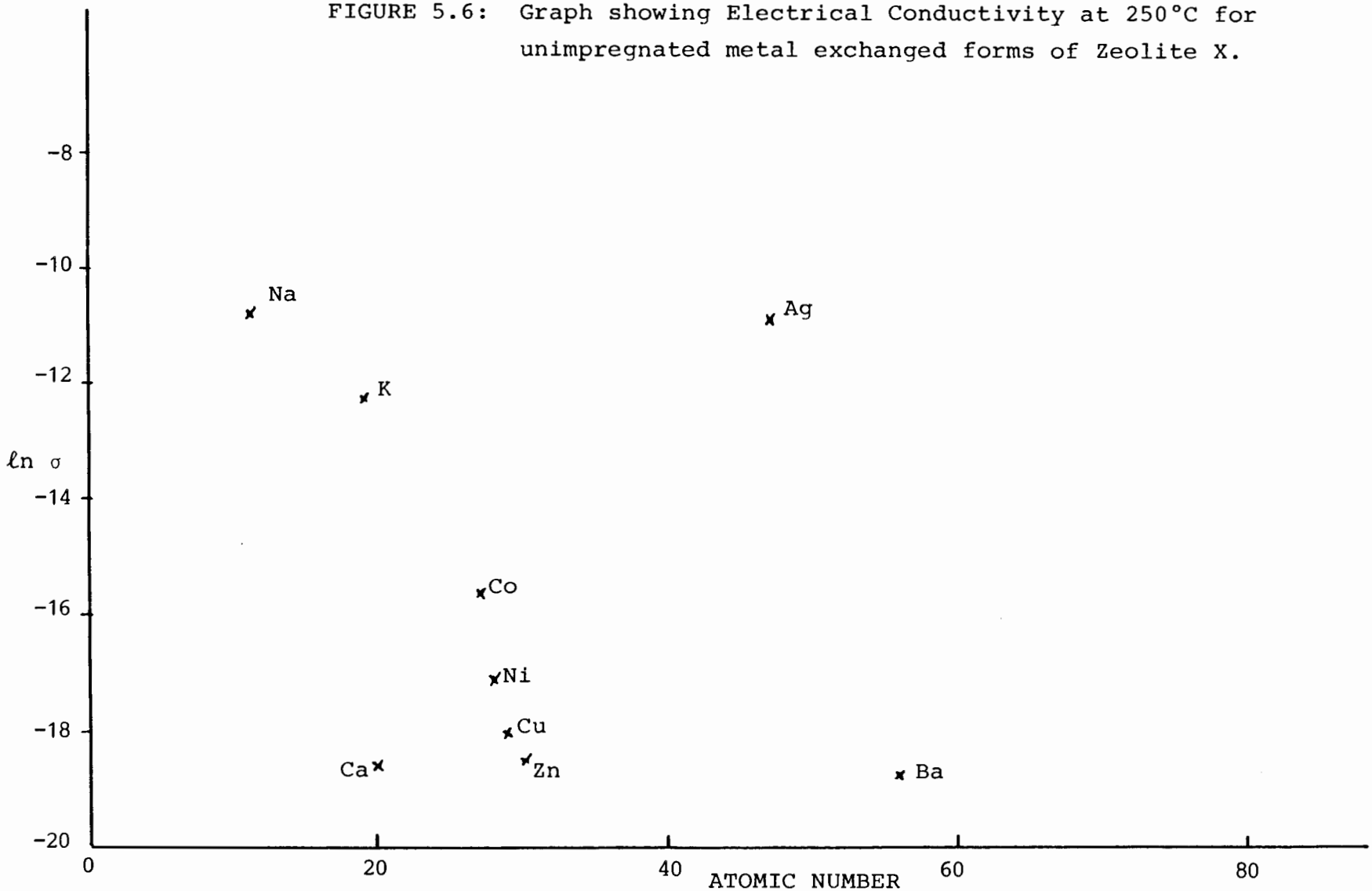

monovalent metal zeolites, hence one could expect a generally lower conductivity value.

No value for the conductivity of the lead-exchanged zeolite could be obtained, since the resistance of the sample remained beyond the limit of the Hewlett Packard LCR meter used in the data collection.

The activation energy ΔE, the Gibbs Free Energy ΔG, the enthalpy ΔH and entropy ΔS for the conduction processes are presented in Table 5.1.

Figure 5.7 shows the relationship between the free energy ΔG and the ionic radius of the metal ions exchanged into the zeolite. For the monovalent ions there is an increase in the free energy with increasing ionic radius. This can be attributed to the steric restriction which affects the larger ions such as K^+ and hence decreases the number of ions capable of migration.

The Group II metal cations also show an increase in free energy with increasing ionic radius. These divalent ions must reside between two relatively widely separated negative charges, thus reducing the bond strength considerably. The increase in ΔG with increasing cation radius therefore reflects the greater ease of bonding to two crystallographically separate sites for the larger more polarisable cations.

The first period transition metals show a decrease in ΔG with increasing ionic radius. This trend could be related to the exchange capacity of the ions, the contribution of the two exchangeable ions partaking in the conduction process and the role of the d-orbital electrons in the bonding of the ions to the zeolite framework.

TABLE 5.1: Thermodynamic parameters of unimpregnated Zeolite forms.

Zeolite	ΔE (kJ/mol.)	ΔG_{400} (kJ/mol.)	ΔH (kJ/mol.)	-ΔS (kJ/mol.)
NaX	22.90	85.48	41.35	110.33
KX	29.98	94.11	59.99	85.28
AgX	28.96	88.92	57.45	78.69
CaX	14.99	98.94	8.38	236.59
BaX	13.69	101.45	1.41	252.60
CoX	30.76	100.93	33.06	169.67
NiX	10.61	101.64	14.91	216.83
CuX	22.19	108.90	46.39	157.27
ZnX	10.15	101.71	14.74	217.43

TABLE 5.2: Thermodynamic parameters of sodium impregnated Zeolite forms.

Zeolite	ΔE (kJ/mol.)	ΔG_{400} (kJ/mol.)	Δ H (kJ/mol.)	-ΔS (kJ/mol.)
NaX	27.01	86.04	34.48	114.00
KX	33.09	91.50	68.48	67.56
AgX	34.23	81.91	76.37	13.85
CaX	35.66	96.01	75.52	51.22
BaX	38.42	89.03	83.19	14.63
CoX	28.02	80.45	65.75	36.75
NiX	35.52	84.40	78.42	14.96
CuX	17.55	71.50	20.74	126.91
ZnX	33.48	80.86	72.74	20.24
PbX	22.85	76.58	53.32	60.65

FIGURE 5.7: Gibbs Free Energy of Conduction for metal exchanged Zeolite 13X

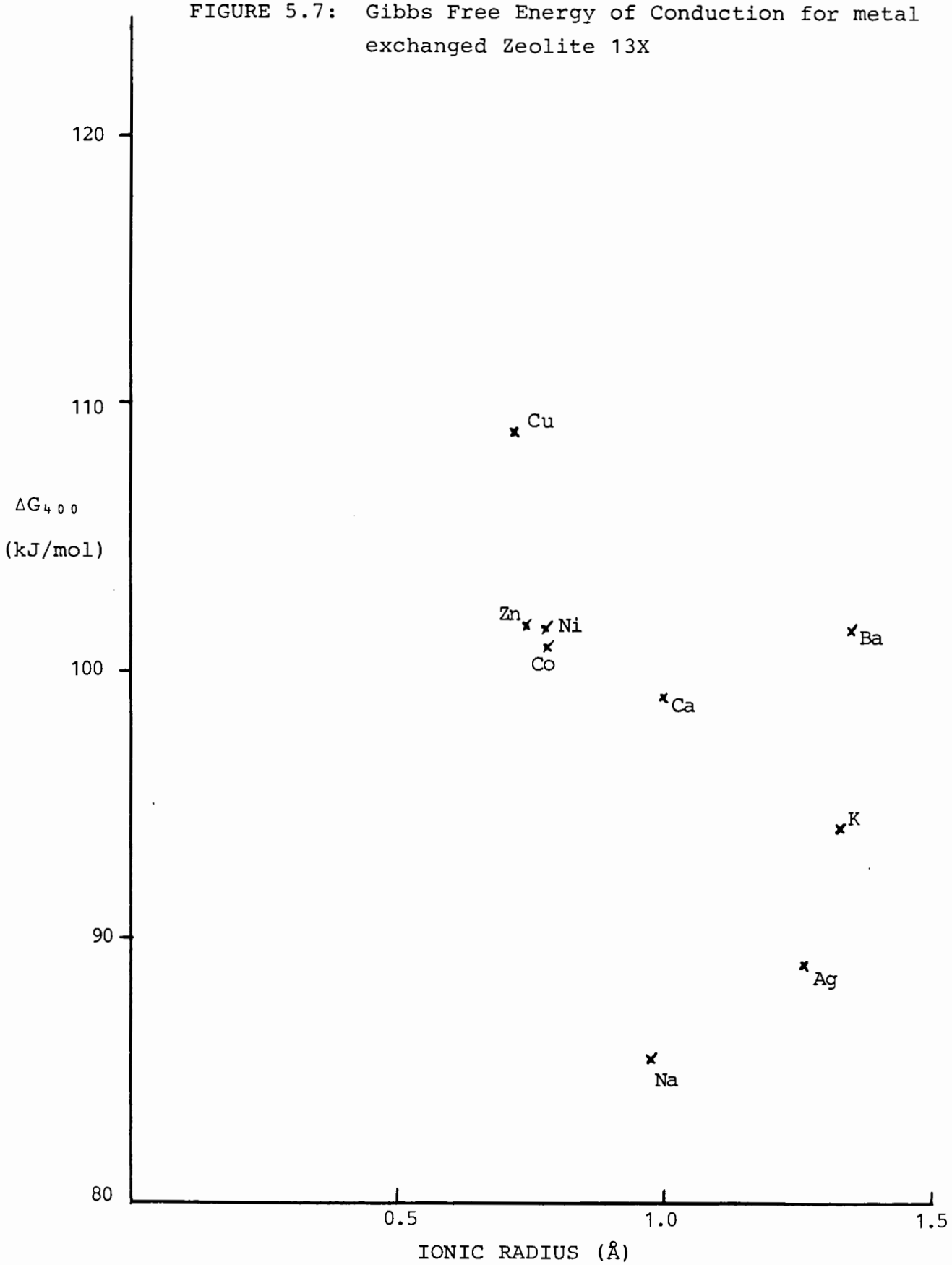

In this instance the conduction process is not fully understood.

The $\log\sigma T$ vs T^{-1} plot for the sodium impregnated monovalent metal-exchanged forms of the zeolite 13X are presented in Figure 5.8. The conductivity for these samples was found to increase with increasing temperature.

The conductivity decreases with increasing ionic size from the Na^+ ion to the K^+ ion, indicating the limit imposed on the mobility of the larger K^+ ions by the steric restriction. The silver-exchanged form exhibits a conductivity higher than the Na^+ and K^+ ions for the conduction process. This could be attributed to the more covalent bonding nature of the silver ion, meaning more mobility for the conduction process. Although some of the silver ions were reduced by the sodium, these metal atoms did not appear to contribute any significant metallic conduction to the overall ionic conduction mechanism. Once again, the remarkable ionic conduction properties of the silver ion are evident in the conductivity values obtained in this instance.

Figure 5.9 illustrates the $\log\sigma T$ vs T^{-1} plot for the sodium impregnated divalent metal-exchanged zeolites. A positive deviation from straight line behaviour is evident at the lower temperatures, characteristic of the samples with two types of exchangeable cations present in the zeolite. The transition metals exhibit a better conductivity than the Group II metal ions. The reason for this is not fully understood, but could be related to the role played by the electrons in the d-orbitals, and the way they affect the bonding of the transition

FIGURE 5.8: Conductivity plot of monovalent metal exchanged Zeolite X impregnated with Sodium.

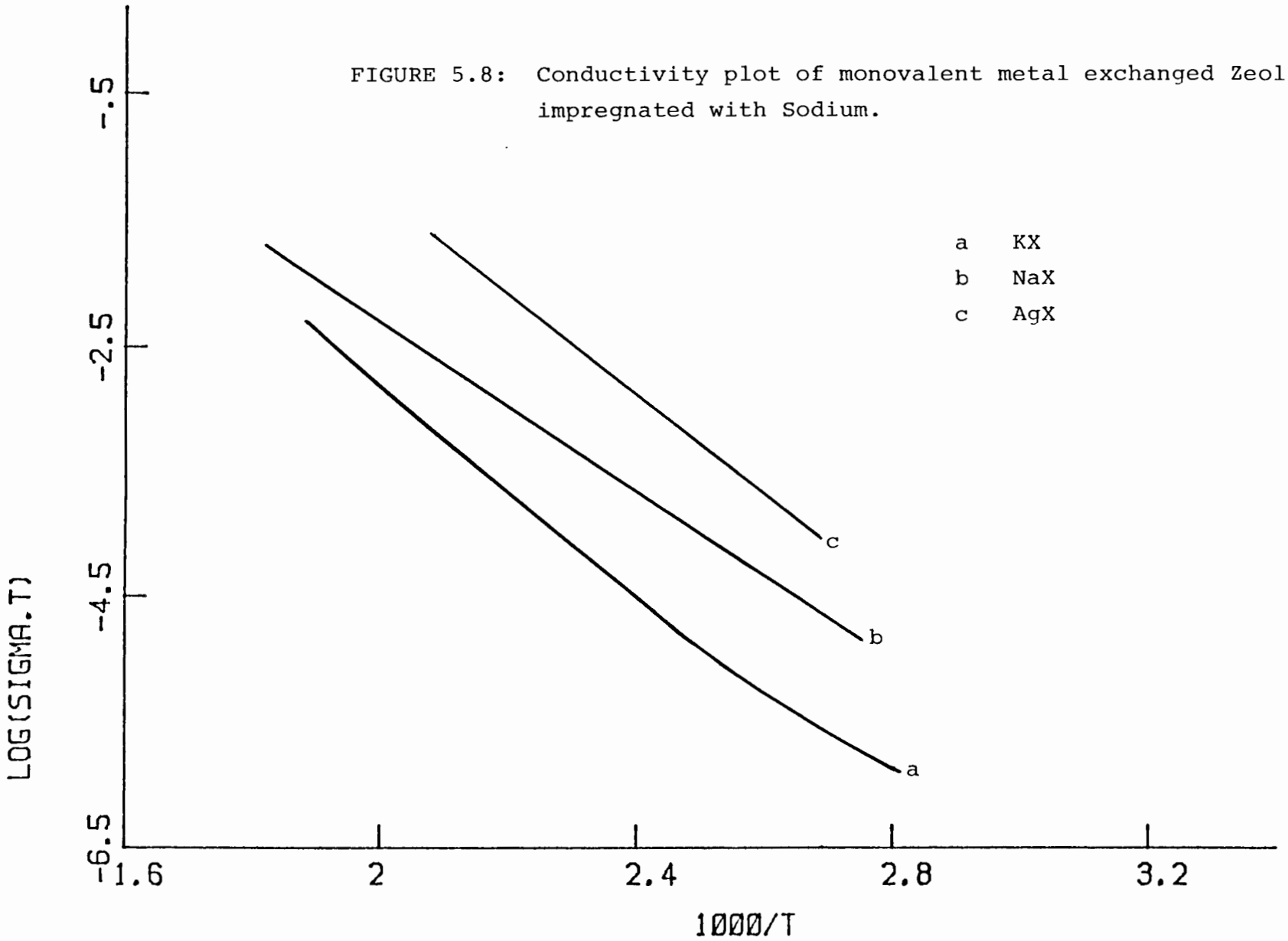

FIGURE 5.9: Conductivity plot of divalent metal exchanged Zeolite X impregnated with sodium.

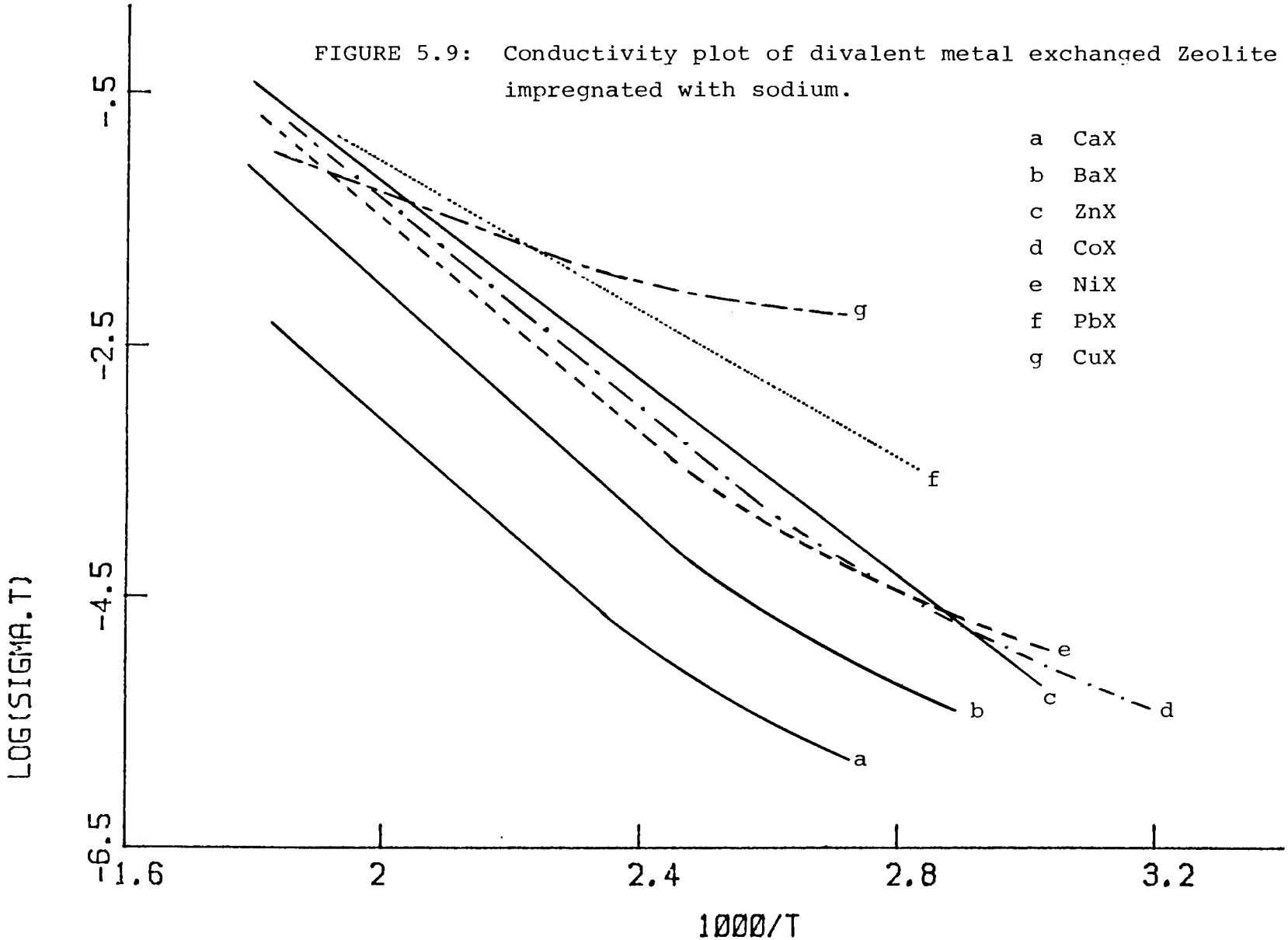

metals to the zeolite framework. The smaller ionic size of the transition metals means less steric restrictions and hence greater ionic mobility.

The presence of metal atoms reduced by the sodium does not appear to impede the ionic conduction mechanism. Therefore contribution to the metallic conduction by these atoms must be small.

Ba^{2+} and Ca^{2+} ions are not reduced by the sodium vapour and hence a metallic conductivity for these ions was not expected.

The thermodynamic parameters ΔG, ΔH and ΔS, as well as the activation energy ΔE for the conduction process are presented in Table 5.2. Figure 5.10 shows the variation of the activation energy with respect to ion size for the metal-exchanged zeolites.

The Group I cations show an increase in activation energy with increasing ionic radius, indicating that the potential energy barrier for the conduction process is larger for the larger ions. The excess sodium doped into the zeolite matrix does not appear to lower the activation energy since the larger ions are still involved in the conduction process.

The activation energy for the silver-exchanged zeolite is higher than the Na^+ and K^+ zeolites. By considering the more covalent nature of the silver ion in bonding to the zeolite framework, one would expect a lower activation energy for the conduction process since the silver ions would be more mobile. The reduction of some of these ions by the sodium vapour, however, could result in the increase in activation energy observed, since there are now Na^+ and Ag^+ ions involved in the conduction mechanism.

FIGURE 5.10: Relationship between activation energy and ion size for sodium impregnated Zeolites.

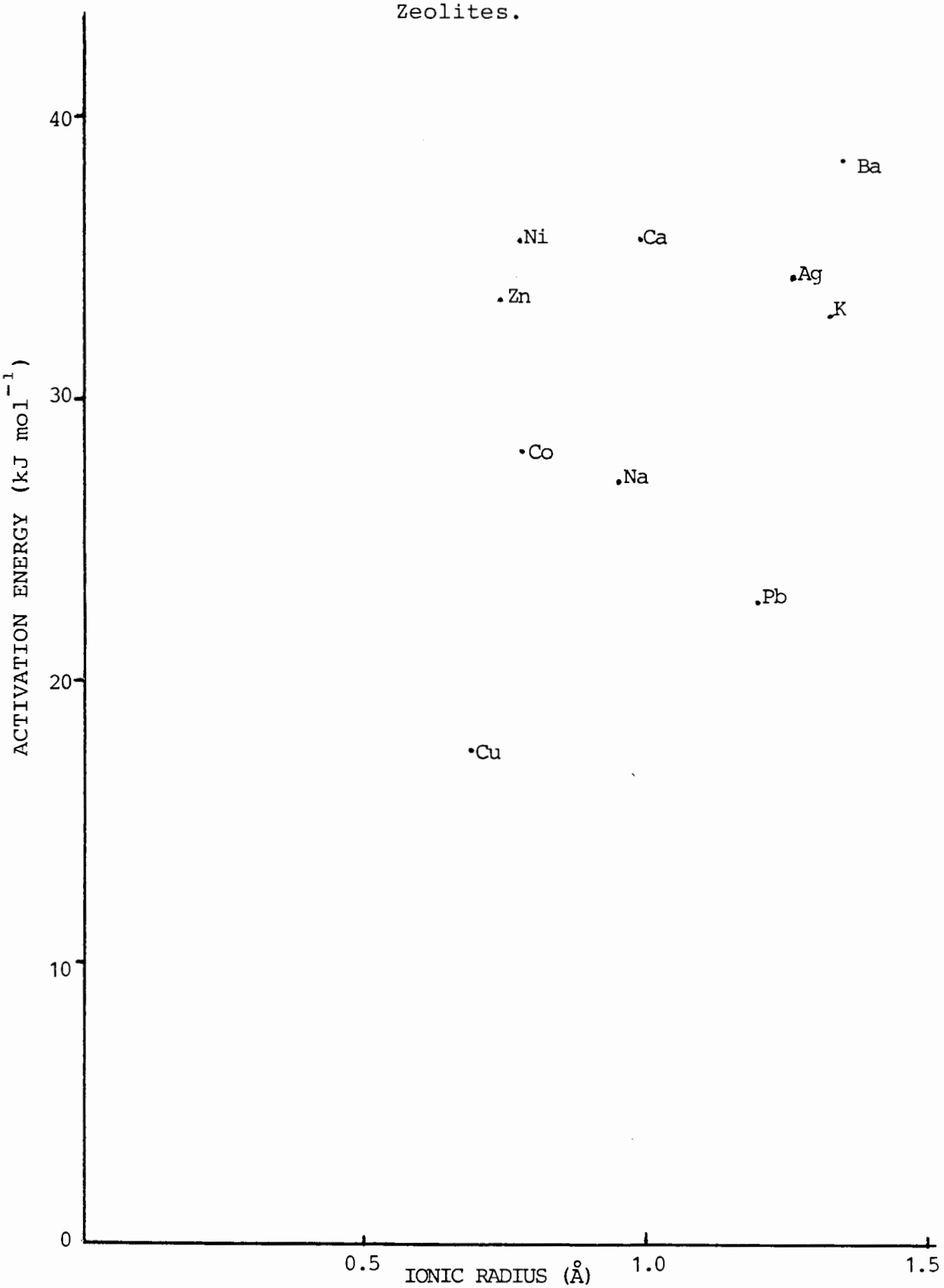

The Group II cations exhibit an increase in activation energy with increasing ionic radius. This can be ascribed to the steric restrictions imposed on the larger Ba^{2+} ions. The activation energies for the Group II cations are on average larger than for the Group I cations. In the Ca and Ba zeolites there are fewer cations in the framework which means that the least favourable sites (lowest binding energy) would not be occupied and hence a higher activation energy would be required to induce cation migration. The Ba^{2+} and Ca^{2+} ions are not reduced by the sodium on impregnation and hence are still involved in the conduction mechanism, contributing to the activation energy.

The first period transition metals show a general increase in activation energy with increase in ionic size. Co^{2+}, however, does not follow this pattern. This trend although obscure could be related to the sites occupied by the ions in the zeolite framework. Cu^{2+} ions are known to occupy sites within the smaller sodalite cages (89). This causes the positive charge density in these cages to increase with a corresponding decrease in activation energy. The ions contributing to the conduction in zeolite X are mostly those located in the large supercages, which in the case of Cu^{2+} zeolite is predominently Na^{+} ions. The location of the other transition metal cations in the zeolite structure is not yet fully apparent, but the trend in activation energies could be due to behaviour similar to that of the Cu^{2+} exchanged zeolite. The fact that most of these metals are reduced by sodium is another factor which could be considered to affect the activation energy for the conduction process.

5.4.2. Conductivity as a function of temperature and pressure.

The electrical conductivity of zeolite NaX was found to increase with increasing temperature and pressure. This is illustrated in Figures 5.11 and 5.12 which show the variation of the conductivity with pressure at different temperatures for the unimpregnated as well as the sodium impregnated zeolite NaX respectively.

In all cases the curves are straight lines at the higher pressures ($> 6.3 \times 10^4$ kPa) with a deviation from straight line behaviour at the lower pressures. This deviation is indicative of a rapid increase in conductivity with an initial increase of pressure. This initial increase in conductivity can be attributed to the compaction process of the powder until it is fully compacted. As the powder is compacted, the volume occupied by the air, which is a non conductor, diminishes, hence the rapid non linear rise in conductivity.

The slopes of the linear sections of the graphs yield the activation volume for the conduction process. These values are presented in Table 5.3.

In general, a negative activation volume is observed. When no pressure is applied, the ions are located on the ionic sites in the framework and hence are energetically stable. When pressure is applied, the contraction of the lattice could displace these ions from their sites to interstitial sites which are energetically less favourable, and hence there is an increase in their ionic mobility.

An increase in temperature increases the activation volume very slightly. This increase is due to the slight thermal expansion of the lattice due to the higher temperatures.

FIGURE 5.11: Conductivity of Zeolite NaX as a function of Pressure at different Temperatures.

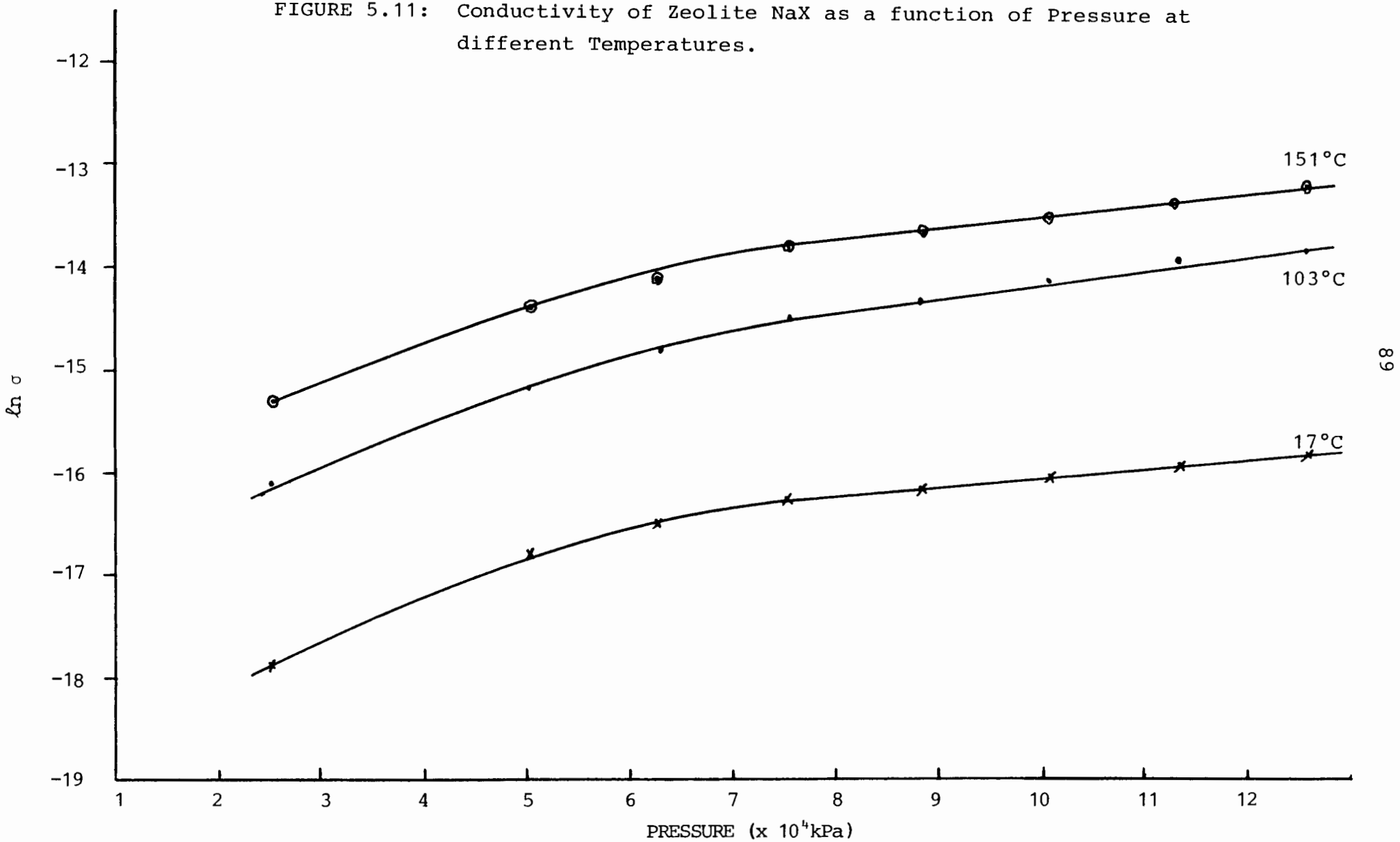

FIGURE 5.12: Conductivity of Sodium impregnated Zeolite NaX as a function of Pressure at different Temperatures.

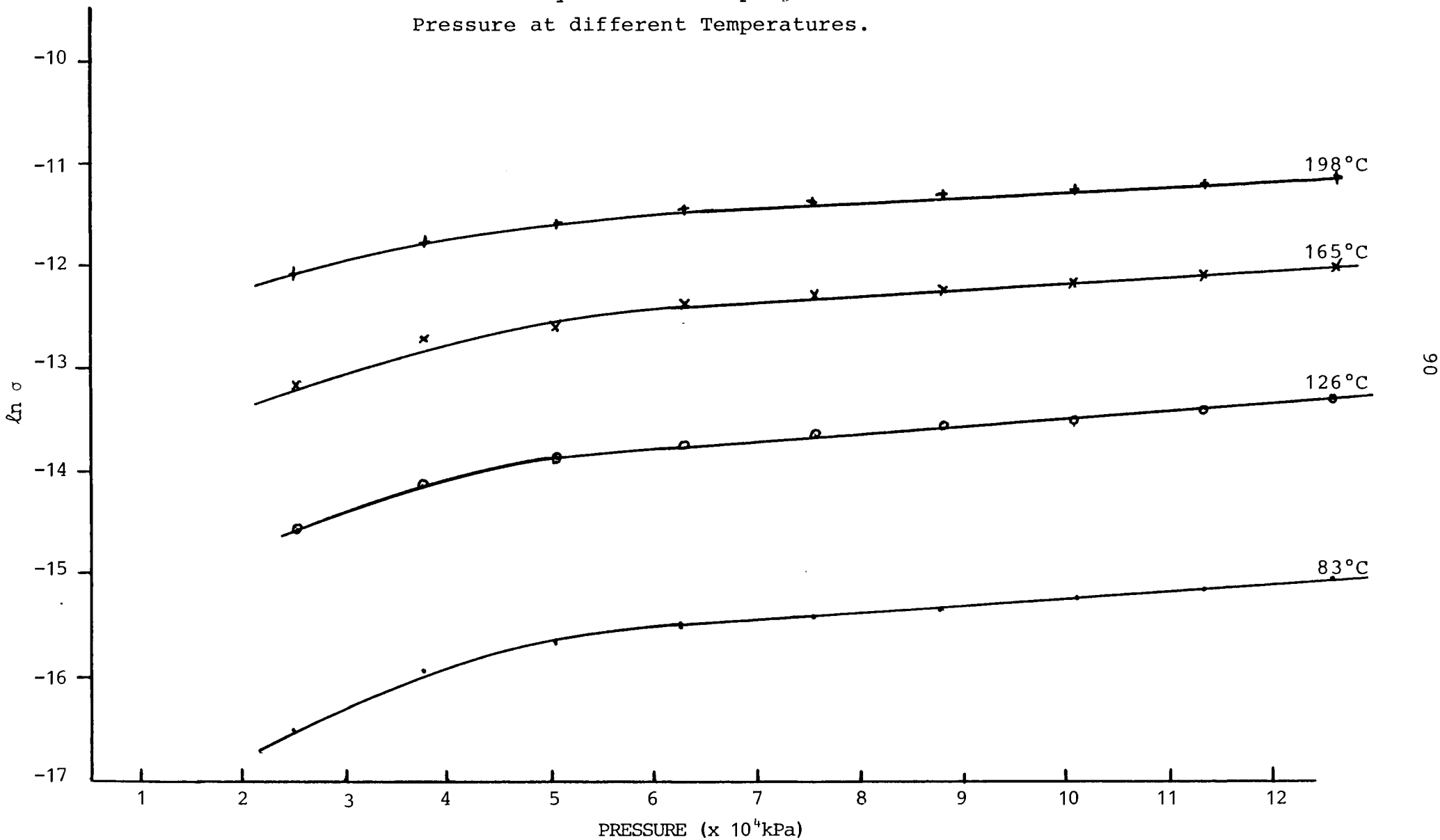

The conductivity of the samples increases with temperature since the ions now possess more energy and tend to a more disordered state, thus increasing their mobility for conduction.

TABLE 5.3: Activation volumes at different temperatures for conduction process.

Zeolite	Temperature(°C)	Activation volume(m^3/mole)
NaX	17	-8.0×10^{-6}
	103	-9.24×10^{-6}
	151	-1.03×10^{-5}
Na doped NaX	83	-7.02×10^{-6}
	126	-6.66×10^{-6}
	165	-5.74×10^{-6}
	198	-5.45×10^{-6}

CHAPTER 6

DISCUSSION AND CONCLUSIONS

The electrical conductivity in zeolite X can be ascribed to the migration of the exchangeable cations present in the zeolite framework (11,88). More specifically, it has been shown that the electrical conductivity can be attributed to the supercage cations located on site S_{II} with a very small contribution from the small cage cations. The elementary jump process for the conduction can be envisaged as a jump from $S_{II} \rightarrow S_{III} \rightarrow S_{II}$ in the supercage. This system of sites constitutes a super lattice type structure similar to that of β-alumina (88,90,91). In general, the ionic conductivity of the zeolite X depends on the number and nature of the exchangeable cations in the zeolite framework.

This is illustrated in the results obtained for the dehydrated metal exchanged forms of the zeolite. A higher number of monovalent cations is required in the structure to maintain electrical neutrality than the divalent cations which require only half the number to maintain electrical neutrality. The monovalent cations exhibit a higher electrical conductivity since there is a higher core of ions in the supercages which are free to migrate. The nature of the cation will dictate in which sites within the framework the cation will be located. This is clearly illustrated by the Cu^{2+} ions which preferentially occupy the sites S_I and $S_{I'}$ in the smaller sodalite cages before occupying the sites in the supercages (89).

On adsorption of sodium into the zeolite matrix an increase in the electrical conductivity of all the zeolite forms is observed with respect to the dehydrated unimpregnated samples. This is illustrated in Figure 6.1(a), (b) and (c), which shows the conductivity as a function of temperature for selected samples of Group I, Group II and the transition metal cations.

This increase in conductivity can be attributed to the Na_6^{5+} colour centres which form when sodium metal is adsorbed into the zeolite X framework (35,40). The increased number of sodium ions occupy site S_{III} in the supercage and hence play a decisive role in enhancing the electrical conductivity of the sample. The exchangeable cations already present in the sample still contribute to the overall electrical conductivity. The actual conduction mechanism in the sodium impregnated samples is more complex than in the unimpregnated samples, due to the migration of more than one ionic species. The detailed mechanism is not fully understood for this reason.

The activation energies for the conduction process in the impregnated samples show a general increase over those values for the unimpregnated samples. This result is rather unexpected, since one would expect the activation energy to decrease due to the high concentration of ions in the form of the Na_6^{5+} centres. The limited understanding of the conduction mechanism makes it difficult to ascertain what causes this phenomenon.

The conduction mechanism is an ionic one and this is indicated by the increase in conductivity with increasing temperature. The incorporation of different ionic species into the zeolite matrix does affect the electrical conduction of the zeolite, the general trend being to lower the conductivity

FIGURE 6.1: Comparison of Conductivities of Selected Metal exchanged Zeolites (1) unimpregnated sample (2) sodium impregnated sample

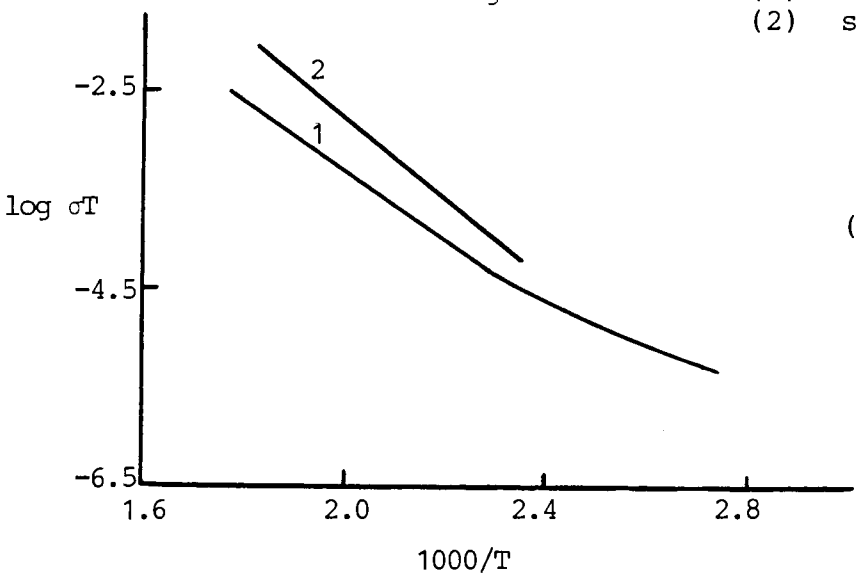

(a) KX

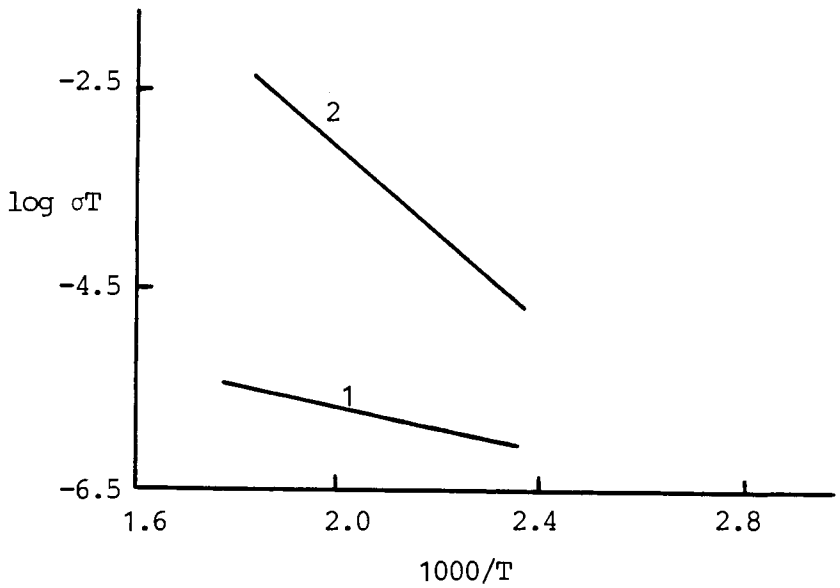

(b) CaX

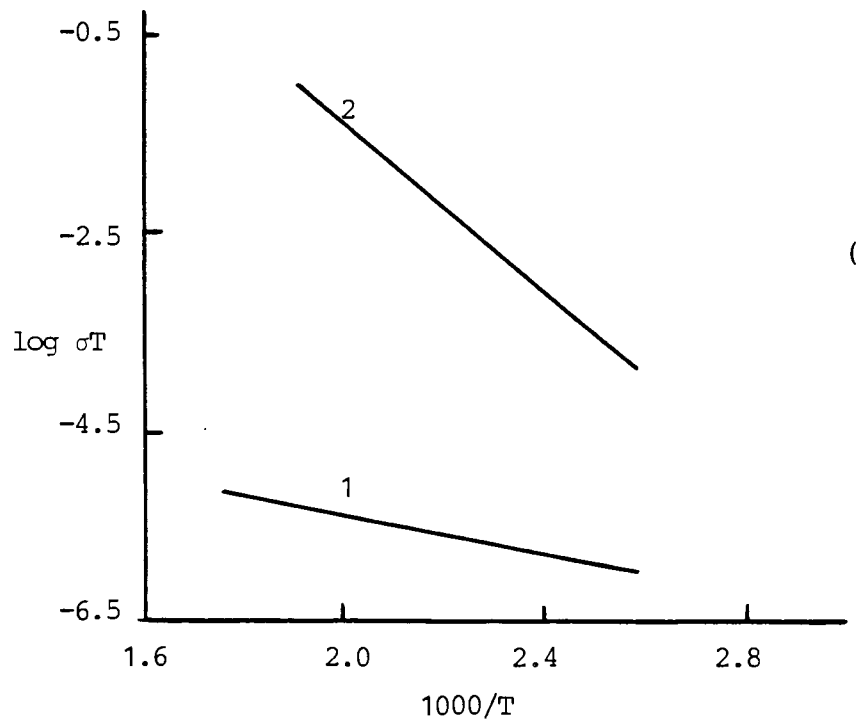

(c) NiX

with respect to the sodium form of the zeolite X. This result is directly related to the type of ion that is exchanged.

The doping of the zeolite forms by sodium metal enhances the electrical conductivity of the zeolites with respect to the non doped forms. The sodium doped zeolites would therefore be the more likely candidates for use as solid electrolytes in solid state batteries.

The most successful solid electrolyte system employed in the high temperature solid state batteries is sodium β-alumina. It has a recorded best conductivity value of $\sim 3.3 \times 10^{-2} \Omega^{-1} cm^{-1}$ at 300 K (79). The best conductivity values obtained on the zeolite samples were obtained on the sodium doped samples and were recorded as $\sim 2.2 \times 10^{-4}$ $\Omega^{-1} cm^{-1}$. This value is some two orders of magnitude lower than that of sodium β-alumina.

The success of zeolites as solid electrolytes in solid state systems is therefore somewhat limited, particularly since there are other problems related to the ceramic strength and the manufacture of zeolite artefacts which impede their use in these applications.

Zeolites must not, however, be ruled out as obsolete solid electrolytes since the scientific technology behind their use as solid electrolytes is nowhere near that of the β-alumina technology.

REFERENCES

1. Smith, J.V.; Mineralogical Society of America Special Paper No 1 (1963), p 281.

2. Pauling, L; Proc. Nat. Acad. Sci. U.S. 16 (1930), p 453.

3. Taylor, W.H.; Z. Krist. 74 (1930), p 1.

4. Barrer, R.M.; British Chem. Engineering (1959), p 267.

5. Clarke, G.; Industrial Minerals, 21 (1980).

6. Bray, L.A., Fullam, H.T.; Zeolite Molecular Sieves, Advances in Chem. Series 101, Amer. Chem. Soc. (1971), p 450.

7. Freeman, D.C. & Durham, N.C.; U.S. Patent No 3,186,875 (1965).

8. J. Coetzer; U.S. Patent No 4,164,608 (1979).

9. Breck, D.W.; Zeolite Molecular Sieves, Wiley & Sons N.Y. (1974), p 5.

10. Breck, D.W., Eversole, W.G., Milton, R.M., Reed, T.B. & Thomas, T.L. J. Amer. Chem. Soc. 78 (1956), p 5963.

11. Freeman, D.C., Stamires, D.N.; J. of Chem. Phys. 35 (1961), p 799.

12. Broussard, L., Shoemaker, D.P.; J. Amer. Chem. Soc. 82 (1960), p 1041.

13. Barrer, R.M.; Zeolites and Clay Minerals, Academic Press (1978), p 4.

14. Barrer, R.M., Chemistry and Industry (1968), p 1203.

15. Kasai, P.H., J. Chem. Phys. 43 (1965), p 3322.

16. Breck, D.W.; Zeolite Molecular Sieves, Wiley & Sons N.Y. (1974), p 29.

17. Breck, D.W., J. of Chem. Education 41 (1964), p 678.

18. Reid, T.B., Breck, D.W.; J. Amer. Chem. Soc. (1956) p 5972.

19. Loewenstein, W.; American Mineralogist 39 (1954), p 92.

20. Meier, W.M.; "Molecular Sieves", Soc. of Chem. Indust. (London) (1968) p 10.

21. Resing, H.A., Thompson, I.K.; Zeolite Molecular Sieves, Advances in Chem. Series 101, Amer. Chem. Soc. (1971), p 473.

22. Boutin, H., Safford, G.J., Danner, H.R.; J. Chem. Phys., 40 (1964) p 2670.

23. Breck, D.W.; Zeolite Molecular Sieves, Wiley & Sons (1974) p 412.

24. Meier, W.M.; "Molecular Sieves", Soc. of Chem. Indust. (London) (1968) p 10.

25. Breck, D.W.; Zeolite Molecular Sieves, Wiley & Sons N.Y. (1974) p 23.

26. Breck, D.W.; IUPAC Info. Bulletin 41 (1975).

27. Breck, D.W.; Zeolite Molecular Sieves, Wiley & Sons N.Y. (1974) p 529.

28. Fischer, K.F., Meier, W.M.; Fortschrift Miner. 42 (1965) p 50.

29. Gal, I.J., Jankovic, O., Malcic, S., Radavanov, P., Todorović, M.; Trans. Faraday Soc. 67 (1971), p 999.

30. Breck, D.W., Eversole, W.G., Milton, R.M., Reed, T.B. & Thomas, T.L.; J. Amer. Chem. Soc. 78 (1956), p 5693.

31. Sherry, H.S.; J. Phys. Chem. 70 (1966), p 1159.

32. Theng, B.K.B, Vansant, E. & Uytterhoven, J.B.; Trans. Faraday Soc. 64 (1968), p 3370.

33. Babo, T; Bull. of Chem. Soc. of Japan, 5 (1930), p 190.

34. McBain, J.W.; The Sorption of Gases and Vapours by Solids, Rutledge & Sons, London; (1932), Chap. 5.

35. Rabo, J.A., Angell, C.L., Kasai, P.H., Shoemaker, V; Dis. of Faraday Soc. 41 (1966), p 328.

36. Barrer, R.M.; Zeolites and Clay Minerals; Academic Press (1978).

37. Breck, D.W.; Zeolite Molecular Sieves, Wiley & Sons N.Y. (1974), p 2.

38. Barrer, R.M., Ibitson, D.A.; Trans. Faraday Soc. 40 (1944), p 206.

39. Barrer, R.M., Whiteman, J.L.; J. Chem. Soc. A, 13 (1967), p 19.

40. Barrer, R.M. & Cole, J.F.; J. Phys. Chem. Solids 29 (1968), p 1755.

41. Rabinowitsch, E. & Wood, W.C.; Trans. Faraday Soc. 32 (1936), p 947.

42. Breck, D.W.; Zeolite Molecular Sieves, Wiley & Sons N.Y. (1974), pp 495, 497.

43. Muratu, K.J.; Amer. Mineralogist 28 (1943), p 545.

44. Breck, D.W.; J. of Chem. Education 41 (1964), p 678.

45. Baur, W.H.; American Mineralogist 49 (1964), p 697.

46. Broussard, L., Shoemaker, D.P. J. Amer. Chem. Soc. 82 (1960), p 1041.

47. Barrer, R.M., Bultitude, F.W. & Sutherland, J.W.; Trans. Faraday Soc. 53 (1957), p 1111.

48. Breck, D.W. & Flannigen, E.M. "Molecular Sieves", Soc. of Chem. Ind. (London) (1967), p 47.

49. Breck, D.W.; Zeolite Molecular Sieves, Wiley & Sons N.Y. (1974), p 93, 96, 98.

50. Smith, J.V., Molecular Sieve Zeolites, Advances in Chem. Series 101, Amer. Chem. Soc. (1971), p 171.

51. Olson, D.H.; J. Phys. Chem. 74 (1970), p 2758.

52. Mortier, W.J., Bosmans, H.J. & Uytterhoven, J.B.; J. Phys. Chem. 76 (1972), p 650.

53. Mortier, W.J. & Bosmans, H.J.; J. of Phys. Chem. 75 (1971), p 3327.

54. Gallezot, P, Ben Taarit, Y & Imelik, B; J. Catalysis 26 (1971), p 481.

55. Rickert, H.; Fast Ion Transport in Solids, ed. W. van Gool North Holland/American Elsevier (1973), p 3.

56. Lehfeldt, W.; Z. Physik 85 (1933), p 717.

57. Lidiard, A.B.; "Handbuch der Physik", ed. S. Flügge, Vol. 20 (1959), p 246.

58. McGeehan, P., Hooper, A.; "Review Fast Ion Conduction Materials", J. of Mat. Sci. 12 (1977), p 1.

59. Armstrong, R.O., Bulmer, R.S., Dickinson, T.; "Fast Ion Transport in Solids", ed. W. van Gool, North Holland/ American Elsevier (1972), p 261.

60. Glasstone, S., Eyring, H. & Laidler, K.J.; "The Theory of Rate Processes", McGraw-Hill Inc., New York (1941), p 516.

61. Beattie, I.R. & Dyer, A.; Trans. of Faraday Soc. 53 (1957), p 61.

62. Stamires, D.N.; J. of Chem. Phys. 36 (1962), p 3174.

63. Barrer, R.M., Baynham, W.J.; J. Chem. Soc. (1959), p 195.

64. Drysdale, D.J.; American Mineralogist 56 (1971), p 1718.

65. Barrer, R.M.; J. Chem. Soc. (1948), p 2158.

66. Breck, D.W.; Zeolite Molecular Sieves, Wiley & Sons N.Y. (1974), pp 249, 295, 304.

67. Charnell, J.F.; J. of Crystal Growth 8 (1971), p 291.

68. Breck, D.W.; J. of Chem. Education 41 (1964), p 678.

69. Breck, D.W.; Zeolite Molecular Sieves, Wiley & Sons N.Y. (1974), p 530, 532.

70. Barrer, R.M., Davies, J.A. & Rees, L.V.C.; J. of Inorg. and Nuclear Chem. 30 (1968), p 3333; 31 (1969), p 2599.

71. Barrer, R.M., Rees, L.V.C. & Shamsuzzoha, M.; J. of Inorg. and Nuclear Chem. 28 (1966), p 629.

72. Sherry, H.S.; J. of Phys. Chem. 70 (1966), p 1158.

73. Sherry, H.S.; J. of Phys. Chem. 72 (1968), p 4086.

74. Ames, L.L.; J. of Inorg. and Nuclear Chem. 27 (1968), p 885.

75. Sherry, H.S.; J. of Colloid and Interface Sci. 28 (1968), p 288.

76. Barrer, R.M. & Bratt, G.C.; J. of Phys. Chem. in Solids 12 (1959), p 130.

77. Barrer, R.M., Buser, W., Grütter, W.F.; Helv. Chimica Acta 39 (1956), p 518.

78. Theng, B.K.G., Vansart, E. & Uytterhoeven, J.B.; Trans. Faraday Soc. 64 (1968), p 3370.

79. Masukazu Iwamoto, Tsuneyasu Hashimoto, Toshikazu Hamano & Shuichi Kagawa, Bull. Chem. Soc. of Japan 54 (1981), p 1332.

80. Bergeret, G., Gallezot, P. & Imellk, B.; J. Phys. Chem. 85 (1981), p 411.

81. Brown, P.J. & Forsyth, J.B.; The Crystal Structure of Solids; Arnold, London (1973).

82. Woldsith, R.; X-ray Energy Spectrometry, Kever Corporation (1973).

83. Coats, A.W. & Redfern, J.P.; Analyst. 88 (1966), p 906.

84. Keattch, C.J. & Dollimore, D.; An Introduction to Thermogravimetry; Heydon & Son (London) (1975).

85. Köhler, B.U.; M.Sc. Thesis: Aspects of the Chemical and Electrical Properties of some A type and other Zeolites, (1982), p 113.

86. Raleigh, D.O.; Electroanal. Chem. 6 (1972), p 87.

87. Ascoli, A; "Fast Ion Transport in Solids" ed. W. van Gool, North Holland/American Elsevier (1973), p 81.

88. Schoonheydt, R.A., Uytterhoeven, J.B.; Molecular Sieve Zeolites - I. Advances in Chem. Series 101, Amer. Chem. Soc. (1971), p 456.

89. Schoonheydt, R.A., Velge, F.; J. Chem. Soc., Faraday Trans. I, 72 (1976), p 172.

90. Schoonheydt, R.A., Jansen, F.J.; J. Chem. Soc., Faraday Trans. I, 69 (1973), p 1338.

91. Schoonheydt, R.A.; Journal de Physique, 41 (1980), p C6 - 261.

APPENDIX

PROGRAMME FOR DATA COLLECTION AND STORAGE.

```
1000 open 7,4,7                                  :rem set printer to lower case
1010 print#7
1020 close 7
1030 poke59468,14                                :rem set screen to lower case
1040 for i = 1 to 3
1050 read cm$(i)
1060 next i
1070 n=1
1080 open4,10                                    :rem dmm i/o channel
1090 print#4,"t0f0r0k0q0s6m0z0w1"                :rem dmm commands
1100 open1,11                                    :rem output channel to bridge
1110 open2,11                                    :rem input channel from bridge
1120 dopen#3,"c-data",l100                       :rem data file-opened for write.
1130 print#1,"c1"                                :rem auto circuit mode.
1140 print#1,"l1"                                :rem loss factor d
1150 print#1,"t3"                                :rem manual trigger
1160 print#1,"s0"                                :rem self test off
1170 print#1,"m0"                                :rem lcr off
1180 print#1,"p0"                                :rem cp low level off
1190 print#1,"d0"                                :rem rqs mode off
1200 print#1,"r9"                                :rem lcr range auto
1210 print#1,"r5"                                :rem dq range auto
1220 input "Enter time in HHMMSS format ";ti$
1230 input "Data collection interval (minutes) ";t1
1240 t1=t1*100
1250 print"■"
1260 rem start of main loop
1270 t=val(ti$)
1280 poke32768,32
1290 for i = 1 to 6
1300 x = asc(mid$(ti$,i,1))                      :rem poke clock on top l.h.s of screen
1310 poke 32768+i,x
1320 next i
1330 if t1=0 then 1350
1340 if t/t1 = int(t/t1)then 1520                :rem measure
1350 get g$
1360 if g$="" then 1260
1370 if g$="t" then gosub 1900                   :rem temperature change
1380 if g$="i" then gosub 4000                   :rem time interval change
1390 if g$="c" then gosub 1930                   :rem circuit mode change
```

```
1400 if g$ = "m" then 1520              :rem measure
1410 if g$ = "o" then 1750              :rem manual instruction
1420 if g$ = "e" then 2050              :rem end experiment
1430 goto 1260
1440 end
1450 :
1460 :
1470 :
1480 :
1490 :
1500 :
1510 :
1520 rem read data subroutine
1530 print#4,"x"                        :rem dmm execute
1540 for xc = 1 to 200:next
1550 input#4,v$                         :rem read dmm voltage
1560 if len(v$)<12 then 1550
1580 v= val(right$(v$,len(v$)-4))
1590 printv
1600 temp= v/.040912*1000               :rem convert dmm voltage to temperature
1610 for f=2 to 3                       :rem read resistance and capacitance,
1620 for h = 1 to 3                     :rem at all three frequencies.
1630 print#1,"f"+right$(str$(f),1)
1640 print#1,"h"+right$(str$(h),1)
1650 print#1,"t3":fori=1to200:next
1651 print#1,"t1":fori=1to2200:next:print#1,"t3t3"
1660 input#2,a$,b$
1670 print ti$;tab(20);a$;tab(40);temp
1680 n=n+1                              :rem increment record count
1690 record#3,(n)
1700 t$=str$(temp)
1710 print#3,t$;",";ti$;",";a$;",";b$   :rem store data on disc
1720 next h
1730 next f
1740 goto 1350
1750 rem - manual instruction
1760 print"refer to 4262a manual page 3-34"
1770 print"for a list of remote program codes"
1780 input#"enter instruction code";ic$
1790 print#1,ic$
1800 print#1,"t3"
1810 input#2,a$,b$
1820 print"result of instruction ";ic$;"is:"
```

```
1830 print
1840 printa$,b$
1850 print"any more instructions"
1860 get g$
1870 if g$="" then 1860
1880 if g$<> "y" then return
1890 goto 1780
1900 rem temperature change
1910 input"new temperature";temp
1920 return
1930 rem circiut mode change
1940 print"Circuit mode options are :-"
1950 print
1960 print"   1.   auto
1970 print"   2.   parallel
1980 print"   3.   serial
1990 print
2000 input "enter required mode";cm
2010 if cm<1 or cm>3 thenprint"there are only three options !!!":goto 1940
2020 print#1,"c"+right$(str$(cm),1)
2030 print"circuit mode "cm$(cm)" selected."
2040 return
2050 rem termination
2060 record#3,1
2070 print#3,n
2080 dclose#3
2090 close1
2100 close2
2110 input"data dump";g$
2120 if left$(g$,1) <> "y" then 2300
2130 dopen#3,"c-data"
2140 record#3,1
2150 input#3,n
2160 open1,4
2170 open8,4,8
2180 print#8
2190 close8
2200 print#1,"■"
2210 print#1,"n■umber of records used = ";n
2220 for i= 2 to n+1
2230 record#3,(i)
2240 input#3,a$,b$,c$,d$
2250 if d$=chr$(13) then d$=""
```

```
 2260 print#1,a$;" ";b$;" ";c$;" ";d$
 2270 next i
 2280 dclose#3
 2290 print#1
 2300 end
 2310 data auto,parallel,serial
ready.
```

PROGRAMME WHICH EXTRACTS REQUIRED DATA AND STORES IT FOR PROCESSING.

```
ready.

 1000 rem this program extracts resistance and temperature data measured at
 1010 rem 1 khz from the data file 'c-data' and stores it in file 'topf'
 1020 rem ready for processing.
 1030 n=0:i=2
 1040 dopen#1,"c-data",d0                    :rem current data file
 1050 dopen#2,"topf",d1,l40                  :rem temporary output file
 1060 n=n+1
 1070 record#1,(n)
 1080 input#1,a$,b$,c$,d$
 1090 if len(a$)<2 then1180                  :rem check for file terminator
 1100 t=val(a$)
 1110 if left$(c$,2)<>"nr" then 1060         :rem check for resistance overflow
 1120 if mid$(c$,4,1)<>"b"then 1060          :rem select 1khz data only
 1130 r=val(right$(c$,len(c$)-4))
 1140 record#2,(i)
 1150 print#2,r;","t                         :rem store resistance & temperature
 1160 i=i+1
 1170 go to 1060
 1180 record#2,1
 1190 print#2,i-1
 1200 dclose
 1210 end
ready.
```

DATA PROCESSING AND GRAPH PLOTTING PROGRAMME

```
READY.

 1000 DEF FNL(X)=LOG(X)/2.303                :REM DEFINE BASE 10 LOGS
 1010 DIMT1$(50),T2$(50),XT$(41),YT$(29),XD(1000),YD(1000)
 1020 OPEN1,4                                :REM OPEN PRINTER CHANNEL
 1030 GOTO1110
 1040 PRINT#1,CHR$(1)CHR$(1)A$
 1050 C$="                          "
 1060 B$="======================"
 1070 B$=LEFT$(B$,LEN(A$))
 1080 PRINT#1,CHR$(1)CHR$(1)B$
 1090 PRINT#1,CHR$(10)CHR$(10)CHR$(10)
 1100 RETURN
 1110 INPUT"DATA IDENTIFIER";A$
 1120 GOSUB 1040:REM PRINT HEADING
 1130 INPUT "AREA,LENGTH";A,L
 1140 REM OUTPUT DATA
 1150 PRINT#1,"RESISTANCE";SPC(5);"TEMP";SPC(11);"SIGMA";SPC(14);"LOG(S)";
 1160 PRINT#1,SPC(9);"1000/T"
 1170 DOPEN#2,"TOPF",D1                      :REM OPEN DATA FILE FOR READ
 1180 RECORD#2,1
 1190 INPUT#2,N                              :REM NUMBER OF DATA POINTS
 1200 FOR I=1 TO N-1                         :REM READ DATA
 1210 INPUT#2,R,T
 1220 T=T+273                                :REM CONVERT TO ABSOLUTE TEMPERATURE
 1230 M=1000/T
 1240 T=INT(T*10)/10
 1250 M=INT(M*10000)/10000
 1260 XD(I)=M                                :REM X-COORDINATE
 1270 S=L/A/R                                :REM SIGMA
 1280 LO=FNL(S*T)                            :REM LOG (SIGMA.T)
 1290 LO=INT(LO*10000)/10000
 1300 YD(I)=LO                               :REM Y-COORDINATE
 1310 R$=STR$(R)+LEFT$(C$,15-LEN(STR$(R))):REM PREPARE DATA FOR OUTPUT
 1320 M$=STR$(M)+LEFT$(C$,15-LEN(STR$(M)))
 1330 S$=STR$(S)+LEFT$(C$,15-LEN(STR$(S)))
 1340 LO$=STR$(LO)+LEFT$(C$,12-LEN(STR$(LO)))
 1350 T$=STR$(T)+LEFT$(C$,10-LEN(STR$(T)))
 1360 PRINT#1,R$;T$;S$;SPC(4);LO$;M$         :REM OUTPUT DATA
 1370 NEXT I
```

```
1380 XD(N+1)=999                          :REM SET PLOTTER TERMINATOR
1390 DCLOSE
1400 PRINT#1:PRINT#1:PRINT#1
1410 REM SET UP DATA FOR PLOT
1420 T1$=A$                               :REM PLOT TITLE
1430 T2$=""
1440 XT$="1000/T"                         :REM X-AXIS TITLE
1450 YT$="LOG(SIGMA.T)                    :REM Y-AXIS TITLE
1460 LT$="L0"                             :REM LINE TYPE
1470 L$="N"
1480 PS=2                                 :REM PLOT SYMBOL
1490 PK$=TI$                              :REM LEGEND TEXT
1500 XL=1.6                               :REM X-AXIS LOWER BOUND
1510 XH=3.4                               :REM X-AXIS UPPER BOUND
1520 YL=-6.5                              :REM Y-AXIS LOWER BOUND
1530 YH=1.0                               :REM Y-AXIS UPPER BOUND
1540 YS=.5                                :REM Y-AXIS STEP SIZE
1550 XS=.2                                :REM X-AXIS STEP SIZE
1560 MA%=1                                :REM PLOT SYMBOL MAGNIFICATION
1570 GOSUB 1590                           :REM CALL PLOT ROUTINE,
1580 END
1590 X1=220:X2=1800:Y1=260:Y2=1550        :REM SET PLOT WINDOW
1600 OPEN9,9                              :REM OPEN PLOTTER CHANNEL
1610 GOSUB1800                            :REM PLOT TITLES & AXES
1620 GOSUB1720
1630 GOSUB1860                            :REM PLOT TICK MARKS & SCALES
1640 GOSUB1990
1650 GOSUB1750                            :REM CHECK FOR FILE TERMINATOR
1660 GOSUB2130                            :REM PLOT DATA
1670 GOTO 1710
1680 IFR$="N"THEN1710
1690 IFR$<>"Y"THEN1670
1700 CC=CC+0.5:GOTO1650
1710 PRINT#9,"H@":CLOSE9:RETURN
1720 PRINT:PRINT"PLOTTER FINISHED TITLES & AXES ?":PRINT"HIT 'Y' WHEN DONE :"
1730 GETR$:IFR$<>"Y"THEN1730
1740 RETURN
1750 FORI=1TO1000
1760 IFXD(I)=999THEN1780
1770 NEXTI
1780 DC=I-1:RETURN
1790 REM*************************************************************** ****
1800 REM PLOT TITLES & AXES
```

```
1810 PRINT#9,";:HOR,0,75,S12,";T1$;CHR$(95);"UH,S12,";T2$;CHR$(95);"U"
1820 PRINT#9,"999,140,S12,";XT$;CHR$(95);"U,90,350,S42,";YT$;CHR$(95);"U"
1830 PRINT#9,X1,Y1;"D";X2,Y1;"U";X1,Y1;"D";X1,Y2;"U"
1840 RETURN
1850 REM************************************************************************
1860 REM PLOT TICK MARKS & SCALES
1870 NN%=((XH-XL)/XS)+.5
1880 IFNN%>7THENXS=XS*2:GOTO1870
1890 FORI=0TONN%
1900 IF(I*XS+XL)>XHTHENPRINT#9,"U":GOTO1940
1910 MM%=(X1+((X2-X1)/((XH-XL)/XS))*I)+.5
1920 PRINT#9,MM%,Y1;"D";MM%,Y1+30;"U"
1930 PRINT#9,MM%-40,Y1-50;"S12,";I*XS+XL;CHR$(95);"U"
1940 NEXTI
1950 PRINT:PRINT"PLOTTER FINISHED X TICK MARKS & SCALE ?"
1960 PRINT"HIT 'Y' WHEN DONE :"
1970 GETR$:IFR$<>"Y"THEN1970
1980 RETURN
1990 NN%=((YH-YL)/YS)+.5
2000 IFNN%>7THENYS=YS*2:GOTO1990
2010 FORI=0TONN%
2020 IF(I*YS+YL)>YHTHENPRINT#9,"U":GOTO2060
2030 MM%=(Y1+((Y2-Y1)/((YH-YL)/YS))*I)+.5
2040 PRINT#9,X1,MM%;"D";X1+30,MM%;"U"
2050 PRINT#9,X1-20,MM%-50;"S42,";I*YS+YL;CHR$(95);"U"
2060 NEXTI
2070 PRINT#9,"H"
2080 PRINT:PRINT"PLOTTER FINISHED Y TICK MARKS & SCALE ?"
2090 PRINT"HIT 'Y' WHEN DONE :"
2100 GETR$:IFR$<>"Y"THEN2100
2110 RETURN
2120 REM************************************************************************
2130 REM PLOT DATA
2140 PS$="M"+RIGHT$(STR$(MAX),1)+CHR$(48+PS)
2150 IFL$="Y"THENPRINT#9,LT$
2160 FORI=1TODC
2170 XP=XD(I):YP=YD(I)
2180 GOSUB2290                          :REM CONVERT DATA TO PLOTTER SPACE
2190 IFL$="N"THEN2220
2200 PRINT#9,XP%,YP%;"D";PS$            :REM LINE
2210 GOTO2230
2220 PRINT#9,XP%,YP%;PS$                :REM NO LINE
2230 NEXTI
```

```
 2240 PRINT#9,"L0U"
 2250 PRINT#9,1800,1350-(CC*100);PS$;"S12, ";PK$;CHR$(95);"U"
 2260 PRINT:PRINT"PLOTTER FINISHED PLOTTING DATA ?":PRINT"HIT 'Y' WHEN DONE :"
 2270 GETR$:IFR$<>"Y"THEN2270
 2280 RETURN
 2290 REM*************************************************************
 2300 REM CONVERT DATA TO PLOTTER SPACE
 2310 XP%=X1+((((XP-XL)*(X2-X1))/(XH-XL))+.5)
 2320 YP%=Y1+((((YP-YL)*(Y2-Y1))/(YH-YL))+.5)
 2330 GOSUB2350
 2340 RETURN
 2350 FORIJ=1TO75
 2360 NEXTIJ
 2370 RETURN
READY.
```